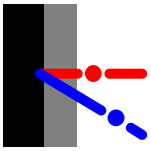

SIMNRA User's Guide

Matej Mayer

Max-Planck-Institut für Plasmaphysik
Boltzmannstr. 2
D-85748 Garching
Germany

email: Matej.Mayer@ipp.mpg.de
Tel.: ++49 89 32991639
Fax.: ++49 89 32992279
www.simnra.com

This manual describes SIMNRA version 6.06

© Max-Planck-Institut für Plasmaphysik, 1997–2011

Additional publications about SIMNRA. The first should be used as general reference for the program:

- M. Mayer, *SIMNRA User's Guide*, Report IPP 9/113, Max-Planck-Institut für Plasmaphysik, Garching, Germany, 1997
- M. Mayer, *SIMNRA, a Simulation Program for the Analysis of NRA, RBS and ERDA*, Proceedings of the 15th International Conference on the Application of Accelerators in Research and Industry, J. L. Duggan and I.L. Morgan (eds.), American Institute of Physics Conference Proceedings **475**, p. 541 (1999)
- W. Eckstein and M. Mayer, *Rutherford Backscattering from layered Structures beyond the Single Scattering Model*, Nucl. Instr. Meth. **B153** (1999) 337
- M. Mayer, *Ion Beam Analysis of Rough Thin Films*, Nucl. Instr. Meth. **B194** (2002) 177
- M. Mayer, K. Arstila, K. Nordlund, E. Edelmann, and J. Keinonen, *Multiple scattering of MeV ions: Comparison between the analytical theory and Monte-Carlo and molecular dynamics simulations*, Nucl. Instr. Meth. **B249** (2006) 823

Contents

Contents . . . iii
Registration and payment information . . . vii
Product license agreement . . . ix
Version history . . . x

1. Overview **1**
1.1. Organization of this manual . . . 1
1.2. Conventions in this manual . . . 2

2. Installation **3**
2.1. System requirements . . . 3
2.2. Installation . . . 3
2.3. Uninstalling SIMNRA . . . 3

3. Using SIMNRA **5**
3.1. Data input forms . . . 5
3.2. Toolbar . . . 5
3.3. Basic steps . . . 5
3.4. File menu . . . 7
3.5. Edit menu . . . 11
3.6. Setup menu . . . 12
3.6.1. Setup: Experiment... . . . 12
3.6.2. Setup: Experiment: More Options . . . 15
3.6.3. Setup: Calculation... . . . 21
3.7. Target menu . . . 28
3.7.1. Target: Target... . . . 28
3.7.2. Layer and substrate roughness . . . 30
3.7.3. Target: Foil... . . . 32
3.8. Reactions menu . . . 34
3.8.1. Replacement of cross section data files . . . 47
3.9. Calculate menu . . . 48
3.9.1. Fit Spectrum... . . . 49
3.9.2. Subtracting pile-up . . . 51

3.10. Tools menu . . . 53
3.10.1. Data Reader . . . 53
3.10.2. Integrate Spectrum . . . 53
3.10.3. Nearest Elements . . . 53
3.11. Plot menu . . . 55
3.12. Options menu . . . 56
3.13. Help menu . . . 57
3.14. Data exchange with other programs . . . 58
3.14.1. Graphics programs: Excel, Origin, ... 58
3.14.2. RUMP . . . 58
3.14.3. IBA data furnace . . . 60
3.15. Importing spectrum data in any format . . . 61
3.16. Adding new cross-section data . . . 62
3.16.1. The R33 file format . . . 62
3.17. Using SRIM stopping powers . . . 66
3.17.1. Trouble shooting . . . 66
3.18. Using user-defined stopping powers . . . 68
3.19. Energy calibration issues . . . 69
3.19.1. Detector nonlinearity . . . 69
3.19.2. Energy calibration for different ion species . . . 69
3.20. Programming support . . . 70
3.20.1. Command line parameters . . . 70
3.20.2. OLE automation . . . 70

4. Physics **71**
4.1. Atomic data . . . 73
4.2. Scattering kinematics . . . 74
4.2.1. Elastic scattering . . . 74
4.2.2. Nuclear reactions . . . 74
4.3. Number of backscattered particles . . . 77
4.4. Cross-section data . . . 78
4.4.1. Rutherford cross-sections . . . 78
4.4.2. Non-Rutherford cross-sections . . . 80
4.5. Evaluation of energy loss . . . 82
4.6. Stopping power data . . . 85
4.6.1. Andersen-Ziegler stopping . . . 85
4.6.2. Ziegler-Biersack stopping . . . 87
4.6.3. KKK stopping . . . 90
4.6.4. SRIM stopping . . . 90
4.6.5. Stopping in compounds . . . 90

4.7. Detector energy resolution . . . 92
4.7.1. Time-of-flight detector . . . 92
4.7.2. Electrostatic detector . . . 92
4.8. Straggling . . . 93
4.8.1. Overview . . . 93
4.8.2. Electronic energy loss straggling . . . 94
4.8.3. Nuclear energy loss straggling . . . 103
4.8.4. Energy loss straggling in compounds . . . 103
4.8.5. Geometrical straggling . . . 103
4.9. Multiple and plural scattering . . . 107
4.9.1. Overview . . . 107
4.9.2. Multiple (small angle) scattering . . . 107
4.9.3. Plural (large angle) scattering . . . 108
4.10. Surface roughness . . . 111
4.10.1. Rough film on a smooth substrate . . . 111
4.10.2. Smooth film on a rough substrate . . . 116
4.11. Live time and pile-up . . . 126
4.11.1. Live time correction . . . 126
4.11.2. Calculation of pile-up . . . 127

5. Examples **137**
5.1. RBS: Rutherford cross-sections . . . 137
5.2. RBS: Non-Rutherford cross-sections . . . 140
5.3. ERDA: Non-Rutherford cross-sections . . . 142

6. Acknowledgements **143**

A. OLE automation reference **145**
A.1. Data types . . . 151
A.2. Simnra.App . . . 151
A.2.1. Properties . . . 151
A.2.2. Methods . . . 156
A.3. Simnra.Setup . . . 164
A.3.1. Properties . . . 164
A.3.2. Methods . . . 171
A.4. Simnra.Calc . . . 172
A.4.1. Properties . . . 172
A.5. Simnra.Target . . . 178
A.5.1. Properties . . . 178
A.5.2. Methods . . . 183

A.6. Simnra.Fit 186
A.6.1. Properties 187
A.6.2. Methods 192
A.7. Simnra.Spectrum 192
A.7.1. Input parameter 192
A.7.2. Properties 193
A.7.3. Methods 195
A.8. Simnra.Stopping 196
A.8.1. Input parameter 196
A.8.2. Methods 196
A.9. Error handling 200
A.10.Programming examples 201

B. The R33 cross section file format **204**
B.1. Introduction 204
B.2. The new R33 Format definition. 205
B.2.1. Syntax of an R33 Entry 206
B.2.2. List of legal entries 206

Bibliography **211**

Index **216**

Registration and payment information

SIMNRA is not free. It is a shareware program – see below for pricing details. You can use SIMNRA for a trial period of thirty (30) days without fee. If you want to use SIMNRA after this period, you have to pay the registration fee and you have to register the program.

The pricing is as follows:

250 €	1 license
450 €	2 licenses
600 €	3 licenses
700 €	4 licenses
800 €	5 licenses
on request	site license

Registered users of any previous version of SIMNRA can upgrade their registration for a reduced fee:

100 €	per license for registered users of any previous version of SIMNRA

Each license is valid for one computer. Installation of SIMNRA on several computers requires several licenses. A site license, which allows installation on all computers of a specific site, is available on request.

To register the program and get a registration number either send an email, a letter by surface mail, or a fax to Dr. Matej Mayer. The address can be found on the title page of this manual. You will receive your registration number and an invoice with full payment details within a few days. Run the program and click `Help:Register...` to enter the registration number.

Most cross-section data files included with SIMNRA have been taken from SigmaBase. These cross-section data files are not included in the shareware fee, but are freely available from SigmaBase. See the file //ibaserver.physics.isu.edu/sigmabase/newuser.html for more information about SigmaBase. The stopping power data files SCOEF.95A and SCOEF.95B have been

taken from the SRIM 97 distribution. These files are not included in the shareware fee, but are freely available for scientific purposes.

SIMNRA was developed at the Max-Planck-Institut für Plasmaphysik, Garching, Germany.

Product license agreement

The product license agreement can be found in the file LICENSE.TXT. The product license agreement is part of SIMNRA.

Version history

Program changes from version 5.0 to 6.0 are described in the file Changes 6.0.txt. Changes between earlier versions are described in Changes 5.0.txt and Changes 4.4.txt.

1. Overview

This report describes the use of the program SIMNRA and the physical concepts implemented therein. SIMNRA is a Microsoft Windows program for the simulation of back- or forward scattering spectra for ion beam analysis with MeV ions. SIMNRA is mainly intended for the simulation of spectra with non-Rutherford backscattering cross-sections, nuclear reactions and elastic recoil detection analysis (ERDA). About 300 different non-Rutherford and nuclear reaction cross-sections for incident protons, deuterons, ^{3}He and ^{4}He-ions are included. SIMNRA can calculate spectra for any ion-target combination including incident heavy ions and any geometry including transmission geometry. Arbitrary multi-layered foils in front of the detector can be used. Several different stopping power data sets are available. Energy loss straggling is calculated including the corrections by Chu and Yang to Bohr's theory. Energy loss straggling propagation in thick layers is considered correctly. Additionally the effects of plural large angle scattering and surface roughness can be calculated approximately. Data fitting (layer thicknesses, compositions etc.) is possible by means of the Simplex algorithm. OLE automation allows automated analysis of large numbers of spectra.

In contrast to other programs for the simulation of backscattering spectra SIMNRA is easy to use due to the Microsoft Windows user interface. SIMNRA makes full use of the graphics capacities of Windows.

1.1. Organization of this manual

This manual is organized in the following way:

- System requirements and the installation of the program are described in chapter 2.
- The use of the program is described in chapter 3. A quick overview about the steps necessary to calculate a spectrum is given in section 3.3. More details are found in the rest of chapter 3.
- The physical concepts implemented in the program are described in detail in chapter 4.
- Some examples for the abilities of the program are shown in chapter 5.

1.2. Conventions in this manual

Links to sections, figures, pages, references, internet web sites and additional text files are highlighted in blue. A click with the mouse will bring you to the link destination.

2. Installation

2.1. System requirements

- SIMNRA requires Windows NT, 2000, XP, Vista, or Windows 7.
- Super-VGA resolution of 1024 × 768 pixels or higher.
- SIMNRA requires about 20 MB free hard disk space.
- User's Guide and help system require Adobe Acrobat or Acrobat Reader. Adobe Acrobat Reader can be downloaded freely from the Adobe web site, see section 3.13 for more details.
- Reading spectrum data in Canberra's CAM-file format requires the Genie-2000 software package. See section 3.4 for more details.
- The use of SRIM stopping powers requires the SRIM software package, version SRIM 2003 or later. SRIM can be downloaded freely from the SRIM home page, see section 3.17 for details.

2.2. Installation

The installation of SIMNRA requires administrator privileges. SIMNRA is distributed with a setup program. To install SIMNRA simply run the setup program and follow the instructions. After running the setup program you should have obtained the files listed in Table 2.1.

To register run SIMNRA, click *Help:Register...* and enter your registration number in the appropriate field.

2.3. Uninstalling SIMNRA

SIMNRA is shipped with an automatic uninstall program. Refer to your Microsoft Windows documentation on how to uninstall programs.

Directory	Files	
	SIMNRA.EXE	Executable program
	README.TXT	Readme file
	CHANGES 6.0.TXT	Describes the changes since version 5.0
	CHANGES 5.0.TXT	Describes the changes since version 4.4
	CHANGES 4.4.TXT	Describes the changes since version 3.0
	LICENSE.TXT	Product license agreement
	MANUAL.PDF	This manual
	DESTINATION.TXT	For internal use by the help system
	libxml2.dll, iconv.dll, zlib1.dll	dynamic link libraries for reading xml files
\ATOM	ATOMDATA.DAT	atomic data
\STOP	STOPH.DAT	electronic stopping power data (Andersen/Ziegler)
	STOPHE.DAT	
	LCORRHI.DAT	
	SCOEF.95A	electronic stopping power data (Ziegler/Biersack)
	SCOEF.95B	
	CHU_CORR.DAT	Chu correction data to Bohr straggling
	SRIM2003_x_y_z.dat	Stopping power data files with SRIM stopping [a]
	ZB_x_y_z.dat	Stopping power data files with Ziegler-Biersack stopping [b]
\CRSEC	*.R33	cross-section data
	*.RTR	
	REPLACE.LST	Replacement of cross-section data files, see subsection 3.8.1
\DLL	*.DLL	dynamic link libraries used by SIMNRA
\SAMPLES	*.NRA	examples
\LAYERS	*.LAY	predefined materials (mylar, stainless steel)
\DEFAULT	SETUP.NRA	default experimental setup
	CALC.NRA	default parameters for calculations
\USERDLL	SAMPLE*.DPR	Code examples in Pascal for user supplied dynamic link libraries, see section 3.15
\XML	IDF_Template.xml	XML template file for xnra files

[a] These files are only created whenever a calculation with SRIM stopping is performed. The number of these files depends on the number of already performed calculations.

[b] These files are only created whenever a calculation with Ziegler-Biersack stopping is performed. The number of these files depends on the number of already performed calculations.

Table 2.1.: Directory structure and files used by SIMNRA.

3. Using SIMNRA

3.1. Data input forms

Input data are entered in different forms. For example, clicking *Setup:Experiment...* will show a window, where experimental parameters are entered. These forms can always remain open: You can modify a parameter and perform a calculation (by clicking *Calculate: Calculate spectrum* or the button in the toolbar) without the need to close the window[1], thus minimizing the number of necessary mouse clicks.

- Do not change parameters while a simulation is being calculated. This may result in unpredictable behavior and may crash the program!

3.2. Toolbar

Often used commands are accessible through a toolbar, see Figure 3.1. Clicking a button is identical to navigating to the corresponding command in the menu. The toolbar can be switched off, see section 3.12.

3.3. Basic steps

This section gives a quick overview about the basic steps necessary to calculate a backscattering spectrum.

Three steps must be performed before a backscattering spectrum can be calculated: In a first step the experimental situation (incident ions, geometry) has to be defined, then the target must be created, and in a third step the cross-sections used for the calculation have to be chosen.

1. Click *Setup:Experiment*. Here you choose the incident ions, the ions energy, define the scattering geometry (see Figure 3.3), and you enter the energy calibration of the experiment.

2. Click *Target:Target*. Here you create the target. Each target consists of *layers*. Each layer consists of different elements with some atomic concentration, which does not change throughout the layer, and each layer has a thickness.

[1] Earlier versions of SIMNRA (version 5.0 and earlier) required these windows to be closed before a calculation could be performed.

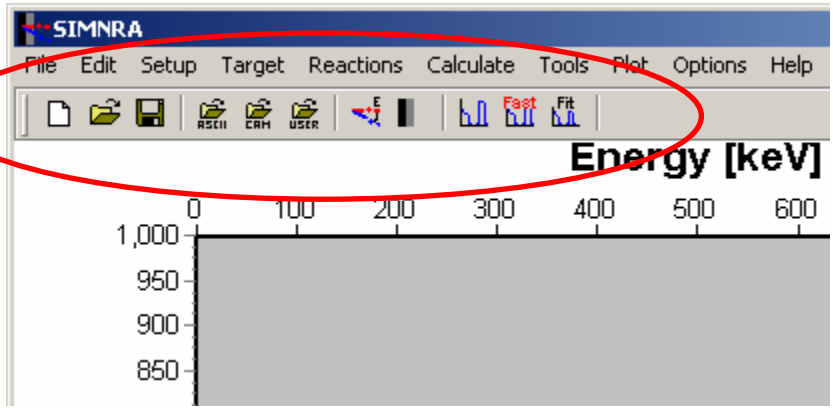

Figure 3.1.: SIMNRA toolbar, marked in red.

3. If there is a foil in front of the detector, then click *Target:Foil* for the definition of a foil. The default is no foil in front of the detector. Like the target, the foil can consist of different layers, and the layers can have different compositions.

4. Click *Reactions*. Here you have to choose which cross-section data should be used for the simulation. The default are Rutherford cross-sections for all elements. You can select non-Rutherford cross-sections instead and you can add nuclear reactions.

5. Now the spectrum can be calculated. Click *Calculate:Calculate Spectrum* for a simulation of the spectrum.

6. With *Setup: Calculation* the parameters for the calculation can be altered. The default values are normally sufficient, and you should change these values only if you know what you are doing.

7. With *File:Read Spectrum Data* a measured spectrum can be imported for comparison with the simulated one and for data fitting.

3.4. *File* menu

In the *File* menu all necessary commands for reading and saving files and data, printing spectra and terminating the program are located.

- *New*: This menu item resets the program to its starting values. All calculated spectra, target, foil and setup definitions are deleted.
- *Open...*: This menu item reads a saved calculation from disk. SIMNRA can open files in the following formats:
  - *nra file format*: SIMNRA version 6 and all earlier versions use the nra file format.
  - *IDF and xnra file formats*: These are xml-files according to the IBA data format (IDF) definition [1]. This file format is very versatile for storing ion beam analysis (IBA) data and spectra and can be used for exchanging data between different IBA simulation programs. SIMNRA 7 and higher use the new xnra file format. This file format is based on the IBA data format (IDF) definition. SIMNRA 6.06 can read xnra files created by SIMNRA 7 and higher. It should be noted, though, that information can be lost if files created by SIMNRA 7 or higher are read with SIMNRA 6.06.
- *Save*: This menu item saves all current parameters, target and foil definitions, experimental and simulated data to disk. See *Save as...* for details. *Save* stores data in nra file format. Use *Save as...*, if you want to store the data in a different format.
- *Save as...*: Like *Save*, but you will be prompted for the name of the file, and you can select in which format the data are saved.

  Data can be saved in the following formats:
  - *nra file format*: SIMNRA version 6 and all earlier versions use the nra file format, and it is recommended to save all files in this format.
  - *xnra file format*: The xnra file format is used by SIMNRA 7 and higher. This file format is based on the IBA data format (IDF) definition.
  - *IBA data format*: These are xml-files according to the IBA data format (IDF) definition [1]. This file format is very versatile for storing ion beam analysis (IBA) data and spectra and can be used for exchanging data between different IBA simulation programs.

  The default file format is nra.

  Depending on the settings in *Options: Preferences: Saving* (see section 3.12) the old NRA-file can be saved to a file named BACKUP.NRA. In the case of erraneous overwriting of a file you can recover the old data from this file.

- *Read Spectrum Data*: This menu item allows the import of experimental data. The availability of menu items depends on the settings in *Options: Preferences*.

  Read Spectrum Data: ASCII...: Allows the import of experimental data in ASCII format.

  The data file format must be as follows: The file may contain an arbitrary number of comment lines at the beginning of the file. A comment line is a line that contains any non-numeric character. These lines will be ignored. The first line that contains only numeric characters will be treated as the first line of data. Each data line must consist of two columns: In the first column the channel number must be given (Integer), in the second column the number of counts must be given (Double). The two columns are separated by an arbitrary number of blanks or tabs. Each line must end with <CR><LF>[2]. The data file may contain up to 8192 channels. An example for a valid data file is given in Figure 3.2.

  Read Spectrum Data: Canberra...: Allows the import of spectral data stored in Canberra's CAM file format.

  SIMNRA uses Canberra's Genie-2000 software package for reading CAM files. The Genie-2000 package is not part of SIMNRA and must be obtained separately from Canberra Industries. This package must be installed correctly before you can read CAM files. The dynamic link libraries sad.dll etc. must be in the search path, and the virtual data manager (VDM) must be installed. SIMNRA has been tested with Genie-2000 versions 1.3 and 1.4.

  Note: SIMNRA reads only spectral data stored in CAM files. Any other information which may be stored in the CAM file, like energy calibration etc., is ignored.

  Read Spectrum Data: IPP...: Reads experimental data stored in the data file format used at the IPP Garching, Germany, until 1999. This data file format will not be described here.

  Read Spectrum Data: ISI...: Reads experimental data stored in the data file format used at ISI, Jülich, Germany. This data file format will not be described here.

  Read Spectrum Data: MCERD...: Reads a spectrum calculated by the Monte-Carlo code MCERD, written by K. Arstila. The data are in the format:

  Energy Counts, with energy in MeV. The energy calibration is taken from the file.

  Read Spectrum Data: User...: Allows to read experimental data stored in any user defined format. A dynamic link library (dll) has to be supplied by the user, which reads the data and passes them to SIMNRA. See section 3.15 for more details.

- *Write Spectrum Data...*: This menu item exports the experimental and simulated data as columns into an ASCII file. You can import this file easily into any plot program, such as Excel, Origin or Mathematica.

[2] <CR> means Carriage Return (#13 decimal), <LF> means Line Feed (#10 decimal).

The file format is as follows: The first line is a comment line which contains information about the contents of the different columns. The first column is the channel number, the second column contains the experimental data (This column is set to zero if experimental data are not available), the third column contains the simulated data (This column is set to zero if simulated data are not available). If the *Element spectra* option in *Setup: Calculation...* is checked, then the next columns will contain the simulated spectra for each element in the target. The columns are separated with blanks. The columns are separated by tabs.

- *RUMP: Read RBS File...*: This menu item allows to read a binary RBS-file produced by RUMP containing experimental parameters (Type of incident particles, incident energy, scattering geometry, etc.) and spectral data.

  Note 1: RUMP stores the description of the sample and the absorber foil in sample description files (*.LCM). You can read sample description files with *RUMP:Read Sample Description File...*.

  Note 2: The RBS-file may contain only one experimental spectrum. Compression level 3 (zero compression) is not implemented. See section 3.14 for more details.

- *RUMP: Read Sample Description File...*: This menu item allows to read a sample description file produced by RUMP or the IBA data furnace NDF. The default file extension of sample description files is *.LCM.

  Note 1: RUMP stores the description of the sample and the absorber foil in sample description files (*.LCM). The experimental parameters (Type of incident particles, incident energy, scattering geometry, etc.) and spectral data are stored in files with extension *.RBS. You can read RBS-files with *RUMP:Read RBS File...*.

  Note 2: SIMNRA supports only a subset of the RUMP sample description commands. Especially the RUMP commands *Equation*, *Species* and *Fuzz* are not supported. If your sample description file contains these commands, they will be neglected and a warning will be shown. See section 3.14 for more details.

- *RUMP: Write Sample Description File...*: This menu item allows to store the structure of the target and the absorber foil in a sample description file in RUMP format. The default file extension is *.LCM. These files can be read by RUMP or the IBA data furnace NDF.

  Note: SIMNRA allows to define a correction factor for the stopping power of each layer for each ion species. The correction factors are not stored in the sample description file.

- *Print...*: This menu item will print all parameters of the calculation and plot the experimental and simulated curves. See also the print preferences on the *Options: Preferences* tab.

```
This line may contain any comment <CR><LF>
This line may contain any comment as well <CR><LF>
 Channel  Counts <CR><LF>
 1          1000 <CR><LF>
 2        1000.0 <CR><LF>
 3         1.0E3 <CR><LF>
 4        +1.0E3 <CR><LF>
 <EOF>
```

Figure 3.2.: Example for a valid data file which can be imported with *File: Read Data: ASCII...*. The first three lines will be ignored by the program. The channel number must be an integer number, counts may be integer or floating point numbers.

Note 1: SIMNRA is not intended to produce high quality graphics. If you want to obtain these, you should use a graphics program such as Excel or Origin. You can exchange data between SIMNRA and any graphics program by file with *File: Write Data...* and via the clipboard with *Edit: Copy Data*.

- *Exit*: Terminates the program.

3.5. *Edit* menu

- *Copy Data*: Copies experimental and simulated data in ASCII format to the clipboard. They can be pasted into any spreadsheet program.

  The format of the data in the clipboard is as follows: The data are organised in three columns. The first column contains the channel number, the second column contains the experimental data, and the third column contains the simulated data. The columns are separated with tabs. Spectra of individual elements or isotopes are not copied to the clipboard. Use *File: Write Spectrum Data...* to export spectra of individual elements or isotopes to a file.

- *Copy Page*: Copies the visible graphics to the clipboard (in enhanced metafile format). You can paste the graphics into any word processing program such as Microsoft Word.

3.6. *Setup* menu

3.6.1. *Setup: Experiment...*

In the *Setup: Experiment...* menu the global parameters of the backscattering experiment are defined. Less often used parameters (necessary for geometrical straggling and pile-up calculations, etc.) can be found in the *Setup: Experiment: More Options* menu.

- *Incident ion*: Selects the incident ions. For incident protons (H), D, T, ^{3}He or ^{4}He ions, the ions are selected by clicking the appropriate radio button.

  For incident heavy ions select *Other* and enter the ions name in *Other ion: Element* (for example Si, Cl, I). Lowercase and uppercase letters in the ions name are treated similar, you can enter silicon as Si, si, SI or sI. The ions mass is selected from the drop down box.

- *Energy*: Energy of the incident ions (in keV).

- *Geometry*: Geometry of the experiment: Incident angle α, exit angle β and scattering angle θ. α and β are measured towards the surface normal, see Figure 3.3. All angles in degrees.

  Note 1: $0° \leq \alpha < 90°$.

  Note 2: $0° \leq \beta \leq 180°$. If $90° < \beta \leq 180°$ then transmission through the target is calculated.

  Note 3: In most experimental setups either IBM or Cornell geometry is used. See Figure 3.10 for a schematic representation of both geometries. You can use *Calculate: Exit Angle Beta...* to calculate β for IBM and Cornell geometry, see section 3.9.

- *Calibration*: Conversion from channels to energy. To account for detector nonlinearities, SIMNRA can use a non-linear energy calibration with a quadratic term of the form

$$E\,[\text{keV}] = A + B \times \text{channel} + C \times \text{channel}^2. \tag{3.1}$$

  E is the particle energy in keV. The calibration offset A must be entered in the *Calibration Offset* field, A in keV. The energy per channel B must be entered in the *Energy per Channel* field, B in keV/channel. C is the quadratic correction term, C in keV/channel^2. For a linear energy calibration $C = 0.0$. A linear calibration is appropriate in most cases, and only if a high accuracy is intended a non-linear calibration should be used.

- *More energy calibration options*: An individual energy calibration may be used for each ion species. This is mainly useful for ERDA measurements with incident heavy ions, where each recoil species may require an individual calibration. By clicking the button an individual nonlinear energy calibration for each ion species may be supplied. If no

individual energy calibration is defined, the major energy calibration entered in the *Calibration* fields of the *Setup: Experiment* form (see above) is used.

Attention: The energy scale, which is plotted at the top of the plot, is obtained with the major energy calibration from the *Calibration* fields of the *Setup: Experiment* form. The energy scale is not valid for particles with individual energy calibrations.

- *Particles*sr*: Number of incident particles times the solid angle of the detector. Solid angle in steradians. The number of incident particles is obtained from the collected charge and the charge state. *Calculate: Particles*sr...* can be used for the calculation.

- *Detector Resolution*: Energy resolution of the detector (in keV). The energy resolution is measured as full width at half maximum (FWHM). This energy resolution is used for all ion species, if no specific resolution for that ion is supplied (see below). *Detector Resolution* is used only for solid state detectors. See section 3.6.2, if you are using a different type of detector, such as a time-of-flight detector.

  SIMNRA can use different detector energy resolutions for different ion species. By pressing the button detector energy resolutions for each ion species may be entered. If no energy resolution for an ion species is supplied, the default resolution (see above) is used.

  Note 1: *Detector Resolution* is only available, if *Detector type* is *Solid state* in the *Setup: Experiment: More Options: Detector type...* menu. *Detector Resolution* is not used for other types of detectors, such as time-of-flight detectors.

  Note 2: SIMNRA uses a constant, energy independent detector resolution for each ion species. This is (more or less) true for light ions (protons and He), but for heavy ions the detector resolution depends on the particle energy. Energy dependent solid-state detector resolutions are not yet implemented in SIMNRA.

- *Energy spread of incident beam*: Usually the incident ion beam is not monoenergetic but has an energy distribution. SIMNRA assumes a gaussian energy distribution of the incident beam with a full width at half maximum which can be entered in the *Energy spread of incident beam* field. If this field is set to 0.0 SIMNRA assumes a monoenergetic incident beam.

The *File*-menu allows to save experimental setups to disk and read experimental setups from disk. All information contained in the *Setup Experiment* form, the *Detector geometry* form, all energy calibrations and all detector resolutions are saved. The NRA data file format is used for saving.

- *Save as Default*: The current experimental setup is stored as startup default for SIMNRA in the file *DEFAULT\SETUP.NRA*.

- *Save Setup as*: Save the current experimental setup to file.

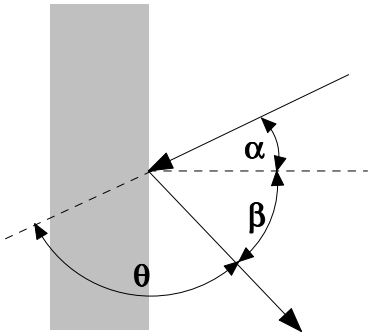

Figure 3.3.: Geometry of a scattering experiment. Incident angle α, exit angle β and scattering angle θ.

- *Read Setup*: Reads an experimental setup from file.
  Note: You can read any NRA-file with *Read Setup*. Only the setup information will be read, any other information (such as target composition, experimental spectra etc.), which may be present in the NRA file, will be ignored.

3.6.2. Setup: Experiment: More Options

Detector type...

The information in this menu is only necessary, if a special detector is used. Special detectors are

1. thin solid state detectors. A solid state detector is thin, if particles are not fully stopped in the detector, but loose only a fraction of their energy. This can be the case for thin transmission detectors (with thicknesses of 10 μm or below), or for nuclear reactions creating high energetic protons: The penetration depth of 10 MeV protons in silicon is about 700 μm, so that these protons are only partly stopped in typical silicon detectors with thicknesses of the order of 100 μm.
2. time-of-flight detectors,
3. electrostatic detectors. These are often used in medium ion scattering (MEIS). SIMNRA is not intended to calculate MEIS spectra, and the agreement to experimental spectra may be poor due to the large influence of plural scattering and neutralization effects. Nevertheless, SIMNRA can be used for a quick overview calculation how a spectrum may look like.

- *Detector type*: Select the type of detector: Either *solid state* (SSD), *time-of-flight* (TOF), or *electrostatic* detector.
- *Solid state detector*:
  - *Detector thickness*: Thickness of the SSD detector, in μm. Select *Infinity*, if the particles are fully stopped in the detector.
  - *Material*: Detector material. Silicon detectors are assumed. This cannot be changed.
- *Time-of-flight detector*:
  - *Free flight path*: Length of the flight path, for which the time of flight is measured, in m.
  - *Time resolution*: Time resolution of the TOF detector, in ps. The full width at half maximum (FWHM) has to be used. The time resolution is used to calculate the energy resolution of the TOF detector, see subsection 4.7.1.
- *Electrostatic detector*:
  - *Delta-E/E*: The energy resolution of electrostatic detectors is usually given by a constant ratio $\Delta E/E$, with ΔE the energy resolution in FWHM and E the particle energy. See also subsection 4.7.2.

Detector Geometry...

In this menu the detailed geometry of the detector (beam diameter, detector diaphragm width, distance sample-detector and shapes of incident beam and detector diaphragm) is entered. This is only necessary if geometrical straggling due to finite widths of the incident beam and detector diaphragm should be calculated. Geometrical straggling is usually small for RBS, but may be considerable for ERDA. See Figure 3.4 for details, how distances and diameters are measured.

- *Calculate geometrical straggling*: Check to include geometrical straggling in the simulation. Geometrical straggling is neglected, if his box is unchecked.
- *Diameter of incident beam*: Diameter of the incident beam in mm. Please note that the size of the beam spot on the sample surface is $d / \cos \alpha$.
- *Shape of incident beam*: Circular or rectangular beams may be selected. A homogeneous current distribution of the incident beam is assumed.
- *Diameter of detector aperture*: Diameter of the detector aperture in mm.
- *Shape of detector aperture*: Circular or rectangular apertures may be selected. Use rectangular also for long narrow slits.
- *Distance sample-detector aperture*: Distance between the sample surface and the detector aperture in mm.

Note: If *Straggling* in the *Setup: Calculation* menu is unchecked, then geometrical straggling (and electronic energy loss straggling) are neglected.

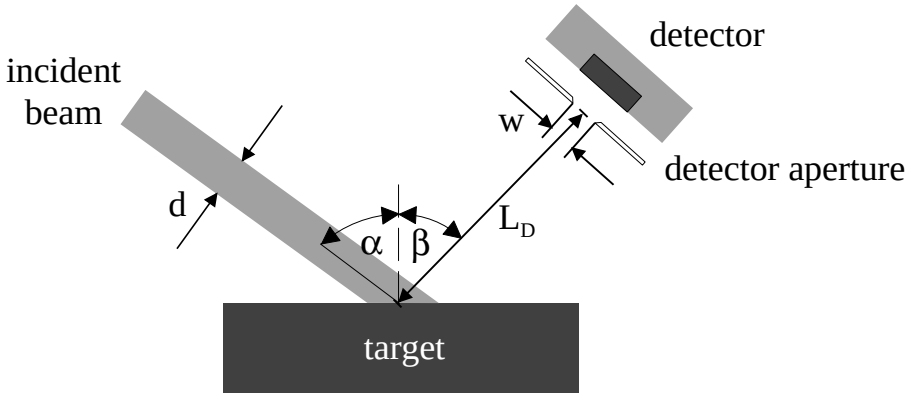

Figure 3.4.: Detector geometry. d is the diameter of the incident beam, w the width of the detector aperture and L_D the distance between sample and the detector aperture. Incident angle α and exit angle β.

Live-time and pile-up...

The parameter for a live-time correction and pile-up simulation are entered in this menu. If experimental data are read from Canberra's CAM-files , some parameters are taken from the information stored in the files.

- *Apply live-time correction*: Check if a live-time correction should be applied to simulated spectra. After checking *Apply live-time correction* you have to enter values for real and live time. Calculation of pile-up is only possible if *Apply live-time correction* is checked.

- *Real time*: Real time of the measurement (in s). The real time is the time it took to measure the spectrum. The real time is necessary for live-time corrections and pile-up calculations.

  If Canberra's CAM-files are used, this parameter is taken from the file.

- *Live time*: Live time of the measurement (in s). The live time is the time interval during the measurement the analog-digital converter (ADC) was able to accept pulses. This value can be obtained from your multi-channel analyzer (MCA). The live time is almost identical to the real time for low pulse rates. The live-time is only necessary for live-time corrections and can be set identical to the real time, if a pile-up calculation is desired without knowing the correct live-time.

  If Canberra's CAM-files are used, this parameter is taken from the file.

- *Calculate pile-up*: Check if pulse pile-up should be calculated for simulated spectra. After checking *Calculate pile-up* you have to enter a value for the pulse rise-time or the fudge time parameter. *Calculate pile-up* is only available if *Apply live-time correction* is checked.

  Note: The pile-up calculation will give incorrect results for ADC offsets other than zero.

- *Pulse rise time*: Rise time of the amplified pulse from zero to its maximum value (in μs). See Figure 3.5 for a schematic definition of the pulse rise time. For Gaussian pulse shaping, the pulse rise time T_p can be derived from the Gaussian shaping time τ_{ST} from [2]

  $$T_p = 2.2 \times \tau_{ST}. \tag{3.2}$$

  The pulse rise time can be measured accurately with an oscilloscope at the amplifier output. However, as SIMNRA approximates the true pulse shape with a parabola (see subsection 4.11.2, Figure 4.28 and Figure 4.29), it is advantageous to use a slightly smaller value for T_p than obtained from Equation 3.2, see Figure 3.6 and Table 3.1.

  If Canberra's CAM-files are used, the pulse rise time is computed from the values for the Gaussian shaping time, DSP rise time, and DSP flat top duration stored in the file according to Table 3.1.

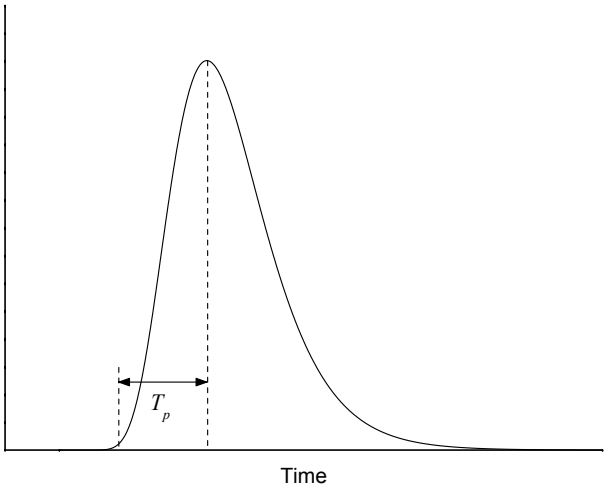

Figure 3.5.: Schematic representation of an amplified pulse with Gaussian shaping. T_p is the pulse rise time.

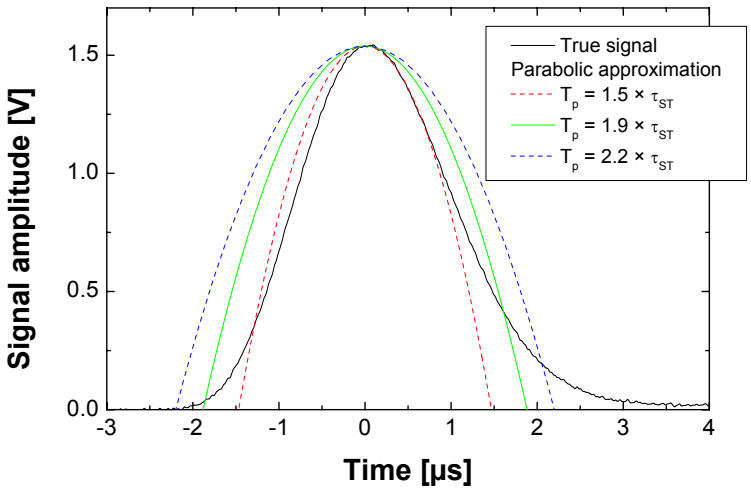

Figure 3.6.: Selection of the pulse rise time T_p for a Gaussian pulse. True pulse from an Ortec 672 spectroscopy amplifier, shaping time $\tau_{ST} = 1\ \mu$s. SIMNRA approximates the Gaussian pulse shape with a parabola. The figure shows parabolas with rise times T_p equal to 1.5, 1.9, and 2.2 times the Gaussian shaping time. The parabola with $T_p = 1.9 \times \tau_{ST}$ usually gives the best approximation to the true pulse shape.

Device	Pulse rise time T_p	
Amplifier (Gaussian shaping)	$T_p = 1.9 \times \tau_{ST}$	τ_{ST}: Gaussian shaping time
Digital signal processor (DSP)	$T_p = 0.8 \times (\tau_{RT} + 0.5 \times \tau_{FT})$	τ_{RT}: DSP filter rise time
		τ_{FT}: DSP filter flat top duration

Table 3.1.: Recommended values for the pulse rise time T_p.

Note: The *Pulse rise time* is only available, if the pile-up model is set to *Accurate* in the *Setup:Calculation* menu, see subsection 3.6.3.

- *Fudge time parameter*: Fudge time parameter for the *Fast* pile-up model (in μs). This parameter can be adjusted to any value matching the measured pile-up in the spectrum. Reasonable values are in the range 0.3–0.5 μs, see section 4.11.2 for more details.

  Note: The *Fudge time parameter* is only available, if the pile-up model is set to *Fast* in the *Setup:Calculation* menu, see subsection 3.6.3.

- *Pile-up rejector*: Switch to *On*, if a pile-up rejector was used during the measurement. Switch to *Off*, if the measurement was made without a pile-up rejector.

  If Canberra's CAM-files are used, this parameter is taken from the file. But note, that this is not always reliable, because it cannot be excluded that the pile-up rejector was enabled, but had no influence due to incorrect or missing cabling.

  Note: This switch is only available, if the pile-up model is set to *Accurate* in the *Setup:Calculation* menu. This switch has no influence, if the pile-up model is set to *Fast*.

- *Pile-up rejector pair-resolution time*: Pair resolution time of the pile-up rejector (in μs). A pile-up rejector (PUR) is only able to recognize two pulses as different, if their time difference is larger than the pair-resolution time. The pair-resolution time is normally specified in the technical manual of the pile-up rejector. Typical values are in the range 0.3–0.5 μs.

  Note: This parameter is only available, if the pile-up model is set to *Accurate* in the *Setup:Calculation* menu. This parameter has no influence, if the pile-up model is set to *Fast*.

3.6.3. *Setup: Calculation...*

In the *Setup: Calculation...* menu the calculation parameters can be altered. This affects the accuracy of the calculation, but also the time necessary to calculate a simulated spectrum.

Parameter tab

- *Isotopes*: If checked, backscattering from all isotopes of all elements in the target is calculated. Especially for heavy elements with many isotopes this will slow down the calculation significantly. If unchecked, the program will use only the mean masses of the elements. Default is checked.

  Important: Non-Rutherford cross-sections and nuclear reactions are only available if *Isotopes* is checked.

- *Straggling*: If checked, electronic energy loss straggling and geometrical straggling (if selected, see section 3.6.2) is taken into account. Default is checked.

- *Multiple Scattering*: If checked, straggling due to multiple small angle scattering will be calculated. Default is unchecked.

- *Dual Scattering*: Most particles are scattered into the detector with only one scattering event with large scattering angle. However, some particles may suffer more than one scattering event with large scattering angle before they reach the detector, see Figure 3.7. This is called plural scattering and results for example in the low background behind the low energy edge of high Z layers on top of low Z elements. The deviations at low energies between simulated and measured spectra are also mainly due to plural scattering.

  SIMNRA can calculate all trajectories with two scattering events. If *Dual Scattering* is unchecked, then only one scattering event is calculated. This is the default. If *Dual Scattering* is checked, additionally trajectories with two scattering events will be calculated.

  Warning: The calculation of dual scattering is a time consuming process. If *Dual Scattering* is checked, this will slow down the calculation of a spectrum by a factor of about 200 (!).

  Note 1: If non-Rutherford cross-sections are selected for some elements, then the selected non-Rutherford cross-sections will be used for the single scattering calculation. The dual scattering calculation, however, is always performed with Rutherford cross-sections: Dual scattering requires cross-sections at all possible scattering angles between $\approx 0°$ and $180°$, which are only available in the case of Rutherford cross-sections. This is reasonable in many cases, because dual scattering is often dominated by heavy elements in the target, where the cross-sections are Rutherford up to high energies. However, this approximation may result in incorrect spectra, if non-Rutherford scattering from light elements is important. SIMNRA will issue a warning message if dual scattering is used with non-Rutherford cross-sections.

Note 2: SIMNRA calculates dual scattering *only* for incident ions and not for recoils or reaction products of nuclear reactions. Additional scattering in a foil in front of the detector (if any) is neglected.

Note 3: If *Dual Scattering* is checked, then *Straggling* must be checked too. SIMNRA will check *Straggling* automatically, if *Dual Scattering* is checked. As long as *Dual Scattering* is checked, *Straggling* cannot be unchecked.

- *Stopping power data*: The selection of stopping power data has a large influence on the shape of the simulated spectra. SIMNRA can use different sets of electronic stopping power data for the stopping of light and heavy ions in all elements:
  - *Andersen/Ziegler*: Electronic stopping power data by Andersen and Ziegler [3, 4, 5].

    Note: If the Andersen/Ziegler stopping power data are used for incident hydrogen isotopes or heavy ions near 1 MeV/amu, artificial steps or kinks may appear in the simulated spectra. This is due to a jump of the stopping power at 1 MeV/amu. See the description of the *High energy stopping* switch for a work-around.
  - *Ziegler/Biersack*: Electronic stopping power data by Ziegler, Biersack and Littmark [5]. These data are identical to Ziegler's SRIM 1997 (formerly TRIM) program. The Ziegler-Biersack data are generally more accurate and reliable than the Andersen-Ziegler data [6]. The energy ranges in which the different stopping power formulas are valid are listed in Table 3.2.
  - *ZB+KKK*: Identical to *Ziegler/Biersack* for most ion/target combinations, except for H, D, T, ^{3}He and ^{4}He in C and Si, in which case the stopping power data by Konac et al. [7, 8] are used. The KKK stopping powers are valid in the energy range $0.01 \leq E \leq 100$ MeV/amu. See subsection 4.6.3 for details about the KKK stopping powers.
  - *SRIM*: Stopping power data from Ziegler's SRIM program, version SRIM 2003 or later. This option will work only, if
    1. SRIM is installed on your computer,
    2. the path to the SRIM directory is registered correctly in *Options: Preferences: Directories*.

    See section 3.17 for more details.
  - *User defined*: User defined stopping powers are used. See section 3.18 for details. But note, that you have to supply stopping power data for all elements present in the target, if *User defined* stopping powers are selected.
- *High energy stopping*: This switch is only available if Andersen-Ziegler electronic stopping power data are used. If checked, the program will use the correct high energy stopping

formula by Andersen and Ziegler for incident protons and heavy ions for $E > 1$ MeV/amu. If unchecked, the program will use the medium energy formula, which is valid only in the range 10 keV/amu–1 MeV/amu, also at higher energies $E > 1$ MeV/amu. The difference between the two formulas usually is small. This switch is necessary because the two stopping power formulas do not fit smoothly together at 1 MeV/amu: The stopping power jumps at 1 MeV/amu resulting in artificial kinks and steps in the simulated spectra. This problem is overcome if *High energy stopping* is unchecked, however this will result in less accurate stopping powers for energies > 1 MeV/amu. A better solution is to use the Ziegler-Biersack stopping powers, where this problem does not occur.

This switch does not have any influence on the calculation of the stopping power of helium ions and is disabled. For helium ions always the medium energy formula is used, which is valid for all energies below 10 MeV. The default is checked.

- *Energy-loss straggling model:* Selects the electronic energy-loss straggling model. Bohr's theory, Chu's theory, or Chu + Yang's theory can be used. Chu's theory takes deviations from Bohr straggling caused by the electron binding in the target atoms into account, and Yang's theory additionally incorporates charge state fluctuations of the ions. See subsection 4.8.2 for more details about electronic energy-loss straggling. Chu + Yang's theory is recommended.

- *Screening to Rutherford cross-section:* Selects the screening function to the Rutherford cross-section due to partial screening of the nuclear charges by the electron shells surrounding both nuclei, see section 4.4.

  – *None*: Rutherford cross-section without screening, see Equation 4.15. This option should be used only for test purposes.

  – *L'Ecuyer*: Screening function according to L'Ecuyer, see Equation 4.16. The L'Ecuyer screening function is only reasonable for RBS with backscattering angles $\theta > 90°$ and should be used only for test purposes. The *Andersen* screening function is generally a better choice.

    Note: If *L'Ecuyer* is selected for recoils, this selection is ignored and replaced by *Andersen*.

  – *Andersen*: Screening function according to Andersen, see Equation 4.17. Andersen's screening function is generally the best choice and the program default.

Options tab

- *Element Spectra*: If checked, individual spectra for each element in the target are calculated and plotted. If unchecked, only the total spectrum is calculated and plotted. Default is unchecked.

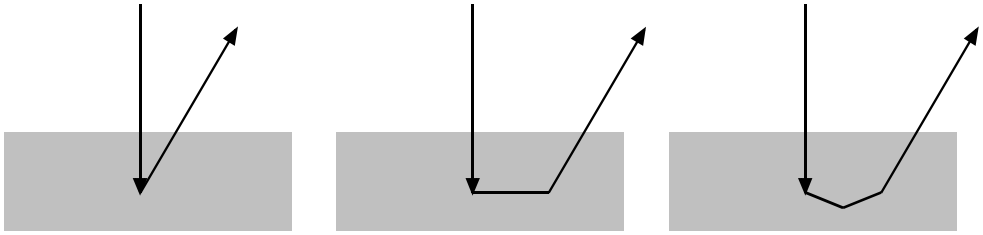

Figure 3.7.: Examples of ion trajectories with one, two and three scattering events.

Incident ion	Andersen-Ziegler (keV/amu)	Ziegler-Biersack (keV/amu)
Hydrogen (H, D, T)	1–100000	1–100000
Helium (^{3}He, ^{4}He)	0.25–2500[a]	1–100000
Heavy ions	1–100000	1–100000

Table 3.2.: Energy ranges in which the different stopping power formulas are valid.

[a] High energy electronic stopping formula for energies > 2.5 MeV/amu from [3] not implemented.

- *Isotope Spectra*: If checked, individual spectra for each isotope in the target are calculated and plotted. Default is unchecked.

  Note: The number of individual spectra is limited to 20. If the target contains many isotopes, not all will be displayed.

- *Logfile*: If checked, a file named SIMNRA.LOG is created. This file contains additional information about each step of the calculation and can be viewed with the program VIEWNRA. The log-file is written to the current directory, if a nra-file was opened or saved. Otherwise it is written to the temporary directory defined by the operating system. Default is unchecked.

Stepwidths tab

- *Stepwidth incident ions*: Stepwidth of the incident ions used in the calculation. See chapter 4 for details. *Automatic* or *Fixed* can be selected. If *Automatic* is selected, the program will choose the stepwidth automatically. This is usually the best choice for obtaining high accuracy and small computing times. *Automatic* is the program default. The automatically determined stepwidth is kept always below the resolution of the experiment. Because the resolution in larger depths degrades due to energy loss straggling the program uses a small stepwidth near the surface and a larger stepwidth in

larger depths.

Fixed stepwidth: The program uses a fixed stepwidth for the calculation. If *Fixed* is selected the default for the stepwidth is 10 keV. For incident heavy ions with energies in the range of several ten MeV this stepwidth can be increased to several 100 keV.

The stepwidth of incident ions affects the time T necessary to perform a calculation strongly. T depends on the stepwidth of the incoming ion ΔE roughly as $T \propto 1/\Delta E$: Decreasing the stepwidth by a factor of two will roughly double the computing time.

Note 1: The stepwidth of incident ions is an important parameter for the accuracy of a simulation. The accuracy may be increased, if a small *Fixed* stepwidth is used instead of *Automatic* step width control, at the cost of higher computing times.

Note 2: If the backscattering cross-section contains narrow resonances, a *Fixed* stepwidth of incident ions (with a step width smaller than the width of the resonances) gives best results. *Automatic* stepwidth control can be used together with narrow resonances in SIMNRA 5.02 and higher[3], but may result in slightly too broad structures in the spectrum.

Note 3: If a *Fixed* stepwidth of incident ions is used and the stepwidth is too high, unwanted oscillations or steps in the simulated spectra may occur. This is due to rounding errors in the routine which calculates the contents of each channel. If these oscillations occur, you have to decrease the stepwidth of incident ions. These problems should never occur with *automatic* stepwidth control: The program always uses a stepwidth which is small enough.

- *Stepwidth outgoing ions*: Stepwidth of outgoing particles used in the calculation. See chapter 4 for details. *Automatic* or *Fixed* can be selected. If *automatic* is selected, the program will choose the stepwidth automatically. This is usually the best choice for obtaining high accuracy and small computing times. *Automatic* is the program default. The automatically determined stepwidth is large at high energies, where the stopping power shows only small variations to decrease computing time. The step width is decreased near the stopping power maximum and at low energies, where the stopping power varies strongly, to increase accuracy.

  Fixed stepwidth: The program uses a fixed stepwidth for the calculation of outgoing particles. The stepwidth will remain constant at all energies and for all outgoing particles. If *Fixed* is selected the default for the stepwidth is 200 keV. For incident heavy ions with energies in the range of several ten MeV this stepwidth can be increased.

  If a small *fixed* stepwidth is used this may increase the accuracy of the calculation, but will slow down the calculation. A very small *fixed* stepwidth may be even more accurate than

[3] *Automatic* stepwidth control should not be used together with narrow resonances in the cross-section with SIMNRA 5.01 and earlier. SIMNRA 5.01 and earlier require a sufficiently small *Fixed* stepwidth, if used with narrow resonances, see section 4.3.

automatic stepwidth control. In contrast a large *fixed* stepwidth decreases the accuracy of the calculation, but will speed up the calculation. There is no easy recipe for the best choice of a *fixed* stepwidth. Usually the best compromise between speed and accuracy is *automatic* stepwidth control.

- *Cutoff Energy*: All particles are calculated until their energy has decreased below the cut-off energy. You may speed up the calculation if you increase the cut-off energy. The lowest possible value for the cut-off energy is 1 keV, the default value is 10 keV.

Pile-up tab

- *Pile-up model:* Selects the model for pile-up calculations, see subsection 4.11.2. The *Fast* model is less accurate, but is calculated fast. The *Accurate* model is closer to physical reality, but the calculation takes much longer. The computing time is about $\propto N^3$ (with N the number of channels in the spectrum) for the *Accurate* model, but only $\propto N^2$ for the *Fast* model: For 1000 channels the *Fast* model is more than 1000 times faster.

  The *Fast* model can be applied, if a pile-up rejector is used and the pulse rise time is larger than about 1 μs. The *Accurate* model should be used, if the measurement was done without a pile-up rejector, or if fast pulses are used, i.e. if the pulse rise time is smaller than 1 μs. See subsection 4.11.2 (especially Figure 4.31) for more details.

  Default is the *Fast* model.

  Note: Several parameters in the *Setup:Experiment:Live time and pile-up* form are only available, if the *Pile-up model* is set to *Accurate*, see section 3.6.2.

Roughness tab

- *Number of thickness steps*: Used for the calculation of layer roughness. A rough layer is approximated by the superposition of N spectra with different layer thicknesses, where N is the number of thickness steps. If N is small, the superposed spectrum may contain steps. Larger values of N result in smoother spectra, but slow down the calculation considerably. Default is $N = 10$.

  Note: One rough layer requires the calculation of N spectra, two rough layers of N^2 spectra, three rough layers of N^3 spectra etc.

- *Number of angular steps*: Used for the calculation of substrate roughness. A rough substrate is approximated by the superposition of M spectra with different incident and exit angles, where M is the number of angular steps. If M is small, the superposed spectrum may contain steps. Larger values of M result in smoother spectra, but slow down the calculation considerably. Default is $M = 20$.

Note: Substrate roughness requires the calculation of M spectra, one rough layers combined with substrate roughness of $N \times M$ spectra, where N is the *Number of thickness steps*, two rough layers combined with substrate roughness of $N^2 \times M$ spectra etc.

- *Dimension of substrate roughness*: Specifies if a 2-dimensional, or an almost 3-dimensional (2.5-dimensional), model of substrate roughness is used. See subsection 4.10.2 for details. The 2.5-dimensional model is more realistic and the program default.

The *File*-menu allows to save setups for calculations to disk and read setups from disk. All information contained in the *Setup Calculation* form is saved. The NRA data file format is used for saving.

- *Save as Default*: The current setup for calculation is stored as startup default for SIMNRA in the file *DEFAULT\CALC.NRA*.
- *Save Setup as*: Save the current setup to file.
- *Read Setup*: Reads a setup from file.
  Note: You can read any NRA-file with *Read Setup*. Only the calculation information will be read, any other information (such as target composition, experimental spectra etc.), which may be present in the NRA file, will be ignored.

3.7. *Target* menu

3.7.1. *Target: Target...*

In this menu the target is created. A target consists of *layers*. Each layer consists of different elements and has some thickness. The composition of a layer does not change throughout his thickness. To simulate a concentration profile you have to use multiple layers.

The layer number 1 is at the surface of the target, the layer number 2 is below layer 1 and so on, see Figure 3.8.

- *Thickness*: Thickness of the layer (in 10^{15} atoms/cm^2). The conversion factor from μg/cm^2 or μm to atoms/cm^2 can be determined with *Calculate: Density...* for pure elements.

- *Number of Elements*: Number of different elements in this layer. The maximum number of different elements in a layer is 20.

- *Element*: Name of the element, for example Si, W, Au. Lowercase and uppercase letters in elements names are treated similar, you can enter silicon as Si, si, SI or sI. XX means that this element is unknown. The special symbols D for deuterium, T for tritium and A for ^{4}He can be used.

- *Concentration or areal density*: Atomic concentration or areal density of the element in the actual layer. The concentration c must be $0.0 \leq c \leq 1.0$. The sum of the concentrations of all elements in one layer must be equal to 1 ($0.999 \leq \sum c_i \leq 1.001$). If the sum of concentrations is not equal to 1, the word concentration is written in red colour, if the sum of concentrations is equal to 1, the word concentration is written in black colour. You can use the small buttons to set the concentration of the element i to 1 minus the sum of concentrations of all other elements, $c_i = 1 - \sum_{i \neq j} c_j$. The areal density is in 10^{15} atoms/cm^2. Whether concentration or areal density of an element is used, is determined by the *Concentration/Areal density* radio button, see below.

- *Isotopes*: These buttons can be used to change the concentrations of isotopes of that element in the actual layer. You will need this only if this element does not have the natural composition of isotopes. You can create for example a layer of enriched ^{13}C on top of ^{12}C, or the like. The sum of concentrations of all isotopes of one element must be equal to 1.

  Note: The *Isotopes* check-box in the *Setup: Calculation...* menu must be checked to manipulate individual isotopes.

- *Concentration/Areal density*: This radio button allows to select if amounts of individual elements are entered as atomic concentration or as areal density. If *Concentration* is

selected, the total layer thickness and the concentrations of all elements are entered. If *Areal density* is selected, the areal density of each element is entered - the total layer thickness is calculated as the sum of all elemental areal densities.

- *Correction factor(s) for stopping power*: SIMNRA uses Bragg's rule to calculate the stopping power of a layer, see subsection 4.6.5 for more details. However, it has been shown experimentally that for several compounds like hydrocarbons or oxides deviations from Bragg's rule occur. To account for deviations from Braggg's rule a correction factor f can be used, and the program will use the stopping power $S(E)$ as function of energy E

$$S(E) = f\, S_{\mathrm{Bragg}}(E) \tag{3.3}$$

  $S_{\mathrm{Bragg}}(E)$ is the stopping power according to Bragg's rule. Note that the factor f is energy independent. An individual factor f for each ion species and each layer may be defined. If no factor f is given the program uses $f = 1$, i.e. uses Bragg's rule.

- *Layer and substrate roughness*: Click the button if the current layer or the substrate is rough. See subsection 3.7.2 for details.

Manipulation of layers

To manipulate layers use the buttons in the *Layer manipulation* box. Additionally layers can be copied to and pasted from the clipboard and layers can be saved to and read from file.

- *Add*: Adds a layer. The added layer will be the last layer. The maximum number of different layers is 100.
- *Ins*: Inserts a layer in front of the current layer. The maximum number of different layers is 100.
- *Del*: Deletes the current layer.
- *Prev*: Go to the previous layer.
- *Next*: Go to the next layer.

Menu bar

- *File: Read Layer...*: Read a layer from file. **Attention:** If a layer is read from file, the current layer is overwritten.
- *File: Save Layer...*: Save the current layer description to file.
- *File: Read Target...*: Read a whole target from file. **Attention:** If a target is read from file, the current target is overwritten.

- *File: Save Target...*: Save the current target to file.
- *File: Write Depth Profile...*: Save the depth profile of all elements in the target to file. The file format is shown in Figure 3.9.
- *Edit: Copy Layer* (or pressing Ctrl C): Copies the current layer to the clipboard.
- *Edit: Paste Layer* (or pressing Ctrl V): Pastes a layer from the clipboard. **Attention:** If a layer is pasted from the clipboard, the current layer is overwritten.
- *Edit: Copy Depth Profile*: Copies the depth profile of all elements in the target to the clipboard. The format is identical to a depth profile file, see Figure 3.9. The depth profile can be pasted into an Origin or Excel worksheet.
- *Show: Target summary* displays the total amounts (in atoms/cm^2) of all elements in the target. This is mainly useful if the target consists of plural layers composed of the same elements in different concentrations. The total amount of each element is the sum of this element in all layers.

3.7.2. Layer and substrate roughness

In this menu the roughnesses of the current layer and of the substrate are defined.

- *Has thickness distribution*: Check, if the current layer is rough, i.e. if the layer thickness is not uniform, but varies from point to point. A rough layer is described by a distribution of layer thicknesses. The distribution is divided into N steps. The step number N can be adjusted by the *Number of thickness steps* in the *Setup: Calculation...* menu, see subsection 3.6.3.
- *FWHM of thickness distribution*: SIMNRA assumes a Gamma distribution of layer thicknesses, see section 4.10 for details, with the layer thickness as mean value. The width and shape of the distribution is determined by the full width at half maximum (FWHM), with

$$\mathrm{FWHM} = 2.35482\,\sigma \tag{3.4}$$

  where σ is the standard deviation [4]. FWHM in 10^{15} atoms/cm^2.

[4] Strictly speaking, the Gamma distribution has only a standard deviation σ, while the full width at half maximum (FWHM) is undefined. However, the Gamma distribution resembles a Gaussian distribution in many cases, which justifies the use of the FWHM. Internally, SIMNRA uses only the standard deviation σ, which is derived from the FWHM through Equation 3.4.

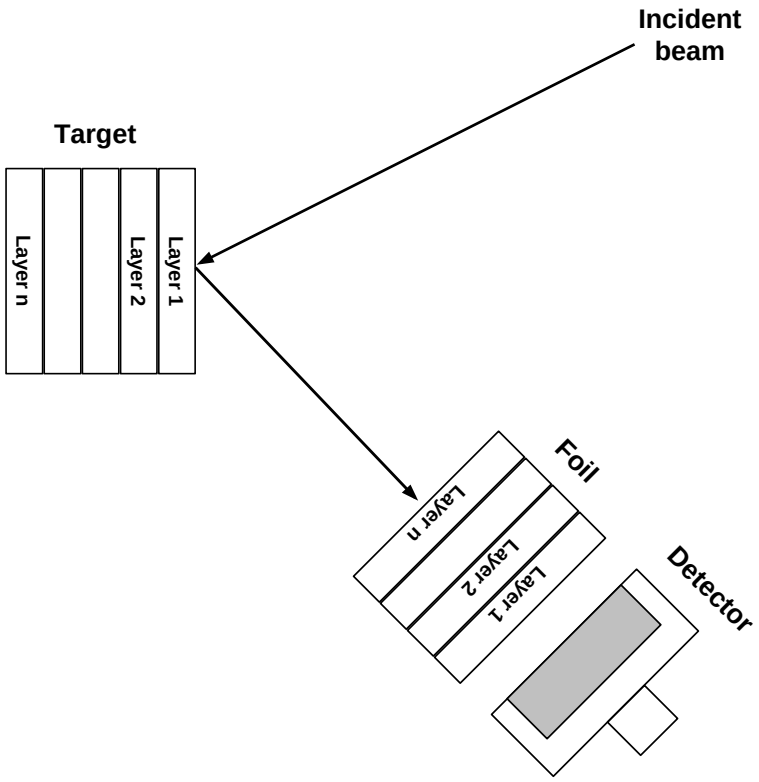

Figure 3.8.: Layer structure of target and foil. For the target, layer 1 is at the surface, the layer with the highest number is the deepest layer. Backscattered particles first penetrate the foil layer with the highest number, the foil layer 1 is in front of the detector.

```
Depth   H     C
0       0.0   0.0
0       0.2   0.8
100     0.2   0.8
100     0.4   0.6
200     0.4   0.6
200     0.3   0.7
300     0.3   0.7
300     0.1   0.9
400     0.1   0.9
```

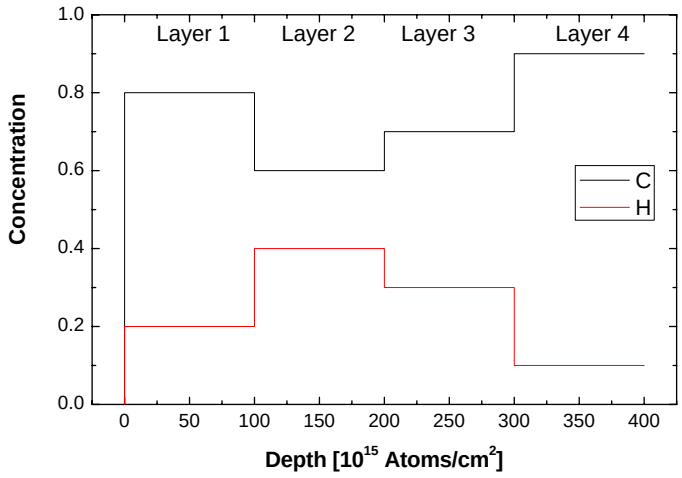

Figure 3.9.: Left: Example for a depth profile file. The target consists of 4 layers. The first line contains the names of the elements (H and C). The depth scale is in 10^{15} atoms/cm^2, the other columns contain the concentrations of the individual elements in the layers. The columns are separated by `tabs`. Right: Graphical representation of the depth profile.

- *Has substrate roughness*: Check if the layers are on top of a rough substrate. A rough substrate is described by a distribution of incident and exit angles and has no other influence. Only one substrate can exist for all layers, i.e. the substrate parameters are identical for all layers. Substrate roughness is not available for foils. The distribution of incident and exit angles is divided into M steps. The step number M can be adjusted by the *Number of angular steps* in the *Setup: Calculation...* menu, see subsection 3.6.3.

- *FWHM of substrate roughness*: SIMNRA assumes a Lorentz distribution of angles. Enter the full width at half maximum (FWHM) of the angle distribution, in deg.

3.7.3. *Target: Foil...*

In this menu a foil in front of the detector can be created. Like the target a foil can consist of multiple layers with different compositions. See the previous section for details. If the foil consists of multiple layers, then backscattered particles first will penetrate layer n, then layer $n-1$ etc., layer 1 is directly in front of the detector (see Figure 3.8).

The default is no foil in front of the detector.

Some common materials used as stopper foils are already stored in the *\LAYERS* directory. The materials and files are listed in Table 3.3. These files can be imported in the *Target* menu with *File: Read layer*.

Filename	Material	Common name
INCON600.LAY	Inconel 600	
INCON625.LAY	Inconel 625	
SS14301.LAY	Stainless steel 1.4301, AISI 304 (US)	
SS14541.LAY	Stainless steel 1.4541	V2A
SS14571.LAY	Stainless steel 1.4571	V4A
SS316.LAY	Stainless steel 316 (US)	
MYLAR.LAY	Polyethylenterephthalat	Mylar, Hostaphan

Table 3.3.: Predefined materials for stopper foils stored in the \LAYERS directory.

3.8. *Reactions* menu

In the *Reactions* menu the cross-sections used for calculation of the simulated spectrum are chosen. Rutherford cross-sections for backscattering of projectiles and creation of recoils are available for all ion-target combinations, if kinematically possible. For heavy projectiles backscattered from light target nuclei two different solutions may be kinematically possible, see Equation 4.4. The solution with the minus sign appears as *Rutherford cross-section (low energy solution)* in the *Reactions* menu.

The buttons *[Rutherford]* and *[No Rutherford]* allow a quick selection of Rutherford/Non-Rutherford cross sections for all isotopes of an element. The button *[Rutherford]* selects Rutherford cross sections for all isotopes and deselects all Non-Rutherford and nuclear reactions cross sections. The button *[No Rutherford]* deselects all Rutherford cross sections.

SIMNRA can handle non-Rutherford cross-sections for backscattering and recoil production and can use nuclear reactions cross-sections. SIMNRA is able to read two different file formats with cross-section data:

1. The R33 file format. Cross-sections for nuclear reactions and non-Rutherford scattering are stored in the R33 file format, originally proposed by I.C. Vickridge. Many files with this extension have been taken from SigmaBase, but several were added by the author. Many of these files, especially the ones containing nuclear reactions cross sections, were digitised from the original publications by G. Vizkelethy from Idaho State University. No guarantee is provided for agreement with the original publication. The references of the original publications are found in the file headers. See subsection 3.16.1 and Appendix B for more details about this file format.

2. The RTR (Ratio To Rutherford) file format. These files contain non-Rutherford cross-sections for backscattering of protons and α-particles. The files contain the ratio of measured to Rutherford cross-sections. The majority of the data has been digitised from the original publications by R.P. Cox, J.A. Leavitt and L.C. McIntyre, Jr. from Arizona University. These cross-section data have been published in [9]. All files with this extension have been taken from SigmaBase. The references of the original publications are found in [9].

SIMNRA distinguishes between three different types of scattering events for each isotope:

1. Backscattering of projectiles

2. Creation of recoils

3. Nuclear reactions.

The chosen cross-sections for each type of scattering event must be unambiguous: You can choose, for example, Rutherford cross-section for backscattering in the energy range from

0.000–0.999 MeV, some non-Rutherford cross-section for backscattering in the energy range from 1.000-1.999 MeV and a different cross-section for backscattering in the energy range from 2.000–3.000 MeV. You cannot choose, however, Rutherford cross-section for backscattering in the range 0.000–2.000 MeV and another cross-section for backscattering in the energy range from 1.000–2.000 MeV: In this case the program does not know which cross-section it should use in the range from 1.000–2.000 MeV, and you will get the error message 'Energy overlap in cross-sections'.

All available cross-section data are listed in Table 3.4, Table 3.5 and Table 3.6. If you want to add new cross-section data files, see section 3.16.

Note 1: Some files contain total cross-section data $\sigma(E)$. In these cases the differentiell cross-section $d\sigma/d\Omega$ is obtained by SIMNRA for all kinematically allowed angles by assuming angular independence of the cross-section in the center of mass system:

$$\left(\frac{d\sigma}{d\Omega}\right)_{CM}(E,\theta) = \frac{1}{4\pi}\sigma(E) \tag{3.5}$$

This cross-section is then transformed from the center of mass to the laboratory system. The assumption of angular independence in the center of mass system is well fulfilled for the ^{3}He(D,p)α-reaction for incident energies below about 1.2 MeV and for the D(^{3}He,p)α-reaction for incident energies below about 1.8 MeV.

Note 2: Use the data files that came with SIMNRA. Some of the original data files at SigmaBase contain small format errors, such as additional blank lines, which confuse the program.

Note 3: Non-Rutherford cross-sections and nuclear reactions are only available if *Isotopes* in the *Setup:Calculation...* menu is checked.

Table 3.4.: Non-Rutherford backscattering cross-sections.

	θ (Lab)	Energy (keV)	File	Reference
D(p,p)D	151	1800–3000	PH_LA76A.RTR	Langley 1976
D(p,p)D	165	2000–2800	HD165_LANGLEY.R33	Langley 1976
T(p,p)T	163.2	2500–3500	PH_LA76B.RTR	Langley 1976
^{3}He(p,p)^{3}He	159.2	2000–3000	PHELA76A.RTR	Langley 1976
^{4}He(p,p)^{4}He	161.4	1500–3700	PHELA76B.RTR	Langley 1976
^{6}Li(p,p)^{6}Li	164	1200–3100	PLIBA51A.RTR	Bashkin 1951
^{7}Li(p,p)^{7}Li	156.7	373–1398	PLIWA53A.RTR	Warters 1953
^{7}Li(p,p)^{7}Li	164	1700–3500	PLIBA51B.RTR	Bashkin 1951
^{7}Li(p,p)^{7}Li	165	1300–2800	PLIMA56A.RTR	Malmberg 1956
^{9}Be(p,p)^{9}Be	142.4	1600–3000	PBEMO56A.RTR	Mozer 1956
^{9}Be(p,p)^{9}Be	158.7	200–1700	PBEMO56B.RTR	Mozer 1956
^{9}Be(p,p)^{9}Be	170.5	2400–2700	PBELE94A.RTR	Leavitt 1994
^{10}B(p,p)^{10}B	100	800–3300	H10B100_CHIARI.R33	Chiari 2001
^{10}B(p,p)^{10}B	105	800–3300	H10B105_CHIARI.R33	Chiari 2001
^{10}B(p,p)^{10}B	110	725–3300	H10B110_CHIARI.R33	Chiari 2001
^{10}B(p,p)^{10}B	115	625–3300	H10B115_CHIARI.R33	Chiari 2001
^{10}B(p,p)^{10}B	120	650–3300	H10B120_CHIARI.R33	Chiari 2001
^{10}B(p,p)^{10}B	125	600–3300	H10B125_CHIARI.R33	Chiari 2001
^{10}B(p,p)^{10}B	130	500–3300	H10B130_CHIARI.R33	Chiari 2001
^{10}B(p,p)^{10}B	135	500–3300	H10B135_CHIARI.R33	Chiari 2001
^{10}B(p,p)^{10}B	140	500–3300	H10B140_CHIARI.R33	Chiari 2001
^{10}B(p,p)^{10}B	145	500–3300	H10B145_CHIARI.R33	Chiari 2001
^{10}B(p,p)^{10}B	150	500–3300	H10B150_CHIARI.R33	Chiari 2001
^{10}B(p,p)^{10}B	154	1000–3000	PB_OV62A.RTR	Overley 1962
^{10}B(p,p)^{10}B	155	500–3300	H10B155_CHIARI.R33	Chiari 2001
^{10}B(p,p)^{10}B	160	500–3300	H10B160_CHIARI.R33	Chiari 2001
^{10}B(p,p)^{10}B	165	500–3300	H10B165_CHIARI.R33	Chiari 2001
^{10}B(p,p)^{10}B	170	500–3300	H10B170_CHIARI.R33	Chiari 2001
^{11}B(p,p)^{11}B	100	800–3300	H11B100_CHIARI.R33	Chiari 2001
^{11}B(p,p)^{11}B	105	825–3300	H11B105_CHIARI.R33	Chiari 2001
^{11}B(p,p)^{11}B	110	725–3300	H11B110_CHIARI.R33	Chiari 2001
^{11}B(p,p)^{11}B	115	625–3300	H11B115_CHIARI.R33	Chiari 2001
^{11}B(p,p)^{11}B	120	650–3300	H11B120_CHIARI.R33	Chiari 2001
^{11}B(p,p)^{11}B	125	600–3300	H11B125_CHIARI.R33	Chiari 2001
^{11}B(p,p)^{11}B	130	500–3300	H11B130_CHIARI.R33	Chiari 2001
^{11}B(p,p)^{11}B	135	500–3300	H11B135_CHIARI.R33	Chiari 2001
^{11}B(p,p)^{11}B	140	500–3300	H11B140_CHIARI.R33	Chiari 2001
^{11}B(p,p)^{11}B	145	500–3300	H11B145_CHIARI.R33	Chiari 2001
^{11}B(p,p)^{11}B	150	500–3300	H11B150_CHIARI.R33	Chiari 2001
^{11}B(p,p)^{11}B	150	500–2000	PB_TA56A.RTR	Trautfest 1956
^{11}B(p,p)^{11}B	155	500–3300	H11B155_CHIARI.R33	Chiari 2001
^{11}B(p,p)^{11}B	155	2200–3300	11BPPB_1.R33	Symons 1963

	θ (Lab)	Energy (keV)	File	Reference
^{11}B(p,p)^{11}B	160	500–3300	H11B160_CHIARI.R33	Chiari 2001
^{11}B(p,p)^{11}B	161.4	1100–3800	11BPPB.R33	Segel 1965
^{11}B(p,p)^{11}B	165	500–3300	H11B165_CHIARI.R33	Chiari 2001
^{11}B(p,p)^{11}B	165	1700–2700	11BPPB_2	Mayer 1998
^{11}B(p,p)^{11}B	170	500–3300	H11B170_CHIARI.R33	Chiari 2001
C(p,p)C	100	340–3000	HC100_MAZZONI.R33	Mazzoni 1998
C(p,p)C	105	340–3000	HC105_MAZZONI.R33	Mazzoni 1998
C(p,p)C	110	340–3000	HC110_MAZZONI.R33	Mazzoni 1998
C(p,p)C	115	340–3000	HC115_MAZZONI.R33	Mazzoni 1998
C(p,p)C	120	340–3000	HC120_MAZZONI.R33	Mazzoni 1998
C(p,p)C	125	340–3000	HC125_MAZZONI.R33	Mazzoni 1998
C(p,p)C	130	340–3000	HC130_MAZZONI.R33	Mazzoni 1998
C(p,p)C	135	340–3000	HC135_MAZZONI.R33	Mazzoni 1998
C(p,p)C	140	340–3000	HC140_MAZZONI.R33	Mazzoni 1998
C(p,p)C	145	340–3000	HC145_MAZZONI.R33	Mazzoni 1998
C(p,p)C	150	340–3000	HC150_MAZZONI.R33	Mazzoni 1998
C(p,p)C	150	1000–3500	12CPPC_1.R33	Amirikas 1993
C(p,p)C	155	340–3000	HC155_MAZZONI.R33	Mazzoni 1998
C(p,p)C	160	340–3000	HC160_MAZZONI.R33	Mazzoni 1998
C(p,p)C	165	340–3000	HC165_MAZZONI.R33	Mazzoni 1998
C(p,p)C	165	100–3500	HC165_GURBICH.R33	Gurbich 1998
C(p,p)C	165	1000–3500	12CPPC.R33	Amirikas 1993
C(p,p)C	170	340–3000	HC170_MAZZONI.R33	Mazzoni 1998
C(p,p)C	170	300–700	PC_LI93A.RTR	Liu 1993
C(p,p)C	170	700–2800	PC_LI93B.RTR	Liu 1993
C(p,p)C	170	300–3000	PC_LI93C.RTR	Liu 1993
C(p,p)C	170	700–2500	PC_RA85A.RTR	Rauhala 1985
C(p,p)C	170	996–3498	PC_AM93A.RTR	Amirikas 1993
C(p,p)C	170	1000–3500	12CPPC_2.R33	Amirikas 1993
^{12}C(p,p)^{12}C	179.2	4000–6600	12CPP179.R33	Tosaki 2000
^{12}C(p,p)^{12}C	168.2	400–4500	PC_JA53A.RTR	Jackson 1953
^{14}N(p,p)^{14}N	140	500–2500	HN140_RAMOS.R33	Ramos 2002
^{14}N(p,p)^{14}N	150	800–1900	PN_TA56A.RTR	Tautfest 1956
^{14}N(p,p)^{14}N	152	1035–1075	PN_HA57A.RTR	Hagedorn 1957
^{14}N(p,p)^{14}N	152	1450–1625	PN_HA57B.RTR	Hagedorn 1957
^{14}N(p,p)^{14}N	152	650–1800	PN_HA57E.RTR	Hagedorn 1957
^{14}N(p,p)^{14}N	155.2	1850–3000	PN_LA67A.RTR	Lambert 1967
^{14}N(p,p)^{14}N	158.7	1735–1760	PN_HA57C.RTR	Hagedorn 1957
^{14}N(p,p)^{14}N	158.7	1785–1815	PN_HA57D.RTR	Hagedorn 1957
^{14}N(p,p)^{14}N	159.5	600–4000	PN_BA59A.RTR	Bashkin 1959
^{14}N(p,p)^{14}N	165	1850–3000	PN_LA67B.RTR	Lambert 1967
^{14}N(p,p)^{14}N	167.2	3600–4100	PN_OL58A.RTR	Olness 1958
^{14}N(p,p)^{14}N	170	1450–2300	PN_RA85A.RTR	Rauhala 1985
^{14}N(p,p)^{14}N	170	2700–3100	HN170_GUOHUA.R33	Guohua 1991

	θ (Lab)	Energy (keV)	File	Reference
^{14}N(p,p)^{14}N	178	500–2500	HN178_RAMOS.R33	Ramos 2002
^{16}O(p,p)^{16}O	149.5	2450–2850	PO_GO65A.RTR	Gomes 1965
^{16}O(p,p)^{16}O	165	100–4080	HO165_GURBICH.R33	Gurbich 1997
^{16}O(p,p)^{16}O	170	1000–3580	PO_AM93A.RTR	Amirikas 1993
^{16}O(p,p)^{16}O	170	700–4000	16OPPO.R33	Gurbich 1997
^{16}O(p,p)^{16}O	178	750–2500	HO178_RAMOS.R33	Ramos 2002
^{19}F(p,p)^{19}F	150	2000–5000	PF_BO93A.RTR	Bogdanovic 1993
^{19}F(p,p)^{19}F	160	500–1300	PF_DE56A.RTR	Dearnaly 1956
^{19}F(p,p)^{19}F	160	1300–2064	PF_DE56B.RTR	Dearnaly 1956
^{19}F(p,p)^{19}F	160	500–1300	PF_DE56C.RTR	Dearnaly 1956
^{19}F(p,p)^{19}F	160	1300–1550	PF_DE56D.RTR	Dearnaly 1956
^{19}F(p,p)^{19}F	165	850–1010	PF_KN89A.RTR	Knox 1989
^{19}F(p,p)^{19}F	165	1000–1875	PF_KN89B.RTR	Knox 1989
^{19}F(p,p)^{19}F	165	1350–1550	PF_KN89C.RTR	Knox 1989
^{19}F(p,p)^{19}F	158.7	600–1800	PF_WE55A.RTR	Webb 1955
^{19}F(p,p)^{19}F	158.7	1300–1500	PF_WE55B.RTR	Webb 1955
^{20}Ne(p,p)^{20}Ne	166 (CM)	1500–2800	PNELA71A.RTR	Lambert 1971
^{23}Na(p,p)^{23}Na	156.5	550–1450	PNABA56A.RTR	Bauman 1956
^{24}Mg(p,p)^{24}Mg	164	400–4000	PMGMO51A.RTR	Mooring 1951
^{24}Mg(p,p)^{24}Mg	164	792–856	PMGMO51E.RTR	Mooring 1951
^{24}Mg(p,p)^{24}Mg	164	1466–1501	PMGMO51F.RTR	Mooring 1951
^{24}Mg(p,p)^{24}Mg	164	1642–1671	PMGMO51G.RTR	Mooring 1951
^{24}Mg(p,p)^{24}Mg	164	1991–2026	PMGMO51H.RTR	Mooring 1951
^{24}Mg(p,p)^{24}Mg	164	2393–2431	PMGMO51I.RTR	Mooring 1951
^{24}Mg(p,p)^{24}Mg	170	700–2540	PMGRA88A.RTR	Rauhala 1988
^{27}Al(p,p)^{27}Al	140	500–2500	HAL140_RAMOS.R33	Ramos 2002
^{27}Al(p,p)^{27}Al	140	800–3000	HAL140_CHIARI.R33	Chiari 2001
^{27}Al(p,p)^{27}Al	150	800–3000	HAL150_CHIARI.R33	Chiari 2001
^{27}Al(p,p)^{27}Al	160	800–3000	HAL160_CHIARI.R33	Chiari 2001
^{27}Al(p,p)^{27}Al	165	800–3000	HAL165_CHIARI.R33	Chiari 2001
^{27}Al(p,p)^{27}Al	170	800–3000	HAL170_CHIARI.R33	Chiari 2001
^{27}Al(p,p)^{27}Al	170	1000–2450	PALRA89A.RTR	Rauhala 1989
^{27}Al(p,p)^{27}Al	178	500–2500	HAL178_RAMOS.R33	Ramos 2002
Si(p,p)Si	160	1500–2100	HSI160_SALOMONOVIC.R33	Salomonovic 1993
Si(p,p)Si	165	1000–3000	HSI165_GURBICH.R33	Gurbich 1998
^{28}Si(p,p)^{28}Si	167.2	1300–4000	PSIVO59A.RTR	Vorona 1959
Si(p,p)Si	170	1500–2000	HSI170_SALOMONOVIC.R33	Salomonovic 1993
Si(p,p)Si	170	1000–3500	SIPPSI.R33	Amirikas 1993
Si(p,p)Si	170	1000–3580	PSIAM93A.RTR	Amirikas 1993
Si(p,p)Si	170	1470–2200	PSIRA85A.RTR	Rauhala 1985
^{31}P(p,p)^{31}P	165	1000–2000	PP_CO63A.RTR	Cohen-Ganouna 1963
^{32}S(p,p)^{32}S	167.4	1300–4000	PS_OL58A.RTR	Olness 1958
S(p,p)S	170	1500–2690	PS_RA88A.RTR	Rauhala 1988
Cl(p,p)Cl	150	2000–5000	PCLBO93A.RTR	Bogdanovic 1993

	θ (Lab)	Energy (keV)	File	Reference
^{40}Ar(p,p)^{40}Ar	159.5	1800–3600	PARBK61A.RTR	Barnhard 1961
^{40}Ar(p,p)^{40}Ar	166 (CM)	1000–2000	PARCO63A.RTR	Cohen-Ganouna 1963
^{40}Ar(p,p)^{40}Ar	166 (CM)	1825–1950	PARCO63B.RTR	Cohen-Ganouna 1963
^{40}Ar(p,p)^{40}Ar	155	1750–2750	PARFR58A.RTR	Frier 1958
^{40}Ca(p,p)^{40}Ca	160	1800–3000	PCAWI74A.RTR	Wilson 1974
^{48}Ti(p,p)^{48}Ti	160	1800–2150	PTIPR72A.RTR	Prochnow 1972
^{48}Ti(p,p)^{48}Ti	160	2150–2500	PTIPR72B.RTR	Prochnow 1972
^{48}Ti(p,p)^{48}Ti	160	2500–2800	PTIPR72C.RTR	Prochnow 1972
^{48}Ti(p,p)^{48}Ti	160	2900–3040	PTIPR72D.RTR	Prochnow 1972
^{48}Ti(p,p)^{48}Ti	170	1000–2600	PTIRA89A.RTR	Rauhala 1989
^{12}C(^{3}He,^{3}He)^{12}C	159.4	1800–5400	12CTTC.R33	Kuan 1964
^{6}Li(α,α)^{6}Li	112	2500–4500	ALIBO72A.RTR	Bohlen 1972
^{7}Li(α,α)^{7}Li	121	2500–4500	ALIBO72B.RTR	Bohlen 1972
^{9}Be(α,α)^{9}Be	136	6000–20000	ABETA65A.RTR	Taylor 1965
^{9}Be(α,α)^{9}Be	157.5	1500–6000	ABEGO73A.RTR	Goss 1973
^{9}Be(α,α)^{9}Be	170.5	575–4200	ABELE94A.RTR	Leavitt 1994
^{10}B(α,α)^{10}B	170.5	975–3275	AB_MC92A.RTR	McIntyre 1992
^{11}B(α,α)^{11}B	150.8	2000–4000	AB_RA72A.RTR	Ramirez 1972
^{11}B(α,α)^{11}B	160.5	4000–8000	AB_OT72A.RTR	Ott 1972
^{11}B(α,α)^{11}B	170.5	980–3300	AB_MC92B.RTR	McIntyre 1992
C(α,α)C	149	4000–12000	AC_MS72A.RTR	Marvin 1972
C(α,α)C	165	1810–9050	AC_FE94A.RTR	Feng 1994
C(α,α)C	167	4000–7500	AC_BI54A.RTR	Bittner 1954
C(α,α)C	170	5000–9000	AC_CH94A.RTR	Cheng 1994
C(α,α)C	170.5	1560–5000	AC_LE89A.RTR	Leavitt 1989
^{12}C(α,α)^{12}C	30	2000–4800	12CAA12C30.R33	Bogdanović Radović 2002
^{12}C(α,α)^{12}C	45	2000–4800	12CAA12C45.R33	Bogdanović Radović 2002
^{12}C(α,α)^{12}C	60	2100–4800	12CAA12C60.R33	Bogdanović Radović 2002
^{12}C(α,α)^{12}C	135	2100–4800	12CAA12C135.R33	Bogdanović Radović 2002
^{12}C(α,α)^{12}C	150	2100–4800	12CAA12C150.R33	Bogdanović Radović 2002
^{13}C(α,α)^{13}C	165	2000–3500	AC_BA65A.RTR	Barnes 1965
^{13}C(α,α)^{13}C	165	3300–6500	AC_KE68A.RTR	Kerr 1968
^{14}N(α,α)^{14}N	163.7	2600–4700	AN_KA58A.RTR	Kashy 1958
^{14}N(α,α)^{14}N	165	2000–6200	AN_FE94A.RTR	Feng 1994
^{14}N(α,α)^{14}N	167	4550–6550	AN_FO93A.RTR	Foster 1993
^{14}N(α,α)^{14}N	167	7090–9070	AN_FO93B.RTR	Foster 1993
^{14}N(α,α)^{14}N	167	8650–9000	AN_FO93C.RTR	Foster 1993
^{14}N(α,α)^{14}N	167.2	2000–4000	AN_HE58A.RTR	Herring 1958
^{15}N(α,α)^{15}N	165.2	1600–2600	AN_SM61A.RTR	Smothich 1961
^{15}N(α,α)^{15}N	165.2	2400–3800	AN_SM61B.RTR	Smothich 1961
^{15}N(α,α)^{15}N	165.2	3800–4800	AN_SM61C.RTR	Smothich 1961
^{15}N(α,α)^{15}N	165.2	4700–5600	AN_SM61D.RTR	Smothich 1961

	θ (Lab)	Energy (keV)	File	Reference
^{15}N(α,α)^{15}N	165.2	1600–5600	AN_SM61E.RTR	Smothich 1961
^{15}N(α,α)^{15}N	165.2	1600–5600	AN_SM61F.RTR	Smothich 1961
^{15}N(α,α)^{15}N	165.2	3800–4800	AN_MO72A.RTR	Mo 1972
^{16}O(α,α)^{16}O	158.6	6000–10500	AO_HU67A.RTR	Hunt 1967
^{16}O(α,α)^{16}O	165	2050–9000	AO_FE94A.RTR	Feng 1994
^{16}O(α,α)^{16}O	165	9200–9900	AO_CA85A.RTR	Caskey 1985
^{16}O(α,α)^{16}O	165	9600–10500	AO_CA85B.RTR	Caskey 1985
^{16}O(α,α)^{16}O	165	10320–10700	AO_CA85C.RTR	Caskey 1985
^{16}O(α,α)^{16}O	165	10650–11100	AO_CA85D.RTR	Caskey 1985
^{16}O(α,α)^{16}O	165	11050–11600	AO_CA85E.RTR	Caskey 1985
^{16}O(α,α)^{16}O	165	11500–12500	AO_CA85F.RTR	Caskey 1985
^{16}O(α,α)^{16}O	165	12150–12750	AO_CA85G.RTR	Caskey 1985
^{16}O(α,α)^{16}O	165	12500–13500	AO_CA85H.RTR	Caskey 1985
^{16}O(α,α)^{16}O	165	9150–12750	AO_CA85I.RTR	Caskey 1985
^{16}O(α,α)^{16}O	165.7	5000–12500	AO_JO69A.RTR	John 1969
^{16}O(α,α)^{16}O	170	2000–9000	AO_CH93A.RTR	Cheng 1993
^{16}O(α,α)^{16}O	170	1770–5000	AO_LE90A.RTR	Leavitt 1990
^{18}O(α,α)^{18}O	160	2400–3500	AO_PO64A.RTR	Powers 1964
F(α,α)F	165	1500–5000	AF_CH93A.RTR	Cheng 1993
^{19}F(α,α)^{19}F	170	1500–2300	AF_CS84A.RTR	Cseh 1984
^{19}F(α,α)^{19}F	170	2300–3700	AF_CS84B.RTR	Cseh 1984
^{19}F(α,α)^{19}F	170	1500–4000	AF_CS84C.RTR	Cseh 1984
Ne(α,α)Ne	167.3	2400–3200	ANEGO54A.RTR	Goldberg 1954
Ne(α,α)Ne	167.3	3200–4000	ANEGO54B.RTR	Goldberg 1954
Ne(α,α)Ne	167.3	2400–4000	ANEGO54C.RTR	Goldberg 1954
Na(α,α)Na	165	2000–6000	ANACH91A.RTR	Cheng 1991
Mg(α,α)Mg	165	2000–9000	AMGCH93A.RTR	Cheng 1993
^{24}Mg(α,α)^{24}Mg	162.5	3150–3900	AMGCS82A.RTR	Cseh 1982
^{24}Mg(α,α)^{24}Mg	162.5	4200–4900	AMGCS82B.RTR	Cseh 1982
^{24}Mg(α,α)^{24}Mg	164	3150–3900	AMGKA52A.RTR	Kaufmann 1952
^{24}Mg(α,α)^{24}Mg	165	5900–6250	AMGIK79A.RTR	Ikossi 1979
^{24}Mg(α,α)^{24}Mg	165	6080–6140	AMGIK79B.RTR	Ikossi 1979
Si(α,α)Si	170	2000–6000	ASICH93A.RTR	Cheng 1993
Si(α,α)Si	170	6000–9000	ASICH93B.RTR	Cheng 1993
^{28}Si(α,α)^{28}Si	165	2400–4000	ASILE72A.RTR	Leung 1972
^{28}Si(α,α)^{28}Si	165	4000–5000	ASILE72B.RTR	Leung 1972
^{28}Si(α,α)^{28}Si	165	5100–6000	ASILE72C.RTR	Leung 1972
^{28}Si(α,α)^{28}Si	165	2400–5000	ASILE72D.RTR	Leung 1972
^{27}Al(α,α)^{27}Al	170	2000–9000	AALCH93A.RTR	Cheng 1993
Cl(α,α)Cl	165	2000–9000	ACLCH93A.RTR	Cheng 1993
Ar(α,α)Ar	170	1800–5200	AARLE86A.RTR	Leavitt 1986
^{39}K(α,α)^{39}K	175.5	6000–8000	AK_FR82A.RTR	Frekers 1982
Ca(α,α)Ca	166	2200–8800	ACAHU90A.RTR	Hubbard 1990
^{40}Ca(α,α)^{40}Ca	145	5000–9000	ACASE87A.RTR	Sellschop 1987

	θ (Lab)	Energy (keV)	File	Reference
C(^{6}Li,^{6}Li)C	165	1800–4700	C6LiLiC.R33	Mayer 2001
^{19}F(^{6}Li,^{6}Li)^{19}F	150	2500–7000	19F6LiLiF.R33	Pastuović 1998
^{27}Al(^{6}Li,^{6}Li)^{27}Al	140	4000–8000	Nurmela-6Li-Al_140.R33	Nurmela 1999
^{27}Al(^{6}Li,^{6}Li)^{27}Al	170	4000–8000	Nurmela-6Li-Al_170.R33	Nurmela 1999
Si(^{6}Li,^{6}Li)Si	140	4500–7750	Nurmela-6Li-Si_140.R33	Nurmela 1999
Si(^{6}Li,^{6}Li)Si	170	4500–7750	Nurmela-6Li-Si_170.R33	Nurmela 1999
Ti(^{6}Li,^{6}Li)Ti	140	5000–11000	Nurmela-6Li-Ti_140.R33	Nurmela 1999
Ti(^{6}Li,^{6}Li)Ti	170	5000–11000	Nurmela-6Li-Ti_170.R33	Nurmela 1999
C(^{7}Li,^{7}Li)C	165	2900–5400	C7LiLiC.R33	Mayer 2001
^{16}O(^{7}Li,^{7}Li)^{16}O	170	2750–6250	16O7LiLiO.R33	Rauhala 1988
^{27}Al(^{7}Li,^{7}Li)^{27}Al	140	4000–7900	Nurmela-7Li-Al_140.R33	Nurmela 1999
^{27}Al(^{7}Li,^{7}Li)^{27}Al	170	3460–7960	27Al7LiLiAl.R33	Räisänen 1993
Si(^{7}Li,^{7}Li)Si	140	4500–7800	Nurmela-7Li-Si_140.R33	Nurmela 1999
Si(^{7}Li,^{7}Li)Si	170	4450–7710	Si7LiLiSi.R33	Räisänen 1993
Ti(^{7}Li,^{7}Li)Ti	140	5250–11000	Nurmela-7Li-Ti_140.R33	Nurmela 1999
Ti(^{7}Li,^{7}Li)Ti	170	4950–11460	Ti7LiLiTi.R33	Räisänen 1993

Table 3.5.: Non-Rutherford ERDA cross-sections.

	θ (Lab)	Energy (keV)	File	Reference
H(^{3}He,H)^{3}He	20	2000–3000	1HTP1X1.R33	Terwagne 1996
H(^{3}He,H)^{3}He	30	1900–3000	1HTP1X2.R33	Terwagne 1996
H(α,H)α	30	2500–4500	1HAP4HE30.R33	Bogdanović Radović 2001
H(α,H)α	40	2500–4500	1HAP4HE40.R33	Bogdanović Radović 2001
H(α,H)α	45	2500–4500	1HAP4HE45.R33	Bogdanović Radović 2001
H(α,H)α	50	2500–4500	1HAP4HE50.R33	Bogdanović Radović 2001
H(α,H)α	55	2500–4500	1HAP4HE55.R33	Bogdanović Radović 2001
H(α,H)α	60	2500–4500	1HAP4HE60.R33	Bogdanović Radović 2001
H(α,H)α	10	600–4800	HHEHHE10_KIM.R33	Kim 1999
H(α,H)α	15	600–4800	HHEHHE15_KIM.R33	Kim 1999
H(α,H)α	20	600–4800	HHEHHE20_KIM.R33	Kim 1999
H(α,H)α	25	600–4800	HHEHHE25_KIM.R33	Kim 1999
H(α,H)α	30	600–4800	HHEHHE30_KIM.R33	Kim 1999
H(α,H)α	35	600–4800	HHEHHE35_KIM.R33	Kim 1999
H(α,H)α	40	600–4800	HHEHHE40_KIM.R33	Kim 1999
H(α,H)α	10	1000–2500	ERD10H.R33	Quillet 1994
H(α,H)α	20	1000–2500	ERD20H.R33	Quillet 1994
H(α,H)α	30	1000–2500	ERD30H.R33	Quillet 1994
H(α,H)α	20	1000–3000	HHEHHE20.R33	Baglin 1992
H(α,H)α	25	1000–3000	HHEHHE25.R33	Baglin 1992
H(α,H)α	30	1000–3000	HHEHHE30.R33	Baglin 1992
H(α,H)α	35	1000–3000	HHEHHE35.R33	Baglin 1992
D(α,D)α	10	1000–2500	ERD10D.R33	Quillet 1994
D(α,D)α	20	1000–2500	ERD20D.R33	Quillet 1994
D(α,D)α	30	1000–2500	ERD30D.R33	Quillet 1994
D(α,D)α	20	1000–3000	DHEDHE20.R33	Kellock 1993
D(α,D)α	25	1000–3000	DHEDHE25.R33	Kellock 1993
D(α,D)α	30	1000–3000	DHEDHE30.R33	Kellock 1993
D(α,D)α	35	1000–3000	DHEDHE35.R33	Kellock 1993
D(α,D)α	40	1000–3000	DHEDHE40.R33	Kellock 1993
T(α,T)α	30	500–2700	THETHE30.R33	Sawicki 1988

Table 3.6.: Nuclear reactions cross-sections. *Total* means that the data file contains total cross-section data. Files without energy range contain only Q-values, but no cross-section data. These files can be used only for kinematic calculations, but not for simulations.

	θ (Lab)	Energy (keV)	File	Reference
D(d,p)T	Total	5–5000	2DDP.R33	Bosch 1992
D(d,t)p	Total	5–5000	2DDT.R33	Bosch 1992
D(d,^{3}He)n	Total	1–5000	2DD3HE.R33	Bosch 1992
D(t,^{4}He)n	Total	1–1370	2DTA_3.R33	Bosch 1992
D(^{3}He,α)p	Total	100–2500	2DTA_1.R33	Möller 1980
D(^{3}He,α)p	Total	10–2240	2DTA_2.R33	Bosch 1992
D(^{3}He,p)α	Total	210–2150	2DTP_1.R33	Möller 1980
D(^{3}He,p)α	Total	280–2400	2DTP_2.R33	Bonner 1952
D(^{3}He,p)α	Total	100–2500	2DTP_3.R33	Möller 1980
D(^{3}He,p)α	Total	10–2240	2DTP_4.R33	Bosch 1992
D(^{3}He,p)α	135	10–6000	2DTP_5.R33	Alimov 2005
T(d,^{4}He)n	Total	1–910	3TDA.R33	Bosch 1992
^{3}He(d,α)p	Total	10–1500	3HEDA_1.R33	Bosch 1992
^{3}He(D,p)α	Total	190–1600	3HEDP_1.R33	Bonner 1952
^{3}He(d,p)α	Total	10–1500	3HEDP_2.R33	Bosch 1992
^{6}Li(p,^{3}He)^{4}He	60	650–2900	6LIP3HE.R33	Marion 1956
^{6}Li(p,α)^{3}He	60	650–2900	6LIPA.R33	Marion 1956
^{6}Li(D,α)^{4}He	150	400–1900	6LIDA_1.R33	Maurel 1981
^{6}Li(^{3}He,p_0)^{8}Be	165	900–5100	6LITP0.R33	Schiffer 1956
^{6}Li(^{3}He,p_1)^{8}Be	165	900–5100	6LITP1.R33	Schiffer 1956
^{7}Li(p,α)^{4}He	150	500–1500	7LIPA.R33	Maurel
^{9}Be(p,α)^{6}Li	Total	30–700	9BEPA.R33	Sierk 1973
^{9}Be(p,α)^{6}Li	138	240–1350	9BEPA_1.R33	Thomas 1949
^{9}Be(p,D)^{8}Be	Total	30–700	9BEPD.R33	Sierk 1973
^{9}Be(p,D)^{8}Be	135	780–3000	9BEPD_1.R33	Weber 1956
^{9}Be(p,D)^{8}Be	138	240 –1330	9BEPD_3.R33	Thomas 1949
^{9}Be(p,D)^{8}Be	165	1400–1500	9BEPD_2.R33	Mayer 2001
^{9}Be(D,α_0)^{7}Li	165	500–1900	9BEDA0.R33	Biggerstaff 1962
^{9}Be(D,α_1)^{7}Li	165	500–1600	9BEDA1.R33	Biggerstaff 1962
^{9}Be(^{3}He,p_0)^{11}B	90	1800–5100	9BETP0_1.R33	Wolicki
^{9}Be(^{3}He,p_1)^{11}B	90	1800–5100	9BETP1_1.R33	Wolicki
^{9}Be(^{3}He,p_0)^{11}B	150	1800–5100	9BETP0_2.R33	Wolicki
^{9}Be(^{3}He,p_1)^{11}B	150	1800–5100	9BETP1_2.R33	Wolicki
^{10}B(p,α_0)^{7}Be	50	1800–10800	10BPA0_1.R33	Jenkin 1964
^{10}B(p,α_1)^{7}Be	50	2350–10100	10BPA1_1.R33	Jenkin 1964
^{10}B(p,α_0)^{7}Be	90	1800–9500	10BPA0_2.R33	Jenkin 1964
^{10}B(p,α_1)^{7}Be	90	2650–7100	10BPA1_2.R33	Jenkin 1964
^{10}B(D,α_0)^{8}Be	156	980–1800	10BDA0.R33	Purser 1963
^{10}B(D,α_1)^{8}Be	156	980–1800	10BDA1.R33	Purser 1963
^{10}B(^{3}He,p_0)^{12}C	90	2000–4000	B10HE3P0T90.R33	McIntyre 1996

	θ (Lab)	Energy (keV)	File	Reference
$^{10}B(^3He,p_1)^{12}C$	90	2000–4000	B10HE3P1T90.R33	McIntyre 1996
$^{10}B(^3He,p_0)^{12}C$	135	2000–4000	B10HE3P0T135.R33	McIntyre 1996
$^{10}B(^3He,p_1)^{12}C$	135	2000–4000	B10HE3P1T135.R33	McIntyre 1996
$^{10}B(^3He,p_0)^{12}C$	90	1300–5000	10BTP0.R33	Schiffer 1956
$^{10}B(^3He,p_1)^{12}C$	90	1300–5000	10BTP1.R33	Schiffer 1956
$^{10}B(\alpha,p_0)^{13}C$	90	1400–5300	10BAP0_1.R33	Chen 2003
$^{10}B(\alpha,p_0)^{13}C$	135	4000–5000	10BAP0.R33	Giorginis 1995
$^{10}B(\alpha,p_1)^{13}C$	135	4000–5000	10BAP1.R33	Giorginis 1995
$^{11}B(p,\alpha_0)^{8}Be$	155	700–6000	11BPA0.R33	Symons 1963
$^{11}B(p,\alpha_0)^{8}Be$	165	1700–2700	11BPA0_1.R33	Mayer 1998
$^{11}B(^3He,p_0)^{13}C$	90	2000–4000	B11HE3P0T90.R33	McIntyre 1996
$^{11}B(^3He,p_0)^{13}C$	135	2000–4000	B11HE3P0T135.R33	McIntyre 1996
$^{11}B(^3He,p_0)^{13}C$	90	3000–5400	11BTP0.R33	Holmgren 1959
$^{11}B(^3He,p_{1,2,3})^{13}C$	90	3000–5400	11BTP123.R33	Holmgren 1959
$^{11}B(^3He,D_0)^{12}C$	90	3000–5400	11BTD0.R33	Holmgren 1959
$^{12}C(D,p)^{13}C$	135	520–2950	12CDP_1.R33	Jarjis 1979
$^{12}C(D,p)^{13}C$	165	800–1950	12CDP_2.R33	Kashy 1960
$^{12}C(^3He,p_0)^{14}N$	90	2100–2300	12CTP0.R33	Tong 1990
$^{12}C(^3He,p_1)^{14}N$	90	2100–2400	12CTP1.R33	Tong 1990
$^{12}C(^3He,p_2)^{14}N$	90	2100–2400	12CTP2.R33	Tong 1990
$^{12}C(^3He,p_0)^{14}N$	159.4	1800–5400	12CTP0_1.R33	Kuan 1964
$^{12}C(^3He,p_1)^{14}N$	159.4	1800–5400	12CTP1_1.R33	Kuan 1964
$^{12}C(^3He,p_2)^{14}N$	159.4	1800–5400	12CTP2_1.R33	Kuan 1964
$^{12}C(^3He,\alpha_0)^{11}C$	159.4	1800–5400	12CTA0.R33	Kuan 1964
$^{13}C(D,p)^{14}C$	135	600–2950	13CDP.R33	Marion 1956
$^{13}C(^3He,p_0)^{15}N$	150	1900–3800	13CTP0.R33	Illsley 1957
$^{13}C(^3He,p_{1,2})^{15}N$	–	–	13CTP12.R33	Illsley 1957
$^{13}C(^3He,p_3)^{15}N$	–	–	13CTP3.R33	Illsley 1957
$^{14}N(D,\alpha_0)^{12}C$	150	600–1400	14NDA0_1.R33	Amsel 1969
$^{14}N(D,\alpha_1)^{12}C$	150	600–1400	14NDA1_1.R33	Amsel 1969
$^{14}N(D,p_0)^{15}N$	150	500–1900	14NDP0_1.R33	Simpson 1984
$^{14}N(D,p_{1,2})^{15}N$	150	600–1400	14NDP12.R33	Amsel 1969
$^{14}N(D,p_3)^{15}N$	150	800–1400	14NDP3.R33	Amsel 1969
$^{14}N(D,p_{4,5})^{15}N$	150	600–1400	14NDP45.R33	Amsel 1969
$^{14}N(D,p_5)^{15}N$	150	600–1400	14NDP45.R33	Amsel 1969
$^{14}N(^3He,p_0)^{16}O$	90	2000–4000	N14HE3P0T90.R33	McIntyre 1996
$^{14}N(^3He,p_0)^{16}O$	135	2000–4000	N14HE3P0T135.R33	McIntyre 1996
$^{14}N(^3He,p_{1,2})^{16}O$	90	2000–4000	N14HE3P1-2T90.R33	McIntyre 1996
$^{14}N(^3He,p_{1,2})^{16}O$	135	2000–4000	N14HE3P1-2T135.R33	McIntyre 1996
$^{14}N(^3He,p_{3,4})^{16}O$	90	2000–4000	N14HE3P3-4T90.R33	McIntyre 1996
$^{14}N(^3He,p_{3,4})^{16}O$	135	2000–4000	N14HE3P3-4T135.R33	McIntyre 1996
$^{14}N(^3He,p_{1,2})^{16}O$	90	1600–2800	14NTP1X1.R33	Terwagne 1994
$^{14}N(^3He,p_{1,2})^{16}O$	135	1600–2800	14NTP1X2.R33	Terwagne 1994
$^{14}N(^3He,p_3)^{16}O$	90	1600–2800	14NTP3X1.R33	Terwagne 1994

	θ (Lab)	Energy (keV)	File	Reference
$^{14}N(^{3}He,p_3)^{16}O$	135	1600–2800	14NTP3X2.R33	Terwagne 1994
$^{14}N(^{3}He,p_4)^{16}O$	90	1600–2800	14NTP4X1.R33	Terwagne 1994
$^{14}N(^{3}He,p_4)^{16}O$	135	1600–2800	14NTP4X2.R33	Terwagne 1994
$^{14}N(^{3}He,p_5)^{16}O$	90	1600–2800	14NTP5X1.R33	Terwagne 1994
$^{14}N(^{3}He,p_5)^{16}O$	135	1600–2800	14NTP5X2.R33	Terwagne 1994
$^{14}N(^{3}He,p_7)^{16}O$	90	1600–2800	14NTP7X1.R33	Terwagne 1994
$^{14}N(^{3}He,p_7)^{16}O$	135	1600–2800	14NTP7X2.R33	Terwagne 1994
$^{14}N(^{3}He,\alpha_0)^{13}N$	90	1600–2800	14NTA0X1.R33	Terwagne 1994
$^{14}N(^{3}He,\alpha_0)^{13}N$	135	1600–2800	14NTA0X2.R33	Terwagne 1994
$^{14}N(\alpha,p_0)^{17}O$	135	4000–5000	14NAP1.R33	Giorginis 1995
$^{15}N(p,\alpha)^{12}C$	140	900–2860	15NPA.R33	Hagedorn 1957
$^{15}N(D,\alpha)^{13}C$	90	400–1600	15NDA90.R33	Vickridge 1996
$^{15}N(D,\alpha)^{13}C$	135	400–2000	15NDA135.R33	Vickridge 1996
$^{15}N(D,\alpha)^{13}C$	150	400–2000	15NDA150.R33	Vickridge 1996
$^{15}N(D,\alpha)^{13}C$	150	800–1300	15NDA_1.R33	Sawicki 1985
$^{16}O(D,\alpha)^{14}N$	135	800–2000	16ODA_2.R33	Amsel 1964
$^{16}O(D,\alpha)^{14}N$	145	760–950	16ODA_1.R33	Turos 1973
$^{16}O(D,\alpha)^{14}N$	165	800–2000	16ODA_3.R33	Amsel 1964
$^{16}O(D,p_0)^{17}O$	135	20–3000	16ODP0_1.R33	Jarjis 1979
$^{16}O(D,p_1)^{17}O$	135	500–3000	16ODP1_2.R33	Jarjis 1979
$^{16}O(D,p_1)^{17}O$	155	400–1100	16ODP1_1.R33	Amsel 1967
$^{16}O(^{3}He,\alpha)^{15}O$	90	1600–2600	16OTA.R33	Abel
$^{18}O(p,\alpha)^{15}N$	155	1500–1800	18OPA_2.R33	Alkemada
$^{18}O(p,\alpha)^{15}N$	165	500–1000	18OPA_1.R33	Amsel 1967
$^{18}O(D,\alpha_0)^{16}N$	165	830–2000	18ODA_1.R33	Amsel 1964
$^{18}O(D,\alpha_1)^{16}N$	165	830–2000	18ODA_2.R33	Amsel 1964
$^{18}O(D,\alpha_2)^{16}N$	165	830–2000	18ODA_3.R33	Amsel 1964
$^{18}O(D,\alpha_3)^{16}N$	165	830–2000	18ODA_4.R33	Amsel 1964
$^{19}F(p,\alpha)^{16}O$	90	700–1900	19FPA_1.R33	Dieumegard 1980
$^{19}F(p,\alpha)^{16}O$	150	700–2000	19FPA_2.R33	Dieumegard 1980
$^{19}F(D,\alpha_0)^{17}O$	150	700–1900	19FDA0_1.R33	Maurel 1981
$^{19}F(D,\alpha_1)^{17}O$	150	1000–1900	19FDA1_1.R33	Maurel 1981
$^{19}F(\alpha,p_0)^{22}Ne$	135	2160–2520	F19AP0T135.R33	Borgardt 1998
$^{19}F(\alpha,p_1)^{22}Ne$	135	2160–2520	F19AP1T135.R33	Borgardt 1998
$^{28}Si(^{3}He,p_0)^{30}P$	–	–	28SITP0.R33	Groeneveld 1970
$^{28}Si(^{3}He,p_1)^{30}P$	–	–	28SITP1.R33	Groeneveld 1970
$^{28}Si(^{3}He,p_2)^{30}P$	–	–	28SITP2.R33	Groeneveld 1970
$^{28}Si(^{3}He,p_3)^{30}P$	–	–	28SITP3.R33	Groeneveld 1970
$^{28}Si(^{3}He,p_4)^{30}P$	–	–	28SITP4.R33	Groeneveld 1970
$^{32}S(D,p_0)^{33}S$	150	1000–2700	32SDP.R33	Healy 1998
$^{32}S(D,p_1)^{33}S$	150	1000–2700	32SDP1.R33	Healy 1998
$^{32}S(D,p_2)^{33}S$	150	1000–2700	32SDP2.R33	Healy 1998
$^{32}S(D,p_3)^{33}S$	150	1000–2700	32SDP3.R33	Healy 1998
$^{32}S(D,p_{456})^{33}S$	150	1000–2700	32SDP456.R33	Healy 1998

	θ (Lab)	Energy (keV)	File	Reference
^{32}S(D,p$_7$)^{33}S	150	1000–2700	32SDP7.R33	Healy 1998

Old File	New File	Version	Reason for replacement
10B3Hep0_135.r33	B10He3p0t135.r33	5.10	Better accuracy
10B3Hep0_90.r33	B10He3p0t90.r33	5.10	Better accuracy
10B3Hep1_135.r33	B10He3p1t135.r33	5.10	Better accuracy
10B3Hep1_90.r33	B10He3p1t90.r33	5.10	Better accuracy
11B3Hep0_135.r33	B11He3p0t135.r33	5.10	Better accuracy
11B3Hep0_90.r33	B11He3p0t90.r33	5.10	Better accuracy
14N3Hep0_135.r33	N14He3p0t135.r33	5.10	Better accuracy
14N3Hep0_90.r33	N14He3p0t90.r33	5.10	Better accuracy
14N3Hep12_135.r33	N14He3p1-2t135.r33	5.10	Better accuracy
14N3Hep12_90.r33	N14He3p1-2t90.r33	5.10	Better accuracy
14N3Hep34_135.r33	N14He3p3-4t135.r33	5.10	Better accuracy
14N3Hep34_90.r33	N14He3p3-4t90.r33	5.10	Better accuracy
CRSDA.DAT	various, see text	5.81	Better accuracy

Table 3.7.: Replacement of cross section data files.

3.8.1. Replacement of cross section data files

Throughout the long history of SIMNRA, cross section data files were renamed, reformated (from RTR to R33), or replaced by more accurate data. To provide backward compatibility, the file REPLACE.LST is used. It lists the original cross section data file, which has been deleted or renamed, and the file it has been replaced with. If an NRA file is opened which references a renamed or replaced cross section data file, this file is automatically replaced and the new data are used for all calculations.

The format of the file REPLACE.LST is as follows:
OldFile, NewFile, TagNr
OldFile is the name of the renamed or replaced file and *NewFile* the name of the file it has been replaced with. *TagNr* is an integer number which is used only together with the file CRSDA.DAT - for any other file 0 should be used.

The replaced files, the SIMNRA version of the replacement, and the reasons for replacement are listed in Table 3.7.

The file CRSDA.DAT, developed at the IPP Garching between 1985 and 1995 and containing polynomial fit coefficients to various cross section data, was deleted in SIMNRA 5.81: The accuracy of the fits was poor, and they were not documented. The fits were replaced by the original data files in REPLACE.LST.

3.9. *Calculate* menu

In the *Calculate* menu all commands for calculating spectra, scattering kinematics, stopping powers and data fitting are located. Additionally some helpful tools (density conversions, particles*sr) can be found here.

- *Calculate Spectrum*: Calculates the simulated spectrum.
- *Calculate Spectrum Fast*: Calculates a simulated spectrum, but with a less accurate and faster integration algorithm. *Calculate Spectrum Fast* can be up to 2 times faster than *Calculate Spectrum*, but is generally less accurate.
- *Fit Spectrum...*: Data fitting to experimental data. See subsection 3.9.1 for details.
- *Kinematics...*: Calculation of scattering kinematics. Allows the calculation of the energies of backscattered particles, recoils and nuclear reaction products.
- *Stopping...*: Calculation of stopping powers for any projectile in any target element and of energy loss in the different layers.
- *Cross Section...*: Calculation of Rutherford cross sections for backscattering and recoils.
- *Density...*: Density conversions (for elements only). Mass density to atomic density and conversion from atoms/cm^2 to μg/cm^2 and nm.
- *Particles*sr...*: Calculation of particles*sr from the collected charge and detector solid angle.
- *Exit Angle Beta...*: Calculation of the exit angle β for IBM and Cornell geometry.

  In IBM geometry incident beam, exit beam and the surface normal are in the same plane, see Figure 3.10, and β is simply given by

  $$\beta = |180^\circ - \alpha - \theta|.$$

  In Cornell geometry incident beam, exit beam and the sample rotation axis are in the same plane, and β is given by

  $$\cos\beta = -\cos\theta\cos\alpha.$$

- *Subtract Pile-up...*: Calculates the pile-up contribution not from simulated, but from experimental data, and allows to subtract the pile-up from the data. See subsection 3.9.2 for details.

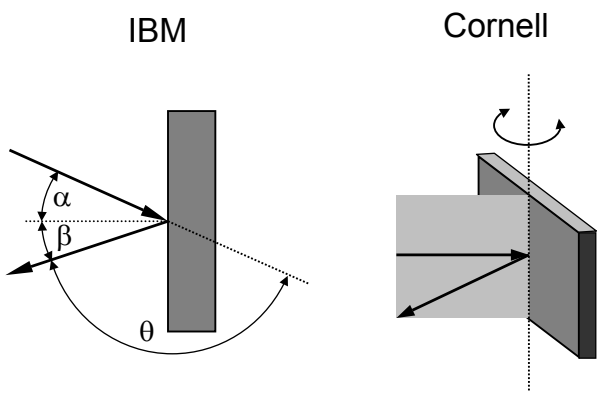

Figure 3.10.: IBM and Cornell geometry.

3.9.1. *Fit Spectrum...*

Data fitting to backscattering spectra is a nontrivial task. In data fitting the quadratic deviation of the simulated from the measured data points

$$\chi^2 = \sum_i \frac{\left(N_{exp}(i) - N_{sim}(i)\right)^2}{\sigma_i^2} \tag{3.6}$$

is minimized by varying the input parameters of the calculation. $N_{exp}(i)$ is the number of counts in the measured spectrum, $N_{sim}(i)$ the number of counts in the simulated spectrum, and σ_i the statistical error[5]. i can be either individual channels or channel regions, see the parameter *Chi2 evaluation*.

Fast fitting algorithms, such as the Levenberg-Marquardt algorithm, tend to be unstable and require the knowledge of the derivatives of χ^2. SIMNRA uses the Simplex algorithm for fitting [10, 11, 12]. The Simplex algorithm is very stable and converges (nearly) always. However, the convergence is not very fast. The Simplex algorithm always uses $n+1$ points (called vertices) in the parameter space for fitting, where n is the number of free parameters.

You can fit:

1. Energy calibration (energy/channel and offset only, quadratic term is not changed)
2. Particles*sr
3. Composition and thickness of a layer
4. Roughness of a layer

[5] SIMNRA uses $\sigma_i = \sqrt{N_{exp}}$ for $N_{exp} > 4$, $\sigma_i = 2$ for $N_{exp} \leq 4$ due to Poisson statistics.

independently or all at once. Check which parameters should be varied. Only one layer at a time can be fitted.

- *Number of fit regions*: Number of different regions where χ^2 is calculated. Up to 10 different regions may be used. At least one region must be specified. The regions should not overlap.
- *From To*: Lower and upper channel of each fit region.
- *Chi2 evaluation*: Determines how χ^2 (see Equation 3.6) is determined.
  - *Channels*:
    $$\chi^2 = \sum_i \frac{\left(N_{exp}(i) - N_{sim}(i)\right)^2}{\sigma_i^2}, \tag{3.7}$$
    where $N_{exp}(i)$ is the number of experimental counts in channel i, and $N_{sim}(i)$ the number of simulated counts in channel i.
  - *Integrals*:
    $$\chi^2 = \sum_i \frac{\left(N_{exp}(i) - N_{sim}(i)\right)^2}{\sigma_i^2}, \tag{3.8}$$
    where $N_{exp}(i)$ is the integrated number of experimental counts in region i, and $N_{sim}(i)$ the number of integrated simulated counts in region i.

  If *Channels* is selected, then the shape of the spectrum is taken into account, resulting in more accurate results in most cases. If *Integrals* is selected, then only count integrals in specified regions are taken into account. This option should be selected, if the agreement between experimental and simulated spectra is poor due to inaccurate energy calibration, complicated peak shapes, and the like: In these cases, the selection of *Channels* may result in poor results, while *Integrals* still may work reliably.
- *Max Iterations*: Maximum number of Simplex iterations. Fitting will be performed until the desired accuracy is obtained or the maximum number of iterations is reached.
- *Fit Accuracy*: Desired accuracy of the fit. The fit has converged if the relative change of all fitted parameters and of χ^2 is below *Fit Accuracy*. The relative change of a parameter A is $\Delta A/A$, where ΔA is the difference between the best vertex (the vertex with the lowest χ^2) and the worst vertex (the vertex with the highest χ^2).
- *Calculate Fit Error*: If checked an error estimate for all fitted parameters is computed. See below for details. This is a time consuming process and may require more computing time than the fit itself. Default is unchecked.

Fit error

An error bar for fitted parameters can be obtained under the following assumptions:

1. The physics model (i.e. stopping powers, cross sections etc.) is assumed to be accurate with zero error. Obviously, in reality this is not the case, and errors introduced by inaccurately known stopping powers or cross sections may largely exceed the computed errors. SIMNRA does not know whether a stopping power or cross section is accurate or not — you should know that.

2. All nonfitted parameters are assumed to be accurate with zero error. Again, usually this will be not the case, but SIMNRA is not able to quantify these errors: It does not know how accurately you determined your energy calibration or performed the ion current measurement.

The error bar Δa of a fitted parameter a is determined by the shape of the χ^2 surface near the minimum: A flat minimum of χ^2 allows a larger variation of a and will result in larger errors of a. On a confidence level of 68.3% (the usual 1σ interval) the error of a is obtained by varying a until χ^2 has increased by 1 [12]:

$$\Delta\chi^2(a_{\Delta=1}) = \chi^2(a_{\Delta=1}) - \chi^2_{min} = 1. \tag{3.9}$$

χ^2_{min} is the minimised χ^2 with an optimised parameter a_{min}, and the error Δa of a is $\Delta a = |a_{\Delta=1} - a_{min}|$.

If we have more than one fit parameter things get more complicated [12]. As an example we consider the case of two fit parameters a_1 and a_2. The $\Delta\chi^2 = 1$ contour now is an ellipse (Figure 3.11) due to correlations between a_1 and a_2, and for more than two fit parameters a multi-dimensional ellipsoid. To find the confidence intervals for a_1 and a_2 we have to do the following: Increase a_1 by some amount (black arrows in Figure 3.11). Now find a new minimum of χ^2 by optimising a_2, a_1 remains unchanged (dotted line in Figure 3.11). Increase a_1 and optimise a_2 again, and so on until $\Delta\chi^2 = 1$. For n fit parameters $a_1 ... a_n$ we have to increase a_1 and optimise $a_2 ... a_n$ until $\Delta\chi^2 = 1$.

As can be seen in Figure 3.11 the error bar $\Delta a_1'$ becomes nonrealistic small if only a_1 is fitted. This is a consequence of the assumption that all nonfitted parameters are accurate. To obtain realistic error bars all parameters should be fitted in one step.

A quantitative measure for the goodness-of-fit of the assumed model can be obtained from the value of χ^2_{min}. See [12, Chapter 14.1] (or any good textbook about statistics) for more information.

3.9.2. Subtracting pile-up

Allows to subtract the pile-up contribution from experimental data. The pile-up is calculated iteratively from *experimental* data (and not from *simulated* data, as is the case if you check

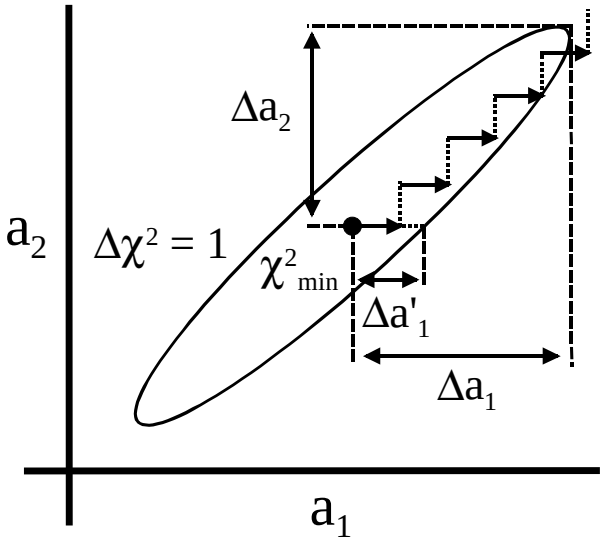

Figure 3.11.: $\Delta\chi^2 = 1$ contour near the χ^2 minimum (black dot) for two fit parameters a_1 and a_2. Δa_1 and Δa_2 are the fit errors for a_1 and a_2 if fitted simultaneously, $\Delta a_1'$ the error for a_1 if only a_1 is fitted.

Calculate pile-up in the *Setup: Experiment: More Options: Live Time and Pile-up...* form, see section 3.6.2). You can use this menu item to subtract pile-up from any type of spectral data, including RBS or ERDA spectra, X-ray spectra (for example PIXE), or γ-ray spectra.

- The parameters *Real time*, *Live time*, *Pulse rise time*, *Fudge time parameter*, *Pile-up rejector*, and *Pile-up rejector pair-resolution time* are described in section 3.6.2, see there.
- *Number of iterations*: The pile-up contribution is calculated iteratively from the data. *Number of iterations* specifies the number of iterations. In most cases 2–3 iterations are sufficient.
- *Calculate pile-up*: Calculates the pile-up contribution from the experimental data.
- *Subtract pile-up*: Subtracts the pile-up contribution from the experimental data.

  Warning: *Subtract pile-up* modifies irreversibly the experimental data.

3.10. *Tools* menu

Several tools for spectrum evaluation are located in the *Tools* menu. These tools appear as floating windows and are updated automatically if the spectrum is recalculated or a new spectrum is loaded from disk.

3.10.1. *Data Reader*

The data reader allows to read out the contents of a specific channel. The data reader is displayed as a small black crosshair with white legend. The data reader control window displays the channel, the energy of this channel and the number of counts in the channel. The data reader is moved by entering the channel number or by using the spin up/spin down buttons in the control window. The data reader is updated automatically if a spectrum is recalculated or if a new spectrum is loaded from disk.

3.10.2. *Integrate Spectrum*

The *Integrate Spectrum* tool allows to integrate a specific spectrum. The integral of a spectrum is the sum of all counts between a lower and an upper channel including the boundary channels. The integration boundaries are displayed as small black vertical lines in the plot. The boundaries are moved by entering the channel numbers or by using the spin up/spin down buttons in the control window. The integral is updated automatically if a spectrum is recalculated or if a new spectrum is loaded from disk.

3.10.3. *Nearest Elements*

The *Nearest Elements* tool marks the channels, in which backscattered particles from specific elements or recoiled particles would appear. This allows easy identification of unknown peaks in the spectrum. The tool shows the three elements, which are closest to the cursor. The cursor is displayed as a black vertical line, and is moved by entering the channel number or by using the spin up/spin down buttons in the control window.

The *Nearest Elements* tool uses the surface approximation, i.e. stopping power effects are neglected. The marked channels are only valid for elements at the surface.

Limitations:

1. Stopping in a foil in front of the detector is neglected, resulting in unrealistic results if foils are present. A warning message is displayed, if a foil is present.

2. The tool assumes that particles are fully stopped in the detector, resulting in unrealistic results for thin detectors.

3. The tool displays energies of scattered particles and recoils, if kinematically possible. It does not display energies of nuclear reaction products.

3.11. *Plot* menu

This section describes all plot related commands, including all commands which are not accessible via menus.

- *Autoscaling*: If checked, the plot will be scaled automatically to minimum and maximum if experimental data are imported or a new calculation is performed. If unchecked, the axis scales remain fixed.
- *Rescale x-Axis*: Scales the x-axis to minimum and maximum of all visible spectra.
- *Rescale y-Axis*: Scales the y-axis to minimum and maximum of all visible spectra.
- *Unzoom*: Undo all zoom operations.
- *x-Axis...*: Scale the x-axis manually by entering the axis minimum and maximum, set logarithmic x-axis. Same as a double-click with the left mouse button on the x-axis.
- *y-Axis...*: Scale the y-axis manually by entering the axis minimum and maximum, set logarithmic y-axis. Same as a double-click with the left mouse button on the y-axis.
- *Legend...*: Allows to alter the text of the legend. Same as a double-click with the left mouse button on the legend.
- *Delete Experimental Data*: Deletes the experimental data from the plot.
- *Delete Simulated Data*: Deletes all simulated data from the plot.
- **Zooming into the plot:** To zoom into the plot click with the left mouse button into the upper left corner of the range you want to zoom in. Keep the mouse button down and tear a rectangle to the lower right corner of the zooming range.
- **Panning:** Click with the right mouse button into the plot, keep the mouse button down and move the mouse.
- **Zooming out:** Click with the left mouse button into the plot. Keep the mouse button down and move the mouse towards the upper left corner. Or use *Plot: Unzoom*.

3.12. *Options* menu

- *Create Reaction List*: SIMNRA uses a file named CRSEC.LST in the cross-sections directory to know which cross-section data are available. *Create Reaction List* will create this file. You have to recreate the reaction list if you add or delete cross-section data files, see section 3.16.

  Note: In some cases files are not readable by SIMNRA due to format errors. These files will be ignored. The program displays a list of all ignored files.

- *Preferences...*: Allows to set global program preferences. These preferences are stored permanently.

  The *Print* tab:

  – *White background for print*: If checked, then the grey background of the graph is changed to white in the printout.

  – *Show "Print What?" dialog*: If checked, then a dialog asking what to print (experimental conditions, graph) is displayed. If unchecked, this dialog is omitted and everything is printed.

  The *Spectrum Data* tab:

  – Determines which menu entries are visible in the *File: Read Spectrum Data* menu.

  The *Saving* tab:

  – *Create BACKUP.NRA when saving*: If checked, the old NRA-file is saved to a file named BACKUP.NRA each time *File: Save* or *File: Save As...* is used. In the case of erraneous overwriting of a file you can recover the old data from this file. In each directory only one BACKUP.NRA can exist.

  The *Directories* tab:

  – Determines in which directories the program looks for atomic, cross-section and stopping power data. This is mainly useful if the data are stored on a network drive and are accessed simultaneously from different computers.

  – *SRIM program directory* : Base directory of the SRIM program for stopping power calculations. SRIM 2003 or later must be installed. See section 3.17 for details.

  The *Appearance* tab:

  – *Toolbar visible*: If checked, a toolbar with speed buttons for opening and saving files, calculating spectra etc. is available. See section 3.2 how to use the toolbar. Program default is *checked*.

  – *Progress window visible*: If checked, a window displaying details about the progress of a calculation is shown during calculations. This slows down the calculations. Program default is *checked*.

3.13. Help menu

- *User's Guide*: Opens the User's Guide in PDF-format using Adobe Acrobat or Adobe Acrobat Reader.
  Note: Adobe Acrobat or Acrobat Reader are not part of SIMNRA. Adobe Acrobat Reader can be obtained freely from the Adobe web site at www.adobe.com.
- *Home Page*: Opens the SIMNRA home page using your default web browser.
- *IBANDL Cross-Sections*: Opens the **I**on **B**eam **A**nalysis **N**uclear **D**ata **L**ibrary (IBANDL) home page using your default web browser. IBANDL contains a large number of cross-section data files for ion beam analysis and is hosted by the International Atomic Energy Agency (IAEA).
- *About...*: Shows the version number of the program.
- *Register...*: Registration of the program.

3.14. Data exchange with other programs

3.14.1. Graphics programs: Excel, Origin, ...

SIMNRA allows to exchange data with graphics programs by two different methods:

1. Via the clipboard. With *Edit: Copy Data* the experimental and simulated spectra are copied in ASCII format to the windows clipboard. They can be pasted into any spreadsheet program. See section 3.5 for details.

2. Via ASCII file. With *File: Write Spectrum Data...* the experimental and simulated data are exported as columns into an ASCII file. You can import this file into any plot program, such as Excel, Origin or Mathematica. See section 3.4 for details.

3.14.2. RUMP

SIMNRA can read and write sample description files (*.LCM) and read RBS files (*.RBS) used by the RUMP program. Sample description files contain the composition of the sample and the absorber foil. These files can be read and written by *File: RUMP: Read Sample Description File* and *File: RUMP: Write Sample Description File*. RUMP stores experimental parameters (Type of incident particles, incident energy, scattering geometry, etc.) and spectral data in binary files with extension *.RBS. These files can be read by *File: RUMP: Read RBS File*. SIMNRA can not write RBS files.

SIMNRA and RUMP use a different naming convention for the three angles (incident angle, scattering angle, exit angle) which define the geometry of an experiment:

- The incident angle is called α in SIMNRA, and Θ in RUMP.
- The scattering angle is called θ in SIMNRA, while RUMP uses the supplement of the scattering angle $\phi = 180° - \theta$: Direct backscattering is $\theta = 180°$ in SIMNRA, but $\phi = 0°$ in RUMP.
- The exit angle is called β in SIMNRA, and ψ in RUMP. This angle is always independent in SIMNRA (i.e. SIMNRA always uses general geometry), while RUMP determines this angle from $\psi = \phi + \theta$ in IBM geometry or $\cos(\psi) = \cos(\phi)\cos(\theta)$ in Cornell geometry.

These relations are summarized in Table 3.8. See Figure 3.3 for a graphical representation of the different angles. SIMNRA adjusts the angles correctly if a RUMP RBS-file is opened.

Sample Description Files

SIMNRA supports only a subset of the RUMP sample description commands. The supported command are listed in Table 3.9. All other commands will be neglected. Note that especially the RUMP commands *Equation*, *Species* and *Fuzz* are not supported. If your sample description file contains these commands, they will be neglected and a warning will be shown.

	SIMNRA	RUMP	Relation
Incident angle	α	Θ	$\alpha = \Theta$
Scattering angle	θ	ϕ	$\theta = 180° - \phi$
Exit angle	β	ψ	$\beta = \phi + \Theta$ (IBM geometry)
			$\cos\beta = \cos\phi \cos\Theta$ (Cornell geometry)
			$\beta = \psi$ (General geometry)

Table 3.8.: Naming conventions for the geometry of an experiment, as used by SIMNRA and RUMP, and the relations between them.

RESET
LAYER
OPEN
NEXT
COMPOSITION[a][b]
THICKNESS[c]
ABSORBER

[a] Partly implemented. Only elements are recognised, but no isotopes. The command *Composition Si 1 O 2 /* will be recognised and the natural isotopic ratios for Si and O will be used. The command *Composition 28Si 1 16O 2 /* will not be recognised properly.

[b] RUMP allows to enter SiO_2 as Si 1 O 2. SIMNRA will convert this to Si 0.33333 O 0.66666.

[c] As units for thickness are possible: */CM2*, *M/CM2*, *A*, *NM*. If *A* for Å or *NM* for nm are used, SIMNRA will use the weighted atomic densities of all elements in the layer to convert Å or nm to 10^{15} atoms/cm^2. It is highly recommended to use the units */CM2* or *M/CM2* instead.

Table 3.9.: RUMP sample description commands which are supported by SIMNRA.

RBS Files

SIMNRA can read RUMP's RBS file format version 1.1 from 8/94 with the following limitations:

1. Data compression level 3 (zero compressed) is not implemented. Levels 0–2 (uncompressed real, uncompressed integer, differential integer) are fully implemented.
2. Each RBS file may contain only one spectrum. Record type 20h is allowed, but may contain only one row.
3. Only one record 120h (RBS spectrum type) or 121h (FRES spectrum type) may be present, i.e. simultaneous RBS and FRES (= ERD) are not allowed.
4. Record types 01h (printed comments), 02h (unprinted comments), 101h (identifier for the data set), 102h (MCA information) and 103h (collection date/time) are recognized, but ignored.
5. Record type 111h (accelerator parameters): Beam current is ignored by SIMNRA, and pile-up is not calculated.
6. Record type 112h (data collection parameters): Starting channel of data is rounded from real to integer. This may result in differences of ±0.5 channels between RUMP and SIMNRA, if a non-integer starting channel is used.

3.14.3. IBA data furnace

The IBA data furnace (NDF, WiNDF) was developed at the University of Surrey and is available from www.ee.surrey.ac.uk/Research/SCRIBA/ndf/. This program converts energy spectra to depth profiles. The depth profiles are stored in RUMP's sample descrition format LCM. You can read these files with the command *File: Read RUMP*, see section 3.14.2.

3.15. Importing spectrum data in any format

SIMNRA can read experimental spectrum data in several formats including ASCII, see section 3.4. But many laboratories have their own spectrum data file formats. SIMNRA offers the possibility to import any type of experimental data by supplying a dynamic link library (DLL), which reads the data and passes them to SIMNRA. This DLL must be supplied by the user and is called if *File: Read Spectrum Data: User...* is clicked. This section describes the details of this DLL.

The DLL-name must be *user.dll*. It must be located in the *SIMNRA\UserDll* subdirectory - otherwise SIMNRA will not find it. The DLL must export a function *ReadData* (exact spelling), defined as follows[6]:

```
Function ReadData  (FileName :  PChar;
                    Var Count :  Integer;
                    Data :  Pointer):      Integer; stdcall;
```

Filename	Input parameter. Null terminated string with the full name including path to the file which shall be read.
Count	Output parameter. Pointer to a 32 bit signed integer value which indicates how many channels were actually read.
Data	Input parameter. Pointer to an array of 32 bit signed integer values which will take the spectrum data. The array starts at channel 0(!) and has a maximum of 8192 channels.

The return value of *ReadData* is a 32 bit signed integer. It must be 0, if the file was read successfully. Any other return value indicates an error condition.

The calling convention of *ReadData* must be *stdcall* in Borland Delphi or *WINAPI* in Microsoft C++.

A small code example in Pascal can be found in *UserDLL\sample.dpr*. A more detailed example is given in *UserDLL\sample1.dpr*.

[6] The code examples are in Pascal (Borland Delphi 4).

3.16. Adding new cross-section data

To add new cross-section data, you have to perform the following steps:

1. Create a cross-section data file in the R33 file format. The easiest way to do this is by using the R33Manager. Alternatively you can use any text editor. The file format is described below.

2. Copy this file into the directory where all other cross-section data files are (subdirectory CRSEC of your SIMNRA installation).

3. Recreate the reaction list by clicking *Options: Create Reaction List*.

   Note: If your file is ignored, SIMNRA was not able to read or understand the file. Carefully read the section about the R33 file format and try again.

The nuclear data section of the International Atomic Energy Agency (IAEA) has created the **I**on **B**eam **A**nalysis **N**uclear **D**ata **L**ibrary IBANDL at `http://www-nds.iaea.org/ibandl/`. This library contains many cross-section data files and is constantly updated. The data files are in R33-format and can be used with SIMNRA.

3.16.1. The R33 file format

The R33 file format is described in full detail by I.C. Vickridge in the file R33Help.htm, which should be present in your SIMNRA installation directory, and in Appendix B. SIMNRA reads the updated R33 file format of April 2002, but is also able to read older R33 files which conform to the original specification from the year 1991[7].

An example for a valid file in the R33 format is shown in Figure 3.12. Each line must end with <CR><LF> (Carriage Return and Line Feed).

SIMNRA uses not only the data points, but also a part of the information supplied in the file header. The following lines are used by SIMNRA and must be present in the file. Though the lines may be arranged in any order, it is recommended to arrange them in the same order as shown in Figure 3.12. Any other entries than the ones listed below are ignored by SIMNRA, but may be necessary to form a valid R33 file. See Appendix B or the file R33Help.htm for details.

- A line containing the string 'Source:'. The rest of the line has to contain a reference or other source for the data and will appear as description in the reaction menu.

- A line containing the string 'Reaction:'. SIMNRA will interpret the nuclear reaction string written in that line (In the example of Figure 3.12 16O(d,a0)14N) to find out which particles are involved in the nuclear reaction. The masses of the particles are ignored.

[7] The original specification can be found in DSIR Physical Sciences Report 33 by I.C. Vickridge

```
COMMENT: These cross sections have been digitised from the publication
cited below.  No error of either the energy and or the sigma is given.
Some errors may be among the data, we are recently checking them.
The Los Alamos Ion Beam Handbook also will contain these data as soon
as it is ready.  If you use this data please refer to the paper below.
Source:  A.Turos, L.Wielunski and a Batcz, NIM, 111(1973), 605
Special comment:
WARNING ! THIS IS MAINLY FOR TEST NO GUARANTY IS PROVIDED FOR EVEN
AGREEMENT WITH THE ORIGINAL PUBLICATION.
File created by R33 Manager version 0.1

Version:  R33
Source:  A.Turos, L.Wielunski and a Batcz, NIM, 111(1973), 605
Name:  Gyorgy Vizkelethy
Address1:  Department of Physics
Address2:  Idaho State University
Address3:  Campus Box 8106
Address4:  Pocatello, ID 83209-8106
Address5:  (208) 236-2626
Address6:  vizkel@physics.isu.edu
Serial Number:  0
Reaction:  16O(d,a0)14N
Distribution:  Energy
Composition:
Masses:  2.000, 16.000, 4.000, 14.000
Zeds:  1, 8, 2, 7
Qvalue:  3110.00, 0.00, 0.00, 0.00, 0.00
Theta:  145.00
Sigfactors:  1.00, 0.00
Enfactors:  1.00, 0.00, 0.00, 0.00
Units:  mb
Data:
761.0     0.0     2.92E+0000     0.0
770.0     0.0     3.65E+0000     0.0
775.0     0.0     3.99E+0000     0.0
780.0     0.0     4.41E+0000     0.0
785.0     0.0     4.55E+0000     0.0
EndData:
```

Figure 3.12.: Example for a cross-section data file in the R33 file format.

- A line containing the string 'Masses:'. SIMNRA will read the masses of the particles from this line. All masses in amu. The first mass is the mass of the incident particle, the second mass is the mass of the target particle, the third mass is the mass of the outgoing particle for which the cross-section is valid and the fourth mass is the mass of the other reaction product. The masses may be rounded to the nearest integer value - SIMNRA will replace the given masses by the exact values.

  Warning: Note that the masses are given in a different order than in the 'Reaction' string! For the reaction 16O(d,a0)14N the correct line is 'Masses: 2, 16, 4, 14'. This is a permanent source of error, so check your input carefully.

  In some cases, for example if the file contains elastic scattering data, the cross section values are not for a specific isotope, but for natural isotopic composition. In this case the mean target mass should be used.

- If the cross section values are for natural isotopic target composition rather than for a specific isotope a line containing the string 'Composition: Natural' has to be present. In this case the given cross section is used for all isotopes. This line has to be omitted if the cross section is for a specific isotope.

  Other compositions than 'Natural' must not be used.

- A line containing the string 'QValue:'. The Q-value is the energy released in the nuclear reaction (in keV). Q = 0.0 for elastic scattering. Up to 5 different Q-values are allowed, for example for multiple particle groups which are not resolved. SIMNRA will use the mean value of all non-zero Q-values.

- A line containing the string 'Theta:'. Theta should be given in degrees. The value of theta is not used by SIMNRA, but this line must be present and contain a value.

- Optionally a line containing the string 'Units:' may be present. Valid values are 'mb' for differential cross sections, 'tot' for total cross sections, and 'rr' for ratio to Rutherford. Differential cross sections have to be in mbarn/sr, and total cross sections in mbarn. If the 'Units' line is omitted, SIMNRA will assume 'mb', i.e. differential cross sections. The value 'tot' indicates that the cross section is integrated over all angles. Thus if 'tot' is used the value of theta has no meaning. Nevertheless, a valid real number has to be given for theta.

- A line containing either the string 'Nvalues:' or 'Data:'. The value of Nvalues is ignored. SIMNRA assumes that the data will start after this line.

- The data are organised in 4 columns: The first column is the energy in keV, the second column is the energy error in keV (ignored by SIMNRA), the third column is the cross-section in the laboratory frame, and the fourth column is the cross-section error (ignored

by SIMNRA). The cross section units have to be mbarn/sr for differential cross sections and mbarn for total cross sections. SIMNRA expects the data to be arranged in order of ascending energy.

- Scale conversion factors ('EnFactors' and 'SigFactors') may be used with SIMNRA 5.02 and higher. Scale conversion factors must not be used with earlier versions of SIMNRA, because they are ignored and will result in incorrect cross section values[8]. Refer to Appendix B how to use scale conversion factors. But note that the use of scale conversion factors is not recommended.

[8] This is only a problem with some files in the IBANDL data library at http://www-nds.iaea.org/ibandl/. These files should not be used with SIMNRA 5.01 and earlier. They can be used with SIMNRA 5.02 and higher.

3.17. Using SRIM stopping powers

SRIM is a program for the calculation of stopping powers and ion ranges. SRIM is not part of SIMNRA, but is developed by J. Ziegler and can be downloaded from www.srim.org. SIMNRA uses SRIM for calculating stopping power tables, which are then used for simulations. SIMNRA requires SRIM 2003 or later and has been tested with SRIM 2003 to SRIM 2010.

In order to use SRIM stopping powers, you must perform the following steps:

1. Download and install SRIM on your computer.
2. Run SIMNRA. Click *Options:Preferences...* and go to the *Directories* tab. Enter the path to the SRIM program directory (i.e. the directory where SRIM 20nn.exe is located. nn is the year, such as 2003, 2008, etc.). You can use the small button to navigate graphically to that directory.
3. Click *Setup:Calculation...* and go to the *Parameter* tab. Select *SRIM* as *Stopping power data*.

SIMNRA uses SRIM to calculate stopping power tables. These tables are stored in the SIMNRA\STOP directory. The file naming convention is SRIM2003_Z1_M1_Z2.dat, where Z1 and M1 are the nuclear charge and mass of the projectile, and Z2 the nuclear charge of the target material. Initially there are no SRIM stopping power files available, but these files will be created successively whenever you are running a simulation.

3.17.1. Trouble shooting

If SIMNRA is not able to use SRIM stopping powers, please read the error message carefully and act according to the following list.

- Error message: *Error running SRIM module.*
  1. Is SRIM 2003 or later installed on your computer? See section 3.17 on how to install SRIM.
  2. Check the path to the SRIM program directory in the *Options:Preferences:Directories* form. See section 3.17 for details.
  3. SIMNRA calls the program *[SRIM]\SR Module\SRModule.exe*, where *[SRIM]* is the SRIM program directory from the *Options:Preferences:Directories* form. This program must exist, and it must be located in the *\SR Module* subdirectory (note the blank between SR and Module). Re-install SRIM, if this program does not exist.
- Error message: *Error creating SRIM Module input file. Cannot write to file xyz.*

  SIMNRA must have write access to the *[SRIM]\SR Module* subdirectory, and it must have write access to the file *[SRIM]\SR Module\SR.IN*, where *[SRIM]* is the SRIM program

directory from the *Options:Preferences:Directories* form. This may be a problem for users with restricted permissions on Windows XP, Vista or Windows 7 systems, especially if SRIM is installed in the *\Programs* branch. This is a bug of the SRIM code, which is not foreseen to be used with restricted permissions – complain to the SRIM author. Ask your administrator to give you write permission to the *[SRIM 20nn]\SR Module* subdirectory.

- Error message: *Error creating SRIM stopping power data file. Cannot write to file xyz.*

  SIMNRA must have write access to the *[SIMNRA\Stop]* directory, where *[SIMNRA\Stop]* is the stopping power data directory in *Options:Preferences:Directories*. This may be a problem for users with restricted permissions on Windows XP,Vista or Windows 7 systems. The SIMNRA setup program gives write permission for the [SIMNRA\Stop] directory to all registered users, but somebody may have changed that later. Ask your administrator to give you write permission to the *[SIMNRA\Stop]* directory.

  Note: Unrestricted write access to the *[SIMNRA\Stop]* directory will not cause a security problem, because this directory contains only data files.

- Anything else: Check the files SRIM2003_Z1_M1_Z2.dat in the *[SIMNRA\Stop]* directory. Delete all files with a length of 0 byte.

```
This is a comment line
This is another comment line
E       Stopping
(keV)   (keV/1E15 at./cm^2)
1       0.5
2       0.6
4       0.7
```

Figure 3.13.: Example of a valid stopping power data file.

3.18. Using user-defined stopping powers

SIMNRA will use user defined stopping powers, if *User defined* stopping powers are selected in *Setup: Calculation*, see subsection 3.6.3.

To use user defined stopping powers, you have to perform the following steps:

1. Stopping power data files must be stored in the SIMNRA\STOP directory.

2. Stopping power data files are selected according to file name. The file naming convention is: STOP_Z_1_M_1_Z_2.DAT, with Z_1 and M_1 the nuclear charge and mass of the ion and Z_2 the nuclear charge of the target element. M_1 is rounded to the nearest integer value. Example: STOP_2_4_14.DAT should contain stopping power data for ^{4}He in Si.

3. The file format is shown in Figure 3.13: The files can start with an arbitrary number of comment lines. These lines are ignored. The stopping power data are organized in two columns as function of energy, with the energy in keV and the stopping power in keV/1E15 at./cm^2. The data have to be be ordered in ascending order. The data points may have irregular energy spacing, i.e. the energy step from one data point to the next may vary. The stopping power must be the total stopping power, i.e. the sum of electronic and nuclear stopping. SIMNRA uses linear interpolation between the data points.

3.19. Energy calibration issues

3.19.1. Detector nonlinearity

A solid state detector, which is used in most ion beam experiments, does not measure the real particle energy, but a somewhat smaller energy. This has been called pulse height defect. The pulse height defect is due to:

1. The energy and particle dependent energy loss in the top electrode and the dead layer of the semiconductor detector [13, 14, 15].
2. Only the electronic energy loss in the active detector region is measured, while nuclear energy loss is not detected [13]. The nuclear energy loss is energy and particle dependent.
3. Heavy ions produce a high density of electron-hole pairs. The electron-hole pairs may recombine before separation by the electric field in the detector. This has been called plasma effect [13]. The plasma effect is energy and particle dependent.

The energy dependence of the pulse height defect results in a nonlinearity of the energy calibration. The energy loss in the top electrode and the dead layer can be accounted in the following way:

- You can create a foil consisting of two layers in front of the detector. Layer 2 is composed of the material of the top electrode (usually Au) and has the thickness of the electrode (usually the thickness is supplied by the manufacturer of the detector). Layer 1 is composed of silicon in the case of a silicon detector and has the thickness of the dead layer (the dead layer is the insensitive region near the electrode). The dead layer thickness can be obtained only experimentally by tilting the detector.

For light ions (protons and He) this should be sufficient to achieve a linear energy calibration. But the nuclear energy loss and the plasma effect, which are both important for heavy ions, are not taken into account by this procedure.

An easier way to account for detector nonlinearities is to use a non-linear energy calibration with a quadratic correction term of the form

$$E\,[\mathrm{keV}] = A + B \times \mathrm{channel} + C \times \mathrm{channel}^2.$$

See subsection 3.6.1 for details.

3.19.2. Energy calibration for different ion species

As already shown in subsection 3.19.1 the pulse height defect depends on the particle species. This requires an individual energy calibration for each ion species if different ion species are detected, as is the case in NRA and ERDA measurements with incident heavy ions. SIMNRA offers the possibility to use an individual nonlinear energy calibration for each detected species, see subsection 3.6.1 for details.

3.20. Programming support

3.20.1. Command line parameters

- */regserver* — Registers the OLE automation server in the Windows Registry. This is done automatically by the setup program, so there should be rarely, if ever, the necessity to use this parameter.
- */unregserver* — Unregisters the OLE automation server from the Windows Registry. This is done automatically by the uninstall program, so there should be rarely, if ever, the necessity to use this parameter.
- */unregister* — Deletes all registry entries used by SIMNRA. This is done automatically by the uninstall program, so there should be rarely, if ever, the necessity to use this parameter.
- Additionally SIMNRA accepts one optional command line parameter, which is the name with full path of a NRA-file. This file is opened upon startup. Use double quotes (") if the file name contains blanks.

  Example: `simnra "c:\test.nra"`

3.20.2. OLE automation

SIMNRA is an OLE 2.0 automation server, which allows other applications to control SIMNRA. This is useful for automatic processing of large numbers of spectra, and allows to implement additional functions, such as the calculation of spectra from laterally inhomogeneous samples [16]. The available OLE objects and methods are described in Appendix A, some sample programs can be found in section A.10.

4. Physics

During the last decade several programs for the simulation of backscattering spectra have been developed. The most common program is Doolittle's RUMP [17, 18]. However, RUMP uses several approximations to save computing time. The increase in computer power during the last years has made it possible to drop several of the approximations used by RUMP. SIMNRA offers more freedom in the use of non-Rutherford cross-sections and nuclear reactions, treats several topics such as straggling and convolution more precise and adds new possibilities such as dual scattering. This section describes the physics involved in the simulation of a backscattering spectrum as performed by SIMNRA.

The target is subdivided into shallow sublayers. Each simulated spectrum is made up of the superimposed contributions from each isotope of each sublayer of the sample target. The thickness of each sublayer is chosen in such a way that the energy loss in each sublayer is about the stepwidth of the incoming particles. When the incident particles penetrate a sublayer, they loose energy due to electronic and nuclear energy loss and the beam energy is spread due to straggling. The calculation of the energy loss is described in detail in section 4.5, and the calculation of straggling in section 4.8. SIMNRA calculates the energy of backscattered particles[1] from the front and the backside of the sublayer, and the energy of these particles when reaching the detector after passing to the target surface and traversing a foil in front of the detector, see Figure 4.1. The contribution of each isotope in each sublayer will be referred to as a brick.

To account for energy straggling and the finite energy resolution of the detector the brick shown in Figure 4.1 is convoluted with a Gaussian function $f(E, \sigma^2)$ with width

$$\sigma^2 = \sigma^2_{\text{Straggling Out}} + \sigma^2_{\text{Detector}}. \tag{4.1}$$

$\sigma^2_{\text{Straggling Out}}$ is the variance of the energy distribution of the outgoing particles due to energy loss straggling, and $\sigma^2_{\text{Detector}}$ is the energy resolution of the detector.

The final contribution to the energy spectrum of each isotope in each sublayer is given by

$$S(E) = \int_0^\infty S_0(E') f(E', \sigma^2(E'))\, dE' \tag{4.2}$$

Here $S_0(E)$ is the energy spectrum before convolution and $S(E)$ the spectrum after the convolution. Note that the width of the Gaussian changes throughout the brick due to different straggling contributions.

[1] A 'backscattered' particle may be a recoil or a product in a nuclear reaction as well.

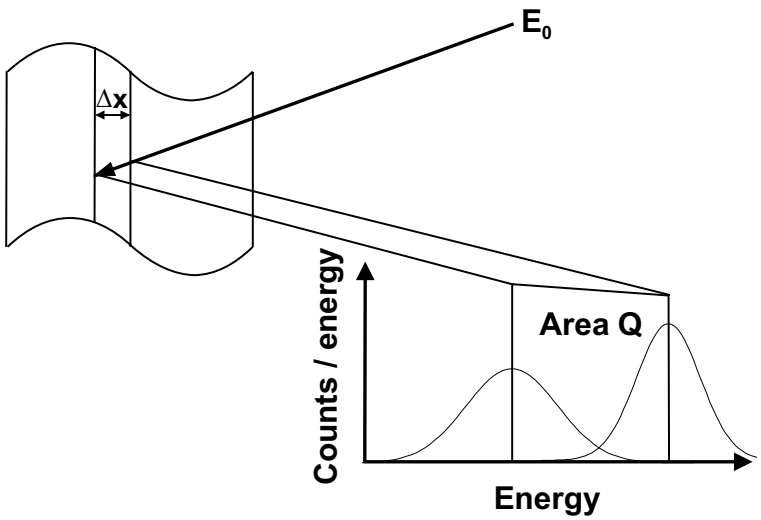

Figure 4.1.: Notation used for a single brick.

The Number of counts N_i in each channel i is given by integrating $S(E)$ over the channel width from the minimum to the maximum energy of each channel:

$$N_i = \int_{E_{min}(i)}^{E_{max}(i)} S(E')\,dE' \tag{4.3}$$

Equation 4.2 and Equation 4.3 can be put together into a 2-dimensional integral, which is computed by SIMNRA by means of a 2-dimensional Gauss-Legendre integration. The accuracy of the integration is about 10^{-4}.

The area Q of the brick in Figure 4.1 is calculated by using the integrated cross-section, see section 4.3, which is stable against fast varying structures in the cross-section, such as sharp resonances.

4.1. Atomic data

The masses of the elements and all isotopes used by SIMNRA have been taken from the recommended values of the 1995 update to the atomic mass evaluation [19]. The abundances of the isotopes have been taken from the recommended values of isotopic abundances in [20]. Isotopic masses and abundances are stored in the file ATOMDATA.DAT. This file contains also the data of some isotopes which do not occur naturally but may be created in nuclear reactions and are necessary for kinematic calculations.

4.2. Scattering kinematics

4.2.1. Elastic scattering

Energy of backscattered projectiles

The energy E_1 of a backscattered projectile with incident energy E_0 and mass M_1 after scattering is given in the laboratory system by

$$E_1 = E_0 \frac{M_1^2}{(M_1+M_2)^2} \left\{ \cos\theta \pm \left[\left(\frac{M_2}{M_1}\right)^2 - \sin^2\theta \right]^{1/2} \right\}^2 \tag{4.4}$$

θ is the scattering angle and M_2 the mass of the target nucleus initially at rest. For $M_1 < M_2$ only the plus sign in Equation 4.4 applies. If $M_1 > M_2$ then Equation 4.4 has two solutions, and the maximum possible scattering angle θ_{max} is given by

$$\theta_{max} = \arcsin\left(\frac{M_2}{M_1}\right). \tag{4.5}$$

The second solution for $M_1 > M_2$ is obtained because different impact parameters d result in the same scattering angle θ. Consider for example the scattering angle $\theta = 0$: This angle is obtained for a head-on collision with $d = 0$, but also for very large impact parameters $d \approx \infty$.

SIMNRA version 3.50 and higher uses both solutions of Equation 4.4, if kinematically possible. Earlier versions of SIMNRA used Equation 4.4 only with the plus sign, the solution with the minus sign was neglected.

Energy of recoils

The energy E_2 of a recoil is given in the laboratory system by

$$E_2 = E_0 \frac{4M_1M_2}{(M_1+M_2)^2} \cos^2\theta. \tag{4.6}$$

E_0 is the energy of the incident projectile, M_1 the mass of the projectile, M_2 the mass of the target nucleus initially at rest and θ the recoil angle, with $0° \le \theta \le 90°$.

4.2.2. Nuclear reactions

For the calculation of nuclear reactions kinematics we use the quantities listed in Table 4.1.

We define the following quantities:

$$A_{13} = \frac{M_1M_3}{(M_1+M_2)(M_3+M_4)} \frac{E_1}{E_T}$$

	Mass	Energy
Incident ion	M_1	E_1
Target nucleus	M_2	0
Light product	M_3	E_3
Heavy product	M_4	E_4
Energy released in reaction		Q
Total energy		$E_T = E_1 + Q = E_3 + E_4$

Table 4.1.: Quantities used for the calculation of nuclear reactions kinematics. The target nucleus is initially at rest. For exotherm reactions $Q > 0$, for endotherm reactions $Q < 0$.

$$
\begin{aligned}
A_{14} &= \frac{M_1 M_4}{(M_1+M_2)(M_3+M_4)} \frac{E_1}{E_T} \\
A_{23} &= \frac{M_2 M_3}{(M_1+M_2)(M_3+M_4)} \left(1 + \frac{M_1}{M_2}\frac{Q}{E_T}\right) \\
A_{24} &= \frac{M_2 M_4}{(M_1+M_2)(M_3+M_4)} \left(1 + \frac{M_1}{M_2}\frac{Q}{E_T}\right)
\end{aligned}
$$

The energy E_3 of the light product created in the nuclear reaction is then given in the laboratory system by

$$E_3 = E_T A_{13} \left[\cos\theta \pm \left(\frac{A_{24}}{A_{13}} - \sin^2\theta\right)^{1/2}\right]^2 \tag{4.7}$$

θ is the emission angle of the light product in the laboratory system. For $A_{13} < A_{24}$ only the plus sign in Equation 4.7 applies. If $A_{13} > A_{24}$ then eq. 4.7 has two solutions, and the maximum possible emission angle θ_{max} of the light product is

$$\theta_{max} = \arcsin\left(\frac{A_{24}}{A_{13}}\right)^{1/2} \tag{4.8}$$

The energy E_4 of the heavy product created in the nuclear reaction is given in the laboratory system by

$$E_4 = E_T A_{14} \left[\cos\Phi \pm \left(\frac{A_{23}}{A_{14}} - \sin^2\Phi\right)^{1/2}\right]^2 \tag{4.9}$$

Φ is the emission angle of the heavy product in the laboratory system. For $A_{14} < A_{23}$ only the plus sign in Equation 4.9 applies. If $A_{14} > A_{23}$ then Equation 4.9 has two solutions, and the

maximum possible emission angle Φ_{max} of the heavy product is

$$\Phi_{max} = \arcsin\left(\frac{A_{23}}{A_{14}}\right)^{1/2} \tag{4.10}$$

SIMNRA uses Equation 4.7 and Equation 4.9 only with the plus sign. The second solution is neglected.

4.3. Number of backscattered particles

The number of backscattered particles Q (i.e. the area of the brick in Figure 4.1) from a thin layer with thickness Δx can be calculated by using the cross-section at the mean energy $\bar{E}$ in the layer:

$$Q = \frac{N\Delta\Omega}{\cos\alpha}\,\sigma(\bar{E})\,\Delta x, \tag{4.11}$$

with $N\Delta\Omega$ the number of incident particles times the solid angle of the detector, $\sigma(\bar{E})$ the differential cross-section evaluated at the mean energy $\bar{E}$, and α the angle of incidence. SIMNRA 5.01 and earlier used Equation 4.11 for the calculation of the number of backscattered particles. This is, however, only valid if the layer is sufficiently thin, i.e. if the energy loss in the layer is small enough, so that the cross-section does not change strongly. If the cross-section has structures such as sharp resonances, this usually requires very thin layers, which cannot be guaranteed if *Automatic* step width control is used, see subsection 3.6.3.

A more accurate approximation than Equation 4.11 is obtained by integrating Equation 4.11:

$$Q = \frac{N\Delta\Omega}{\cos\alpha}\int_{x_0}^{x_1}\sigma(E(x))\,dx \tag{4.12}$$

$$= \frac{N\Delta\Omega}{\cos\alpha}\int_{E_0}^{E_1}\sigma(E)\frac{dx}{dE}\,dE \tag{4.13}$$

with x_0 and x_1 the start and end depths of the thin layer, and $E_0 = E(x_0)$, $E_1 = E(x_1)$ the corresponding energies. By assuming a constant stopping power $S = dE/dx(\bar{E})$ throughout the layer, we get $E(x) = E_0 - Sx$, and

$$Q = \frac{N\Delta\Omega}{\cos\alpha}\,\frac{1}{S}\int_{E_1}^{E_0}\sigma(E)\,dE. \tag{4.14}$$

Equation 4.14 is used by SIMNRA 5.02 and higher, providing a higher accuracy and better stability than Equation 4.11 in the case of narrow structures in the cross section. While Equation 4.11 neglects all stopping power effects, Equation 4.14 takes a constant stopping power into account, neglecting effects due to the variation of the stopping power.

4.4. Cross-section data

4.4.1. Rutherford cross-sections

The Rutherford cross-section for backscattering is given in the laboratory system by

$$\sigma_R\,[\mathrm{mb/sr}] = 5.1837436 \times 10^6 \left(\frac{Z_1 Z_2}{E\,[\mathrm{keV}]}\right)^2 \frac{\left\{\left(M_2^2 - M_1^2 \sin^2\theta\right)^{1/2} + M_2 \cos\theta\right\}^2}{M_2 \sin^4\theta \left(M_2^2 - M_1^2 \sin^2\theta\right)^{1/2}} \tag{4.15}$$

θ is the scattering angle, Z_1 and M_1 are the nuclear charge and the mass of the projectile, respectively, and Z_2 and M_2 are the nuclear charge and the mass of the target atom, respectively. σ_R is the differential cross-section in the laboratory system[2].

Experimental measurements indicate that actual cross-sections deviate from Rutherford at both high and low energies for all projectile-target pairs. The low-energy departures are caused by partial screening of the nuclear charges by the electron shells surrounding both nuclei [21, 22, 23, 9]. This screening is taken into account by a correction factor F:

$$\sigma = F\sigma_R$$

For $\theta > 90°$ the correction factor by L'Ecuyer *et al.* [21] is widely used:

$$F_{\text{L'Ecuyer}} = 1 - \frac{0.04873\, Z_1 Z_2^{4/3}}{E_{CM}} \tag{4.16}$$

E_{CM} is the energy in the center of mass system (in keV). Tabulated values of $F_{\text{L'Ecuyer}}$ can be found for example in [9]. But note, that L'Ecuyer used the factor 0.049 instead of the correct 0.04873 [24] in his original article. The correction for backscattering angles $\theta > 90°$ at typical energies used in ion beam analysis usually is small. For 1 MeV ^{4}He ions on gold the correction is only about 3.5%.

The correction factor by L'Ecuyer (Equation 4.16) is a first order correction and does not take into account the influence of the scattering angle θ. For $\theta < 90°$ Equation 4.16 will underestimate the necessary correction to the Rutherford cross-section. A more accurate approximation is the angular- and energy dependent correction factor by Andersen *et al.* [23]:

$$F_{\text{Andersen}} = \frac{\left(1 + \frac{1}{2}\frac{V_1}{E_{CM}}\right)^2}{\left\{1 + \frac{V_1}{E_{CM}} + \left[\frac{V_1}{2E_{CM}\sin\theta_{CM}/2}\right]^2\right\}^2} \tag{4.17}$$

[2] For $M_1 > M_2$ there may exist two different solutions of the kinematic equation Equation 4.4. The cross-section given by Equation 4.15 applies for the solution with the plus sign. The cross-section for the second solution of Equation 4.4 is obtained by calculating the scattering angle in the centre-of-mass system θ_{CM} from $\theta_{CM} = \theta - \arcsin[M_1/M_2 \sin\theta] + \pi$, calculating the Rutherford backscattering cross-section in the centre-of-mass system and transforming into the laboratory system.

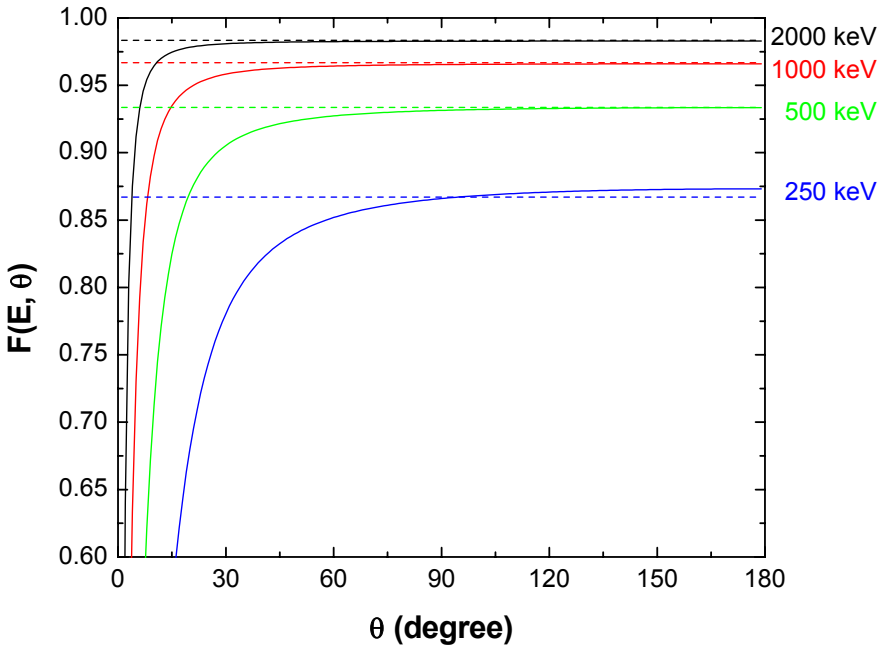

Figure 4.2.: Angular dependence of the correction factors for the Rutherford cross-section by L'Ecuyer (Equation 4.16, dashed lines) and Andersen (Equation 4.17, solid lines) for ^{4}He backscattered from gold at different energies.

θ_{CM} is the scattering angle in the center of mass system. The increase in the kinetic energy V_1 is given by

$$V_1\,[\mathrm{keV}] = 0.04873\, Z_1 Z_2 \left(Z_1^{2/3} + Z_2^{2/3}\right)^{1/2}$$

The dependence of the correction factor F_{Andersen} from the scattering angle θ for ^{4}He scattered from gold is shown in Figure 4.2 for different ^{4}He energies. Dashed lines are the angular independent correction factor by L'Ecuyer. For large scattering angles the correction factors by L'Ecuyer and Andersen are near to unity and similar, however, for small scattering angles the correction by Andersen becomes large and the angle-independent L'Ecuyer correction underestimates the deviations from the Rutherford cross-section.

The Rutherford cross-section for recoils is given in the laboratory system by

$$\sigma_R^{ERD}\,[\mathrm{mb/sr}] = 2.0731 \times 10^7 \frac{\left[Z_1 Z_2 (M_1 + M_2)\right]^2}{\left(2 M_2 E\,[\mathrm{keV}]\right)^2 \cos^3\theta} \tag{4.18}$$

θ is the recoil angle in the lab system. SIMNRA applies the correction to the Rutherford cross-section from Equation 4.17 also for the recoil cross-section.

4.4.2. Non-Rutherford cross-sections

High energy deviations

At high energies the cross-sections deviate from Rutherford due to the influence of the nuclear force. A useful formula above which energy E_{NR} deviations from Rutherford can be expected was given by Bozoian [25, 26, 27]:

$$E_{NR}\,[\mathrm{MeV}] = \frac{M_1 + M_2}{M_2}\frac{Z_2}{10} \quad \text{for } Z_1 = 1$$
$$E_{NR}\,[\mathrm{MeV}] = \frac{M_1 + M_2}{M_2}\frac{Z_1 Z_2}{8} \quad \text{for } Z_1 > 1$$

E_{NR} is the energy at which the deviation from the Rutherford cross-section gets $> 4\%$.

SIMNRA does not check if the cross-sections at a given energy are Rutherford or not. It is in the responsibility of the user to choose the correct cross-sections. The above formulas may be useful to estimate if the cross-section is still Rutherford or not.

For non-Rutherford cross-sections SIMNRA uses experimentally determined differential cross-sections taken from SigmaBase. The use of non-Rutherford cross-sections is described in full detail in section 3.8. SIMNRA uses linear interpolation between the given data points.

Mott scattering

The scattering of identical particles in forward direction (such as ^{4}He on ^{4}He, ^{12}C on ^{12}C, ^{28}Si on ^{28}Si etc.) results in a quantum-mechanical interference term and deviates from Rutherford scattering already at low energies [28, 29]. This is called Mott scattering and is shown in Figure 4.3. The Rutherford cross-section is a linear superposition of the Rutherford scattering and recoil cross-sections from Equation 4.15 and Equation 4.18. The experimental data deviate significantly from the Rutherford prediction and have to be described by the Mott cross-section. This case may occur in heavy ion ERDA, if the incident ion is present as element in the sample.

Warning: Mott scattering is currently not implemented in SIMNRA. The use of Rutherford scattering and recoil cross-sections for identical particles in forward direction ($0° \leq \theta \leq 90°$) may result in incorrect cross-section data. If you apply scattering of identical particles, do not use Rutherford scattering- and recoil cross-sections in the *Reactions* menu (section 3.8). Define a reaction cross-section according to the Mott scattering formula.

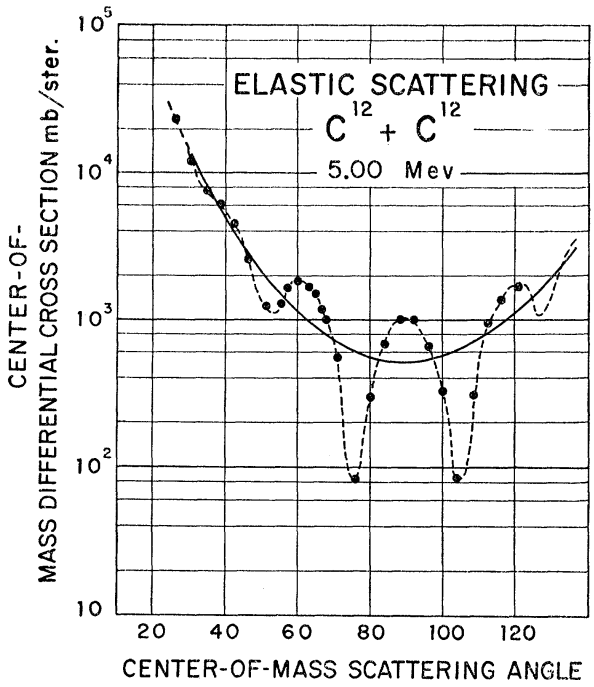

Figure 4.3.: Angular distribution for elastic scattering of ^{12}C on ^{12}C at a center-of-mass energy of 5 MeV. The solid curve is the Rutherford prediction; the dashed curve is the Mott prediction. Dots are experimental data. From [29].

4.5. Evaluation of energy loss

The energy E of a particle after passing through a layer of material with thickness x is given by the integral equation

$$E(x) = E_0 - \int_0^x \frac{dE}{dx'}(E(x'), x')dx' \tag{4.19}$$

Here we assume that the particle starts with initial energy E_0 at the surface ($x = 0$), and $dE/dx'(E(x'), x')$ is the energy and depth dependent stopping power. x is the path length into the material, measured in areal density (10^{15} atoms/cm^2). By differentiating Equation 4.19, we obtain the differential equation

$$\frac{dE}{dx} = -\epsilon(E), \tag{4.20}$$

where this is the defining equation for $\epsilon(E)$, the energy dependent stopping cross-section.

All SIMNRA versions before 5.70 used the algorithm of Doolittle for the evaluation of energy loss, initially developed for the RUMP program [17]. Doolittle expands the particle energy into a Taylor series, and the energy E_1 after a layer of material with thickness Δx, is given by

$$E_1 = E_0 + \Delta x \frac{dE}{dx}(E_0) + \frac{1}{2}\Delta x^2 \frac{d^2E}{dx^2}(E_0) + \frac{1}{6}\Delta x^3 \frac{d^3E}{dx^3}(E_0) \tag{4.21}$$

where $\epsilon' = d\epsilon/dE$ is the first and $\epsilon'' = d^2\epsilon/dE^2$ the second derivative of ϵ. ϵ, ϵ' and ϵ'' are evaluated at the incident energy E_0. The terms in Equation 4.21 look as follows:

$$\frac{dE}{dx} = -\epsilon \tag{4.22}$$

$$\frac{d^2E}{dx^2} = \frac{d}{dx}(-\epsilon) = -\frac{d\epsilon}{dE}\frac{dE}{dx} = \epsilon'\epsilon \tag{4.23}$$

$$\frac{d^3E}{dx^3} = \frac{d}{dx}(\epsilon'\epsilon) = \frac{d\epsilon'}{dx}\epsilon + \epsilon'\frac{d\epsilon}{dx} = -\epsilon''\epsilon^2 - \epsilon'^2\epsilon \tag{4.24}$$

With ϵ, ϵ' and ϵ'' evaluated at E_0. This gives the final result

$$E_1 = E_0 - \Delta x\epsilon + \frac{1}{2}\Delta x^2\epsilon\epsilon' - \frac{1}{6}\Delta x^3\left(\epsilon''\epsilon^2 + \epsilon'^2\epsilon\right) \tag{4.25}$$

ϵ' and ϵ'' were calculated by SIMNRA by numerical differentiation of the stopping power data.

Mayor disadvantage of Equation 4.25 is the need of the first and second derivative of the stopping power. Stopping powers supplied by the SRIM program don't have smooth derivatives, and the use of Equation 4.25 can result in large errors (see below). Moreover, Equation 4.25 does not provide a criterion how to select the step width Δx in order to obtain a desired accuracy, and it does not provide an error estimate.

Therefore Equation 4.25 was replaced by a more accurate and stable Runge-Kutta algorithm in SIMNRA 5.70 [12]. Equation 4.20 is a first order differential equation with initial values

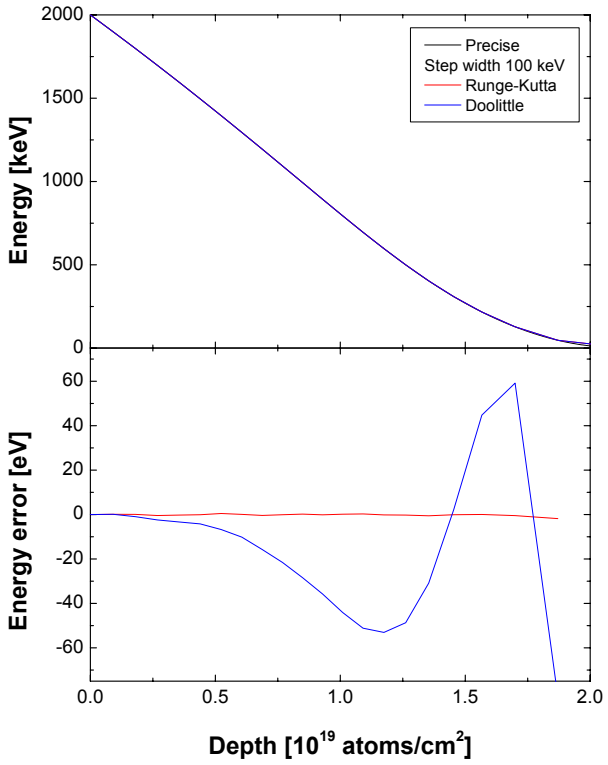

Figure 4.4.: Slowing down of 2 MeV ^{4}He in Au with Ziegler/Biersack stopping, calculated with different numerical methods. Top: ^{4}He energy as a function of depth. Bottom: Error of the calculated energy. The 'Precise' result was obtained with a Runge-Kutta method using a step width of 1 keV.

$E(x=0)=E_0$ and $dE/dx(x=0)=-\epsilon(E_0)$. SIMNRA uses a fifth order Runge-Kutta method with embedded forth order Runge-Kutta with Cash-Karp parameters for an error estimate and automatic step width control [12]. The error is some eV for energy losses of the order of 1 MeV.

The energy loss of ^{4}He ions in Au and the numerical error of the energy loss calculation are shown in Figure 4.4 for Ziegler/Biersack stopping. The Ziegler/Biersack stopping, as used by SIMNRA (see subsection 4.6.2, especially section 4.6.2), is smooth with continuous second derivative due to spline interpolation of the input data, and the energy loss calculation according to Doolittle's formula (Equation 4.25) results in a maximum error of about 50 eV. Runge-Kutta with identical step width is more accurate, with a maximum error below 1 eV. The same calculation, but with SRIM 2003 stopping powers, is shown in Figure 4.5. The SRIM 2003 stopping power has no continuous derivative, and Doolittle's method results in serious deviations. The Runge-Kutta method still gives accurate results with a maximum error of about 20 eV.

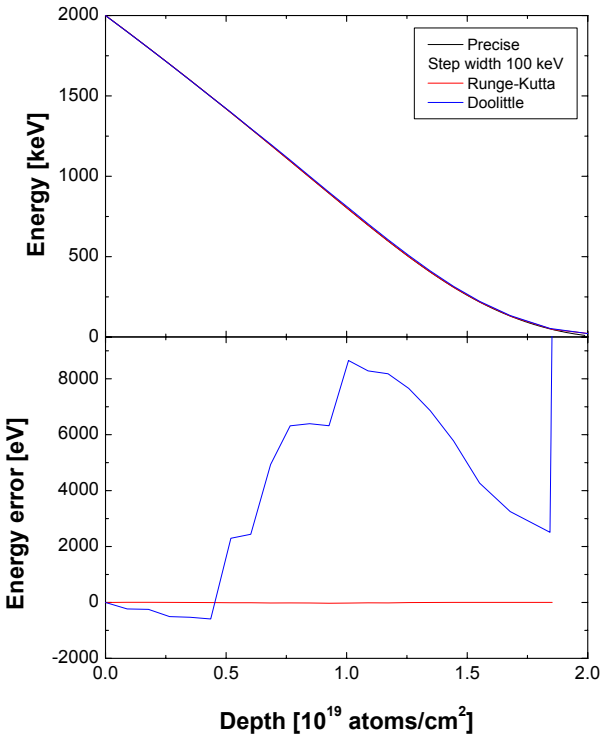

Figure 4.5.: Slowing down of 2 MeV ^{4}He in Au with SRIM 2003 stopping, calculated with different numerical methods. Top: ^{4}He energy as a function of depth. Bottom: Error of the calculated energy. The 'Precise' result was obtained with a Runge-Kutta method using a step width of 1 keV.

4.6. Stopping power data

SIMNRA offers the possibility to use several different sets of electronic stopping power data for the stopping of light and heavy ions in all elements. The differences between the data sets are typically < 5%, but may be larger in some cases, especially for ions other than H or He. See [30, 31, 32] for a discussion of the accuracy of stopping powers. An up-to-date compilation of stopping power data can be found in [33].

4.6.1. Andersen-Ziegler stopping

Hydrogen

If Andersen-Ziegler stopping is selected SIMNRA uses the electronic stopping power data by Andersen and Ziegler [3] for the stopping of incident protons, deuterons and tritons in all elements. The electronic stopping power S_e in eV/(10^{15} atoms/cm^2) for an incident hydrogen ion with energy/mass E in keV/amu is given by

$$\frac{1}{S_e} = \frac{1}{S_{Low}} + \frac{1}{S_{High}} \tag{4.26}$$

with

$$S_{Low} = A_2 E^{0.45} \tag{4.27}$$

and

$$S_{High} = \frac{A_3}{E} \ln\left[1 + \frac{A_4}{E} + A_5 E\right] \tag{4.28}$$

$A_2 - A_5$ are fitting coefficients and tabulated in [3]. They are stored in the file STOPH.DAT. Equation 4.26 to Equation 4.28 are valid for 10 keV $\leq E <$ 1 MeV. For energies in the range 1 MeV–100 MeV the electronic stopping power S_e is given by

$$S_e = \frac{A_6}{\beta^2}\left[\ln\frac{A_7\beta^2}{1-\beta^2} - \beta^2 - \sum_{i=0}^{4} A_{i+8}(\ln E)^i\right] \tag{4.29}$$

$A_6 - A_{12}$ are tabulated in [3], $\beta = v/c$, with v the ion velocity and c the speed of light. Equation 4.29 is used only if the switch *High energy stopping* in the *Setup: Calculation* menu is checked. If unchecked, the program will use Equation 4.26 to Equation 4.28 at all energies. The program default is checked. The difference between Equation 4.26 and Equation 4.29 is small in most cases. The main problem using Equation 4.29 is that the first and second derivatives of Equation 4.26 and Equation 4.29 do not fit smoothly together at 1 MeV/amu. This may result in the appearance of kinks in the spectrum.

Nuclear stopping for incident hydrogen, deuterium and tritium ions is negligible for incident energies above about 10 keV/amu [3] and is neglected by SIMNRA.

Helium

If Andersen-Ziegler stopping is selected then for incident ^{3}He and ^{4}He ions the electronic stopping power data by Ziegler [4] are used for all elements. The electronic stopping power S_e in eV/(10^{15} atoms/cm^2) for incident ^{4}He ions with energy E in keV is given by

$$\frac{1}{S_e} = \frac{1}{S_{Low}} + \frac{1}{S_{High}} \tag{4.30}$$

with

$$S_{Low} = A_1 E^{A_2} \tag{4.31}$$

and

$$S_{High} = \frac{A_3}{E} \ln\left[1 + \frac{A_4}{E} + A_5 E\right] \tag{4.32}$$

$A_1 - A_5$ are fitting coefficients and tabulated in [4]. They are stored in the file STOPHE.DAT. Equation 4.30 to Equation 4.32 are valid for 1 keV $\leq E <$ 10 MeV. ^{4}He-stopping at higher energies (above 10 MeV) is not implemented in the program.

The stopping power of ^{3}He is identical to the stopping power of ^{4}He at the same velocity [4]. The stopping power of ^{3}He with energy E is obtained by taking the stopping power value at the energy $E(^4\text{He}) = 4/3\,E(^3\text{He})$. The stopping power for ^{3}He is valid in the energy range 10 keV $\leq E <$ 7.5 MeV.

Nuclear stopping for incident helium ions is calculated with the Krypton-Carbon (Kr-C) potential [34]. The nuclear stopping S_n in eV/10^{15} atoms/cm^2 for He-ions with incident energy E (in keV) is given by:

$$S_n = s_n \frac{8.462\, Z_1\, Z_2\, M_1}{(M_1 + M_2)\left(Z_1^{2/3} + Z_2^{2/3}\right)^{1/2}} \tag{4.33}$$

s_n is the reduced nuclear stopping and Z_1, M_1 are the nuclear charge and mass of the helium ion and Z_2, M_2 are the nuclear charge and mass of the target element. The reduced nuclear stopping s_n has the simple form

$$s_n = 0.5 \frac{\ln(1+\epsilon)}{\epsilon + 0.10718\,\epsilon^{0.37544}} \tag{4.34}$$

ϵ is the reduced energy and is given by

$$\epsilon = \frac{32.53\, M_2\, E}{Z_1 Z_2 (M_1 + M_2)\left(Z_1^{2/3} + Z_2^{2/3}\right)^{1/2}} \tag{4.35}$$

Nuclear stopping is only important at incident energies $E <$ 100 keV, at higher energies nuclear stopping becomes negligible.

Heavy ions

The electronic stopping power of heavy ions in all elements is derived from the stopping power of protons using Brandt-Kitagawa theory [5, 35]. The formalism is described in detail in ref. [5], a short overview is given in [35]. The screening length Λ (eq. 3-29 of ref. [5]) is multiplied by an empirical correction factor which has been digitised from fig. 3-25 of ref. [5]. The correction factor for all elements is stored in the file LCORRHI.DAT.

Note that the switch *High energy stopping* in the *Setup: Calculation* menu has influence on the calculation of the stopping power for heavy ions with incident energies above 1 MeV/amu.

Nuclear stopping for incident heavy ions is calculated with the universal potential from ref. [5]. The reduced nuclear stopping s_n with the universal potential is given by

$$s_n = \frac{\ln(1 + 1.1383\,\epsilon)}{2\left[\epsilon + 0.01321\,\epsilon^{0.21226} + 0.19593\,\epsilon^{0.5}\right]} \tag{4.36}$$

for $\epsilon \leq 30$. For $\epsilon > 30$ s_n is given by

$$s_n = \frac{\ln(\epsilon)}{2\epsilon} \tag{4.37}$$

The reduced energy ϵ in Equation 4.36 and Equation 4.37 is calculated using the universal screening length a_U, which is $\propto 1/(Z_1^{0.23} + Z_2^{0.23})$ instead of the Firsov screening length $a_F \propto 1/(Z_1^{2/3} + Z_2^{2/3})^{1/2}$, which is used in Equation 4.35. The difference between Equation 4.34 and Equation 4.36 is only some percent.

The nuclear stopping component for heavy ions may be large and cannot be neglected.

4.6.2. Ziegler-Biersack stopping

Hydrogen

If Ziegler-Biersack stopping is selected SIMNRA uses the electronic stopping power data by Ziegler, Biersack and Littmark [5] for the stopping of incident protons, deuterons and tritons in all elements. The electronic stopping power S_e in eV/(10^{15} atoms/cm^2) for an incident hydrogen ion with energy/mass E in keV/amu is given by

$$S_e = \frac{S_{Low} S_{High}}{S_{Low} + S_{High}} \tag{4.38}$$

with

$$S_{Low} = C_1 E^{C_2} + C_3 E^{C_4} \tag{4.39}$$

and

$$S_{High} = \frac{C_5}{E^{C_6}} \ln\left(\frac{C_7}{E} + C_8 E\right) \tag{4.40}$$

$C_1 - C_8$ are fitting coefficients and partly tabulated in [35]. They are stored in the file SCOEF.95A for all elements. Equation 4.38 to Equation 4.40 are valid in the energy range 10 keV/amu $\leq$

$E < 10$ MeV/amu. For energies in the range 10–100 MeV/amu the electronic stopping power S_e is given by

$$S_e = C_9 + C_{10}x + C_{11}x^2 + \frac{C_{12}}{x} \tag{4.41}$$

with $x = \ln(E)/E$. $C_9 - C_{12}$ are fitting coefficients and tabulated in the file SCOEF.95B.

For energies below 10 keV/amu the electronic stopping power S_e is given by

$$S_e(E) = S_e(10)\left(\frac{E}{10}\right)^y \tag{4.42}$$

where $S_e(10)$ is the stopping power at 10 keV/amu and $y = 0.45$ for $Z_2 > 6$ and $y = 0.35$ for $Z_2 \leq 6$.

Nuclear stopping for incident hydrogen, deuterium and tritium ions is negligible for incident energies above about 10 keV/amu [3] and is neglected by SIMNRA.

Helium

If Ziegler-Biersack stopping is selected then for incident ^{3}He and ^{4}He ions the electronic stopping power data by Ziegler, Biersack and Littmark [5] are used for all elements.

The electronic stopping of He ions in elements S_e is derived from the stopping power of protons for the same velocity S_p by using [5, 35]

$$S_e = S_p\left(\gamma_{He} Z_{He}\right)^2 \tag{4.43}$$

Z_{He} is the helium charge and γ_{He} can be obtained from the simple polynomial fit

$$\gamma_{He}^2 = 1 - \exp\left[-\sum_{i=0}^{5} C_i E^i\right] \tag{4.44}$$

with E in keV/amu. The coefficients C_i are tabulated in [35].

Nuclear stopping for incident helium ions is calculated with the universal ZBL potential [5]. The nuclear stopping S_n in eV/10^{15} atoms/cm^2 for He-ions with incident energy E (in keV) is given by:

$$S_n = s_n \frac{8.462\, Z_1\, Z_2\, M_1}{(M_1 + M_2)\left(Z_1^{0.23} + Z_2^{0.23}\right)} \tag{4.45}$$

s_n is the reduced nuclear stopping and Z_1, M_1 are the nuclear charge and mass of the helium ion and Z_2, M_2 are the nuclear charge and mass of the target element. The reduced nuclear stopping s_n has the simple form

$$s_n = \frac{\ln(1 + 1.1383\epsilon)}{2(\epsilon + 0.01321\,\epsilon^{0.21226} + 0.19593\,\epsilon^{0.5}} \tag{4.46}$$

for $\epsilon \leq 30$ and

$$s_n = \frac{\ln \epsilon}{2\epsilon} \tag{4.47}$$

for $\epsilon > 30$. ϵ is the reduced energy and is given by

$$\epsilon = \frac{32.53\, M_2\, E}{Z_1 Z_2 \left(M_1 + M_2\right) \left(Z_1^{0.23} + Z_2^{0.23}\right)} \tag{4.48}$$

Nuclear stopping is only important at incident energies $E < 100$ keV, at higher energies nuclear stopping becomes negligible.

Heavy ions

The electronic stopping power of heavy ions in all elements is derived from the stopping power of protons using Brandt-Kitagawa theory [5, 35]. The formalism is described in detail in ref. [5], a short overview is given in [35]. Fermi velocities of all target elements are stored in the file SCOEF.95A, a small correction to the Fermi velocity in the file SCOEF.95B. The ion's screening length Λ as a function of fractional charge is stored in the file SCOEF.95B.

Nuclear stopping for incident heavy ions is calculated with the universal ZBL potential from ref. [5]. The formalism is the same as for He ions, see Equation 4.45 to Equation 4.48. For Z_1 and M_1 the ions nuclear charge and mass, respectively, have to be used.

The nuclear stopping component for heavy ions may be large and cannot be neglected.

Differences between SIMNRA and SRIM 97

The program SRIM (formerly TRIM) by J. Ziegler is a widely used program for stopping power and range calculations. If Ziegler-Biersack stopping is selected SIMNRA uses the same stopping power routines and input data as SRIM 97 for elemental targets. The routines for stopping power calculations have been taken from the SRIM source code, the input data have been taken from the SRIM distribution. For incident hydrogen and helium ions SIMNRA therefore uses exactly the same electronic and nuclear stopping powers as the SRIM program[3]. For incident heavy ions, however, there are *small* differences between SIMNRA and SRIM. SRIM uses linear interpolation for some input data, resulting in stopping powers with a noncontinuous derivative. SIMNRA uses spline interpolation instead of linear interpolation, resulting in stopping powers with continuous second derivative. The stopping powers calculated by SIMNRA are therefore more smooth than the original stopping powers calculated by SRIM, the differences are typically below 1%.

[3] For low energetic hydrogen ions ($E < 10$ keV) there are differences because SIMNRA neglects nuclear stopping of hydrogen.

4.6.3. KKK stopping

As was shown by Konac et al. [7, 8], the SRIM 97 stopping power values (which are used by SIMNRA if Ziegler/Biersack stopping is selected) are somewhat inaccurate for the stopping of ions in C and Si. Konac et al. fitted their experimental values with the formulas

$$S_e(E) = E^s \ln(e + \beta E)/P(E)P(E) = \alpha_0 + \alpha_1 E^{1/2} + \alpha_2 E + \alpha_3 E^{1+s}, \tag{4.49}$$

where the constants α_i, β and s are tabulated in [8]. S_e is the electronic stopping, E is in MeV/amu, and S_e is in eV/10^{15} atoms/cm^2. The fit is valid in the range $0.01 \leq E \leq 100$ MeV/amu. SIMNRA uses the KKK stopping for H, D, T, ^{3}He and ^{4}He in C and Si. Nuclear stopping is calculated using the universal potential, see subsection 4.6.2.

4.6.4. SRIM stopping

SRIM is a program for calculating stopping powers of ions ions matter. SRIM stopping is obtained by calling the SRIM program, which has to be downloaded and installed separarely. See the SRIM documentation for details of stopping power calculations.

4.6.5. Stopping in compounds

SIMNRA uses Bragg's rule [36] for the determination of the stopping power in compounds. Bragg's rule is a simple linear additivity rule of the stopping contributions of the different compound elements, assuming that the interaction of an incident ion with a target atom is independent of the surrounding target atoms. For a compound consisting of different elements i with atomic concentrations c_i ($\sum c_i = 1$) the total stopping power S is given by

$$S = \sum c_i S_i \tag{4.50}$$

S_i is the stopping power of each element.

Bragg's rule assumes that the interaction between the ion and the atom is independent of the environment. The chemical and physical state of the medium is, however, observed to have an effect on the energy loss. The deviations from Bragg's rule predictions are most pronounced around the stopping power maximum and for solid compounds such as oxides, nitrides and hydrocarbons. The deviations from Bragg's rule predictions may be of the order of 10–20% [35, 37]. For compounds with heavier atoms such as Fe_2O_3, NbC, NbN, Ta_2O_5, WO_3, Au alloys etc. deviations from Bragg's rule disappear (deviation $< 2\%$) [35, 38].

Ziegler and Manoyan [35] have developed the 'cores and bonds' (CAB) model, which assumes the electronic energy loss to have two contributions: The effect of the cores and the effect of the bonds, such as C-H and C-C. The CAB-model allows better predictions for the stopping in compounds, however, the bond structure has to be known. Currently the CAB-model (or any other model which allows better predictions for the stopping in compounds) is not implemented

in SIMNRA. However, a correction factor f may be used for each ion species and each layer, see section 3.7 for details. If a factor f is defined for a layer, then the program will use the stopping power $S(E)$, with E the ion energy,

$$S(E) = f\, S_{\mathrm{Bragg}}(E) \tag{4.51}$$

$S_{\mathrm{Bragg}}(E)$ is the stopping power according to Bragg's rule. Note that the factor f is energy independent.

4.7. Detector energy resolution

4.7.1. Time-of-flight detector

A time-of-flight (TOF) detector is characterized by its time resolution, which determines the energy resolution. The energy E is given by

$$\begin{aligned} E &= \frac{1}{2}mv^2 \\ &= \frac{1}{2}m\frac{L^2}{T^2}, \end{aligned}$$

where m is the ion mass, v the ion velocity, L the free flight path, and T the time of flight.

The energy resolution ΔE is determined from the time resolution ΔT according to

$$\begin{aligned} \Delta E &= m\frac{L^2}{T^3}\Delta T \\ &= 2E\frac{\Delta T}{T}. \end{aligned} \tag{4.52}$$

Equation 4.52 is used by SIMNRA to calculate the energy resolution of TOF detectors.

4.7.2. Electrostatic detector

The energy resolution of electrostatic detectors is given by the constant ratio

$$c = \frac{\Delta E}{E}, \tag{4.53}$$

with ΔE the detector energy resolution (full width at half maximum, FWHM) and E the particle energy. This relation is used for all particle species.

4.8. Straggling

4.8.1. Overview

When a beam of charged particles penetrates matter, the slowing down is accompanied by a spread in the beam energy. This phenomenon is called straggling. It is due to statistical fluctuations of the energy transfer in the collision processes.

Energy loss straggling has different contributions:

1. Electronic energy loss straggling due to statistical fluctuations in the transfer of energy to electrons.
2. Nuclear energy loss straggling due to statistical fluctuations in the nuclear energy loss.
3. Geometrical straggling due to finite detector solid angle and finite beam spot size, resulting in a distribution of scattering angles and different pathlengths for outgoing particles.
4. Straggling due to multiple small angle scattering, resulting in angular and energy spread on the ingoing and outgoing paths.
5. Straggling due to surface and interlayer roughness and thickness inhomogeneities of absorber foils.

An additional contribution to the energy broadening visible in experimental spectra is the energy resolution of the detector. The different straggling contributions (excluding roughness) have been reviewed by Szilágy *et. al.* [39, 40], and can be included in SIMNRA calculations. The details are described in the following sections.

4.8.2. Electronic energy loss straggling

There are four main theories describing electronic energy loss straggling [41, 42, 43], each applicable in a different regime of energy loss. With ΔE the mean energy loss of the beam, and E the energy of the incident beam, we can distinguish:

$\Delta E/E < 10\%$	**Vavilov's Theory**[44, 42]. For thin layers and small energy losses. The energy distribution is non-Gaussian and asymmetrical. This energy range is not described properly by SIMNRA.
$10 - 20\%$	**Bohr's Theory**[45, 46]. As the number of collisions becomes large, the distribution of particle energies becomes Gaussian.
$20 - 50\%$	**Symon's Theory**[41]. This theory includes non-statistical broadening caused by the change in stopping power over the particle energy distribution. If the mean energy of the beam is higher than the energy of the stopping power maximum, then particles with a lower energy have a higher stopping power, and particles with higher energy have a smaller stopping power. This results in a nonstatistical broadening of the energy distribution. The width of the particles energy distribution in Symon's theory is significantly higher than predicted by Bohr's theory. The distribution of particle energies is still Gaussian.
$50 - 90\%$	**Payne's and Tschalärs Theory** [47, 48, 49]. When the energy losses become very large and the mean energy of the beam decreases below the energy of the stopping power maximum, the particle energy distribution again become skewed, because now particles with lower energy have a lower stopping power than particles with higher energy. The distribution is about Gaussian.

SIMNRA always assumes that the particles energy distribution is Gaussian. This is only an approximation for thin layers: In this case the energy distribution is described by the Vavilov distribution [44, 42]. However, the straggling contribution of thin layers to the total energy broadening is much smaller than the contribution of the finite energy resolution of the detector.

SIMNRA calculates the non-statistic broadening (or skewing) of the energy distribution when penetrating a layer in the following way [39]:
Assume two particles with energies E_1 and E_2

$$\begin{aligned} E_1 &= E_0 + \frac{\Delta E}{2} \\ E_2 &= E_0 - \frac{\Delta E}{2} \end{aligned}$$

centered around a mean energy E_0. The energy difference $E_1 - E_2$ of the two particles is ΔE. After penetrating a layer the particles have the energies E_1' and E_2' centered around a mean

energy E_0'. The energy difference $\Delta E'$ behind the layer is given by

$$\Delta E' = \frac{\epsilon(E_0')}{\epsilon(E_0)}\Delta E = \frac{\epsilon_f}{\epsilon_i}\Delta E \tag{4.54}$$

with the stopping power $\epsilon = dE/dx$. ϵ_f is the stopping power at the exit of the layer and ϵ_i the stopping power at the entrance of the layer. If $\epsilon_f > \epsilon_i$, which is the case for all energies above the stopping power maximum, the energy difference increases and the distribution function is broadened. If $\epsilon_f < \epsilon_i$, the energy difference decreases and the distribution function gets skewed. The shape of the distribution remains unchanged: a Gaussian distribution remains gaussian, but the width of the Gaussian is changed according to Equation 4.54[4].

To the non-statistic broadening we have to add the statistical effects. When the incident beam with initial energy E_0 and initial beam width σ_0^2 (σ^2 is the variance of the energy distribution, the full width at half maximum (FWHM) is $2\sqrt{2\ln 2}\,\sigma = 2.355\,\sigma$) penetrates a layer of matter with thickness Δx, then the beam width σ_1^2 after penetrating the layer is given by:

$$\sigma_1^2 = \left(\frac{\epsilon_f}{\epsilon_i}\right)^2 \sigma_0^2 + \sigma^2 \tag{4.57}$$

ϵ_f and ϵ_i are the stopping powers of the material at the entrance and exit of the layer and σ^2 is the energy loss straggling in the layer. The first term in Equation 4.57 describes the non-statistical broadening of the beam according to Equation 4.54 due to the energy dependence of the stopping power, the second term adds the statistical effects.

The electronic energy-loss straggling in Bohr approximation σ_{Bohr}^2 is given by [45, 46]:

$$\sigma_{Bohr}^2\ [\mathrm{keV}^2] = 0.26\, Z_1^2\, Z_2\, \Delta x\ [10^{18}\,\mathrm{atoms/cm}^2] \tag{4.58}$$

In Chu's theory the Bohr straggling is modified by a correction factor H [50, 46]:

$$\sigma_{Chu}^2 = H(E/M_1, Z_2)\sigma_{Bohr}^2 \tag{4.59}$$

Bohr's theory of electronic energy loss straggling is valid in the limit of high ion velocities. In this case the electronic energy loss straggling is almost independent of the ion energy. For lower

[4] SIMNRA versions before 3.30 used the equation

$$\Delta E' = \left(1 - \frac{d\epsilon_i}{dE}\Delta x\right)\Delta E \tag{4.55}$$

instead of Equation 4.54. Equation 4.55 is obtained by a taylor expansion of ϵ_f around ϵ_i considering only the linear term:

$$\epsilon_f = \epsilon_i - \frac{d\epsilon}{dE}\epsilon_i \Delta x \tag{4.56}$$

where $d\epsilon/dE$ is the derivative of the stopping power and Δx the layer thickness. $\epsilon_i \Delta x$ is the energy loss in the layer. By putting the above equation into Equation 4.54 we obtain Equation 4.55. The difference between Equation 4.54 and the previously used Equation 4.55 is only 1-2% because of the relatively small stepwidths used by SIMNRA.

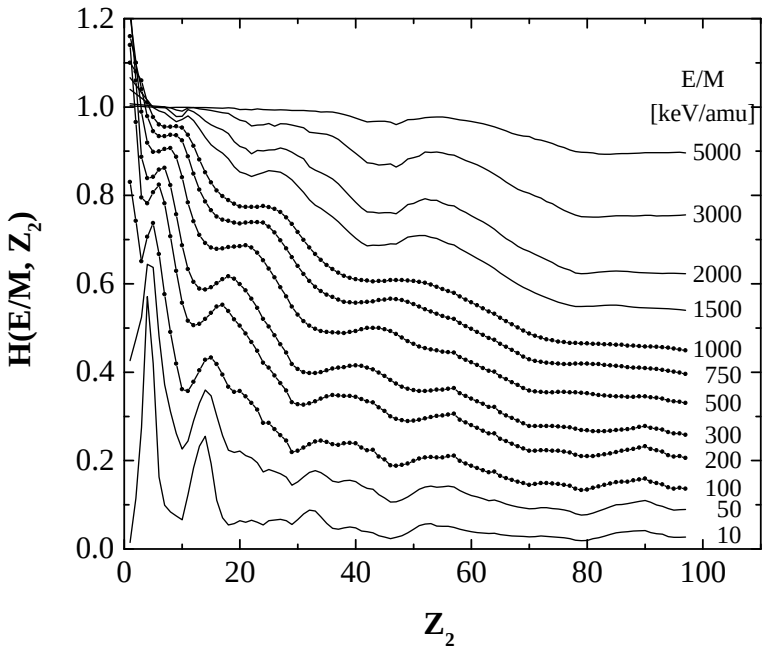

Figure 4.6.: The Chu straggling correction for several values of E/M_1 as a function of the nuclear charge of the target Z_2. Dots are original data from Chu [46], solid lines are extrapolated data taken from [39].

ion energies the Bohr straggling is multiplied by the Chu correction factor $H(E/M_1, Z_2)$, which depends only on E/M_1 and the nuclear charge of the target atoms Z_2. H takes into account the deviations from Bohr straggling caused by the electron binding in the target atoms. Chu [50, 46] has calculated H by using the Hartree-Fock-Slater charge distribution. This calculation gives straggling values which are considerably lower than those given by Bohr's theory. The correction factor H, as used by SIMNRA if Chu straggling is selected, is shown in Figure 4.6. The Z_2 oscillations are clearly visible. The Chu correction is mainly necessary for high Z_2 and low energies. For high energies H approaches 1 and becomes independent of Z_2 and energy. For E/M_1 values in the range 100–1000 keV/amu the data have been taken from ref. [46], data for lower and higher E/M_1 values are based on an extrapolation performed in ref. [39]. Tabulated values for H are stored in the file CHU_CORR.DAT. For not tabulated values SIMNRA uses linear interpolation.

Charge state fluctuations of the ions result in an additional straggling contribution, which was taken into account empirically by Yang et al. [51]. In Yang's theory, the total straggling is expressed by

$$\frac{\sigma^2_{Yang}}{\sigma^2_{Bohr}} = \gamma^2(Z_1, Z_2, \nu)\frac{\sigma^2_{Chu}}{\sigma^2_{Bohr}} + \frac{\Delta\sigma^2}{\sigma^2_{Bohr}}, \tag{4.60}$$

where $\gamma(Z_1, Z_2, v)$ is the effective charge factor for ions in matter, v the ion velocity, and $\Delta\sigma^2$ is the additional straggling due to correlation effects.

For hydrogen ions in matter, Yang always assumes a charge state of one, i.e. $\gamma = 1$. A fit to about 600 different empirical data points with a deformed resonant function gave

$$\left(\frac{\Delta\sigma^2}{\sigma^2_{Bohr}}\right)_H = \frac{B_1\Gamma}{(E-B_2)^2+\Gamma^2}, \tag{4.61}$$

with

$$\Gamma = B_3[1-\exp(-B_4E)], \tag{4.62}$$

where E is the energy in MeV/amu and B_1–B_4 are fitted constants.

Helium and heavier ions are not always fully stripped, but the charge state is a constantly changing parameter, fluctuating along the trajectory. The effective charge state $\gamma(Z_1, Z_2, v)$ was calculated by Ziegler [5], and is also used by Yang. The extra contribution to energy straggling $\Delta\sigma^2$ of helium and heavy ions is fitted by

$$\left(\frac{\Delta\sigma^2}{\sigma^2_{Bohr}}\right)_{HI} = \frac{Z_1^{4/3}}{Z_2^{1/3}}\frac{C_1\Gamma}{(\mathscr{E}-C_2)^2+\Gamma^2}, \tag{4.63}$$

with

$$\Gamma = C_3[1-\exp(-C_4\mathscr{E})], \tag{4.64}$$

and

$$\mathscr{E} = \frac{E}{Z_1^{3/2}Z_2^{1/2}}, \tag{4.65}$$

where E and $\mathscr{E}$ are the energies in MeV/amu and C_1–C_4 are fitted constants. The above equations are for solid targets.

Figure 4.7 compares the beam width (FWHM) of 2.5 MeV ^{4}He ions in silicon calculated by SIMNRA using Equation 4.57 with Bohr's theory. For small energy losses the beam width calculated by SIMNRA is slightly smaller than predicted by Bohr's theory due to the Chu correction. However, this is counterbalanced by the nonstochastic broadening due to the characteristics of the stopping power curve, and for larger energy losses the beam width gets larger than in Bohr's theory. When the mean beam energy has decreased below the energy of the stopping power maximum, the beam width becomes skewed.

As can be seen from Figure 4.6 the deviation of the Chu correction from Bohr's theory is largest for high Z_2 and low energies. Figure 4.8 shows the beam width (FWHM) of 1 MeV ^{4}He penetrating through gold. The deviation from Bohr's theory is large. The stopping power maximum is at about 960 keV. For low energy losses the beam width increases due to the statistical broadening because the nonstochastic skewing, which occurs for beam energies below the stopping power maximum, is small and the stochastic broadening wins. For larger energy losses however the beam width gets skewed.

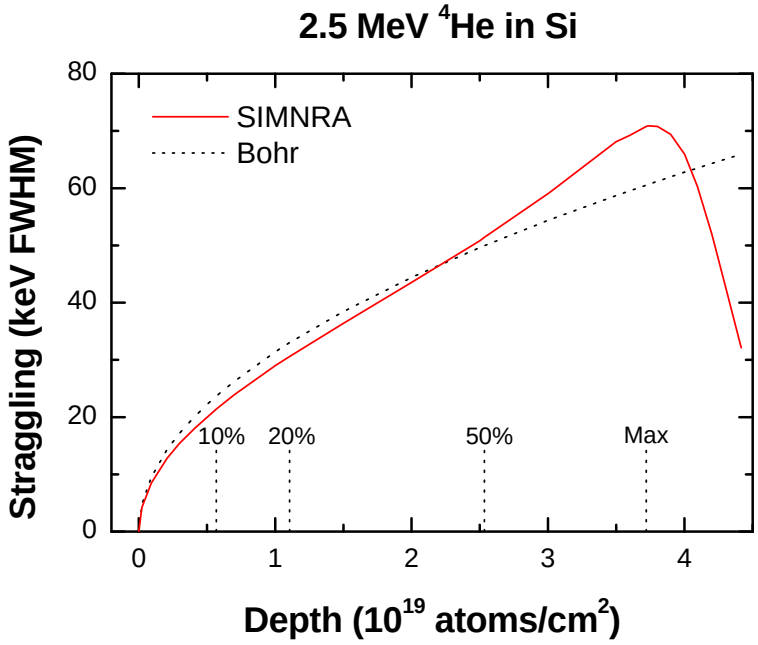

Figure 4.7.: Beam width (FWHM) of 2.5 MeV ^{4}He ions penetrating through silicon. The solid line is the beam width calculated by SIMNRA using Equation 4.57, the dashed line is the prediction of Bohr's theory. The vertical lines denote the mean depth at which the beam has lost 10%, 20% and 50% of its initial energy. Max denotes the depth at which the mean energy of the beam has decreased to the energy of the stopping power maximum.

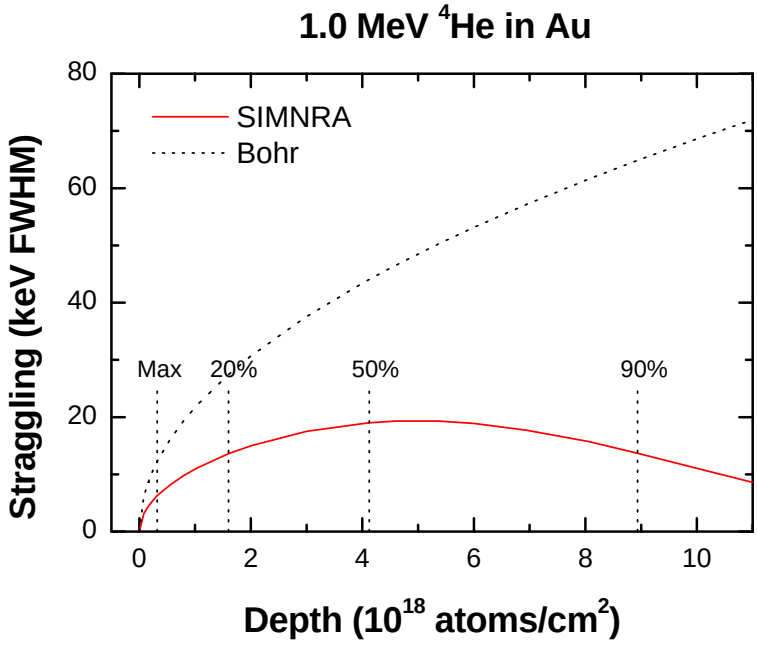

Figure 4.8.: Beam width (FWHM) of 1.0 MeV ^{4}He ions penetrating through gold. The solid line is the beam width calculated by SIMNRA using Equation 4.57, the dashed line is the prediction of Bohr's theory. The vertical lines denote the mean depth at which the beam has lost 20%, 50% and 90% of its initial energy. Max denotes the depth at which the mean energy of the beam has decreased to the energy of the stopping power maximum.

Figure 4.9 shows the measured RBS-spectrum for 1.0 MeV ^{4}He ions incident on a gold layer with a thickness of about 100 nm and a scattering angle of 165° compared with simulations using Bohr straggling and Chu straggling. As can be seen at the low energy edge of the layer, the Bohr straggling is broader than the experimental data. The Chu straggling fits the measured curve relatively well, except of the multiple scattering contribution.

The straggling of outgoing particles is calculated with Equation 4.57 as well. Outgoing particles always start with an energy distribution with variance σ^2_{out} which is given by

$$\sigma^2_{\text{out}} = K^2 \sigma^2_{\text{in}} \tag{4.66}$$

with K the kinematic factor and σ^2_{in} the variance of the energy distribution of the incident beam.

Accuracy of electronic energy-loss straggling calculations

SIMNRA uses Equation 4.57 for the calculation of straggling. However, Equation 4.57 is only correct for infinitesimal thin layers, i.e. if Δx (see Equation 4.58) is sufficiently small. It gets more and more inaccurate for thicker layers, because the straggling propagation for the second term in Equation 4.57 is neglected.

The error $\Delta\sigma^2$ for σ^2_1 (see Equation 4.57) can be estimated to be

$$\Delta\sigma^2 \leq \begin{cases} \left|1 - \left(\frac{\epsilon_f}{\epsilon_i}\right)^2\right| G\Delta x & \text{if } |1 - (\epsilon_f/\epsilon_i)^2| > 0.03 \\ 0.03\, G\Delta x & \text{else.} \end{cases} \tag{4.67}$$

G depends on theory: For Bohr straggling it is given by Equation 4.58, and for Chu and Yang straggling by Equation 4.59 and Equation 4.60, respectively. 0.03 is based on extensive tests of Equation 4.67: Using only the upper half of the equation results in unrealistically small error estimates (and too large step widths) around the stopping power maximum, where $\epsilon_f \approx \epsilon_i$ on both sides of the maximum.

The step width Δx for electronic energy-loss straggling calculations is selected in such a way, that

$$\frac{\Delta\sigma^2}{\sigma^2_1} \leq \delta, \tag{4.68}$$

where δ is the desired accuracy. SIMNRA uses a default of $\delta = 1\%$. An estimate of the accuracy of straggling calculations can be obtained with the program VIEWNRA.

An example for the accuracy of straggling calculations and the error estimate is shown in Figure 4.10. The error of the straggling calculation is obtained by comparison to a calculation with very small fixed step width. The error estimate based on Equation 4.67 gives the correct sign and magnitude of the real error.

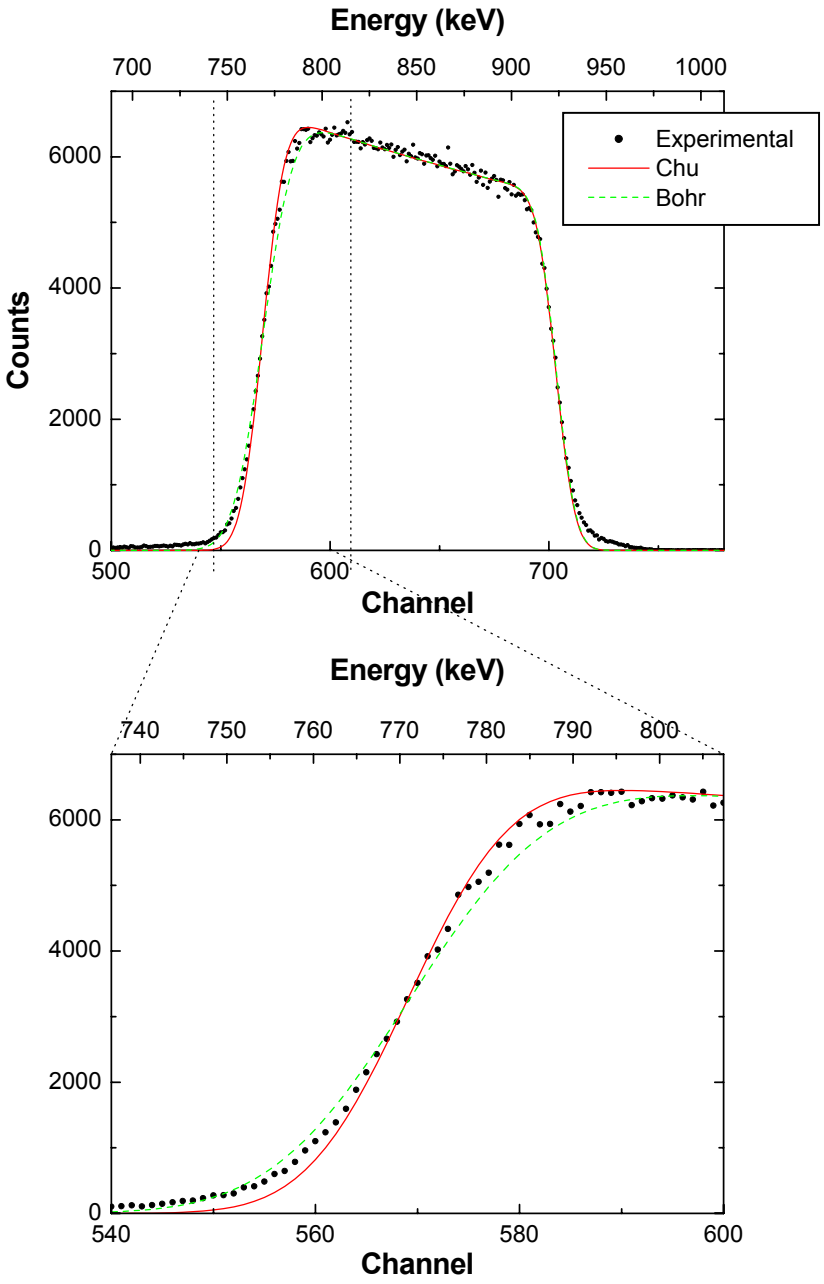

Figure 4.9.: Measured and simulated spectra using Bohr and Chu straggling of 1.0 MeV ^{4}He ions incident on 100 nm Au on Si, scattering angle 165°. Bottom: Magnification of the low energy gold edge.

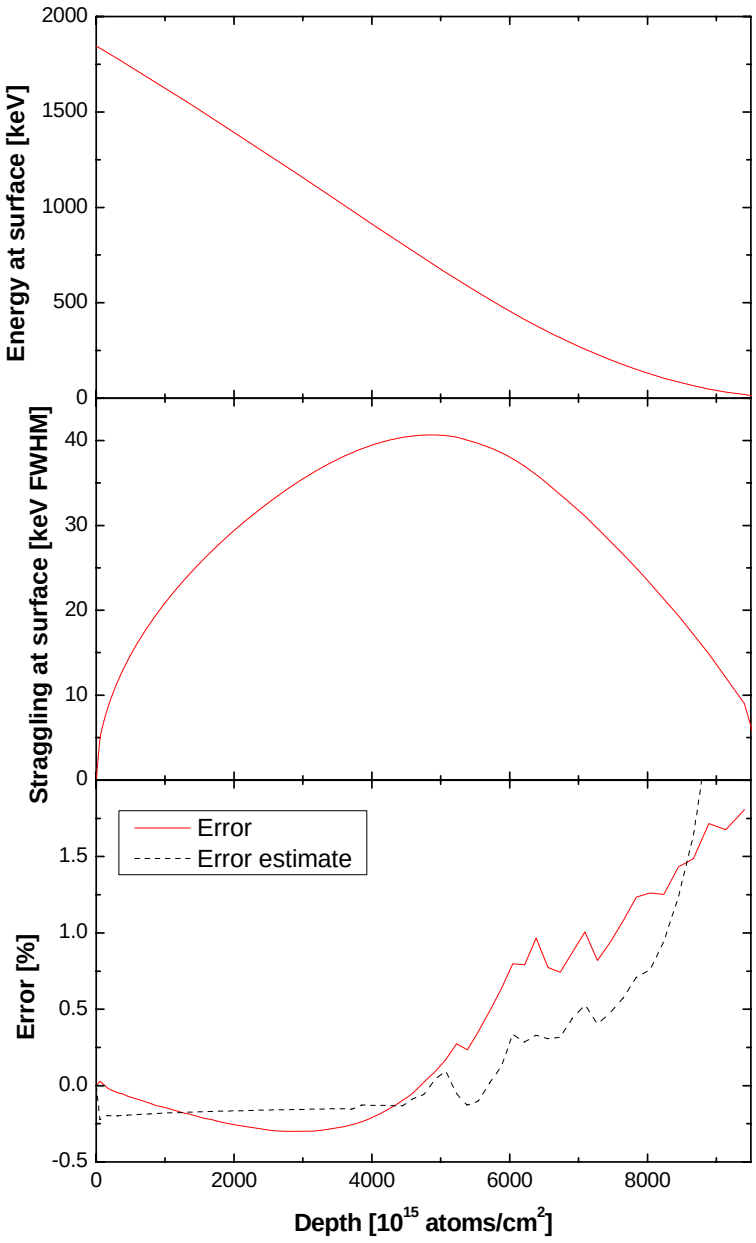

Figure 4.10.: Energy and energy loss straggling of backscattered ^{4}He ions at the target surface in Au. Incident angle $\alpha = 0°$, exit angle $\beta = 15°$, scattering angle $\theta = 165°$, Yang straggling. Top: Energy of backscattered ions at the target surface; Middle: Electronic energy-loss straggling at the target surface; Bottom: Error of the straggling calculation and error estimate based on Equation 4.67.

4.8.3. Nuclear energy loss straggling

Fluctuations in the number of nuclear collisions lead to nuclear energy loss straggling, which can be described by Bohr's theory of nuclear straggling. The variance σ_n^2 in Bohr's approximation is given by:

$$\sigma_n^2\,[\mathrm{keV}^2] = 0.26\, Z_1^2\, Z_2^2 \left(\frac{M_1}{M_1+M_2}\right)^2 \Delta x\;[10^{18}\,\mathrm{atoms/cm}^2] \tag{4.69}$$

Nuclear energy loss straggling is small compared to electronic energy-loss straggling for light ions (protons or helium ions), and can be neglected. Nuclear straggling becomes more important for heavy ions, and variance of nuclear straggling may exceed electronic energy-loss straggling, see Equation 4.58 and Equation 4.69. However, it has been shown experimentally for 60 MeV ^{58}Ni ions in different target materials, that the width of the total straggling distribution is only somewhat larger than electronic energy loss straggling alone [52]. The nuclear straggling energy distribution is broad with a long tail towards low energies, which cannot be described by a Gaussian distribution. This tail leads to the large variance of nuclear straggling. However, the tail contains only a small fraction of all particles, and the width of the total energy distribution (electronic plus nuclear straggling) is still dominated by electronic energy-loss straggling [52]. This justifies to neglect nuclear straggling for all ion species [5].

4.8.4. Energy loss straggling in compounds

For compounds a simple additivity rule for energy loss straggling is used [46]. The straggling in a compound consisting of elements i with atomic concentration c_i is calculated with

$$\sigma^2 = \sum_i c_i\, \sigma_i^2 \tag{4.70}$$

with σ_i^2 being the straggling in each element.

4.8.5. Geometrical straggling

The finite size of the incident beam and the width of the detector aperture result in a spread $\Delta\beta$ of the exit angle β for outgoing particles. This angular spread leads to different energies of the particles at the target surface due to

1. a spread $\Delta\theta$ of the scattering angle θ and therefore a spread of the transferred energy in the scattering process

[5] SIMNRA versions before 4.70 used a quadratic addition of the nuclear and electronic energy loss straggling contributions, i. e. $\sigma^2 = \sigma_n^2 + \sigma_e^2$, with σ_n^2 the variance of the nuclear straggling and σ_e^2 the variance of the electronic straggling. Due to the different shape of the two distributions this is incorrect and results in an overestimation of the total straggling. This error is negligible for light ions (H^+, He^+), but may play a role for heavy ions.

2. different path lengths of the outgoing particles in the material.

These two contributions to geometrical straggling are not independent of each other and have to be considered simultaneously.

The spread $\Delta\beta$ of the exit angle β is given by [53, 39]:

$$(\Delta\beta)^2 = \left(\frac{g_d w}{L_D}\right)^2 + \left(\frac{g_b d \cos\beta}{L_D \cos\alpha}\right)^2 \tag{4.71}$$

where d is the diameter of the incident beam[6], w is the width of the detector aperture and L_D is the distance between the sample and the detector aperture, see Figure 3.4. g_b and g_d take into account the shapes of the beam and the detector aperture. For circular detectors or circular beams with uniform current density $g = 0.59$. $g = 0.68$ for rectangular shapes, as in the case of narrow slits [53].

SIMNRA calculates geometrical straggling by calculating the energy at the surface of particles with exit angles $\beta - \Delta\beta/2$ and $\beta + \Delta\beta/2$ and corresponding scattering angles $\theta - \Delta\theta/2$ and $\theta + \Delta\theta/2$. The spread of θ is given by

$$\Delta\theta = \frac{\partial\theta}{\partial\beta}\Delta\beta. \tag{4.72}$$

This equation can be solved only if the relation between β and θ is known.

In IBM geometry (see Figure 3.10 and section 3.9) the incident and outgoing trajectories are in the same plane with

$$180^\circ = \alpha + \beta + \theta. \tag{4.73}$$

The spread in θ is then simply given by

$$\Delta\theta = -\Delta\beta. \tag{4.74}$$

Note the minus sign: If β increases then θ decreases and vice versa.

In Cornell geometry (see Figure 3.10 and section 3.9) the relation between the angles α, β and θ is given by

$$\cos\beta = -\cos\theta\,\cos\alpha, \tag{4.75}$$

and the spread of θ can be obtained from

$$\frac{\partial\theta}{\partial\beta} = -\frac{1}{\sin\theta}\frac{\sin\beta}{\cos\alpha}. \tag{4.76}$$

In general geometry the relation between the angles α, β and θ is undefined, and $\partial\theta/\partial\beta$ cannot be determined. *Calculation of geometrical straggling is not possible for general geometry.* Geometrical straggling is only calculated for IBM and Cornell geometries. SIMNRA will automatically determine if IBM or Cornell geometry is present.

[6] Note that the beam spot size on the sample surface is $d/\cos\alpha$.

Energy loss straggling, geometrical straggling and the detector resolution are independent and are added quadratically.

Figure 4.11 gives as examples the different straggling contributions at the sample surface for 2.6 MeV ^{4}He incident on $C_{0.99}D_{0.01}$ as a function of depth for typical RBS and ERDA geometries. An energy independent detector resolution of 15 keV FWHM is used. For RBS geometry the contribution of geometrical straggling is small compared to energy loss straggling and the resolution of the detector and may be neglected without penalty. For the ERDA geometry however, geometrical straggling cannot be neglected. Note that geometrical straggling first decreases until it reaches zero and then increases again. This is due to the minus-sign in Equation 4.74: If the exit angle β decreases (the outgoing path is closer to the surface normal) then the scattering angle θ increases: The backscattered or recoiled particles start with a smaller energy. However, the path length in the material is smaller due to the exit angle which is closer to normal resulting in a smaller energy loss. Near the surface the path lenght differences are small and geometrical straggling is governed by the kinematic spread. With increasing depth the two effects compensate each other more and more until in large depths the path length differences become dominant and geometrical straggling increases.

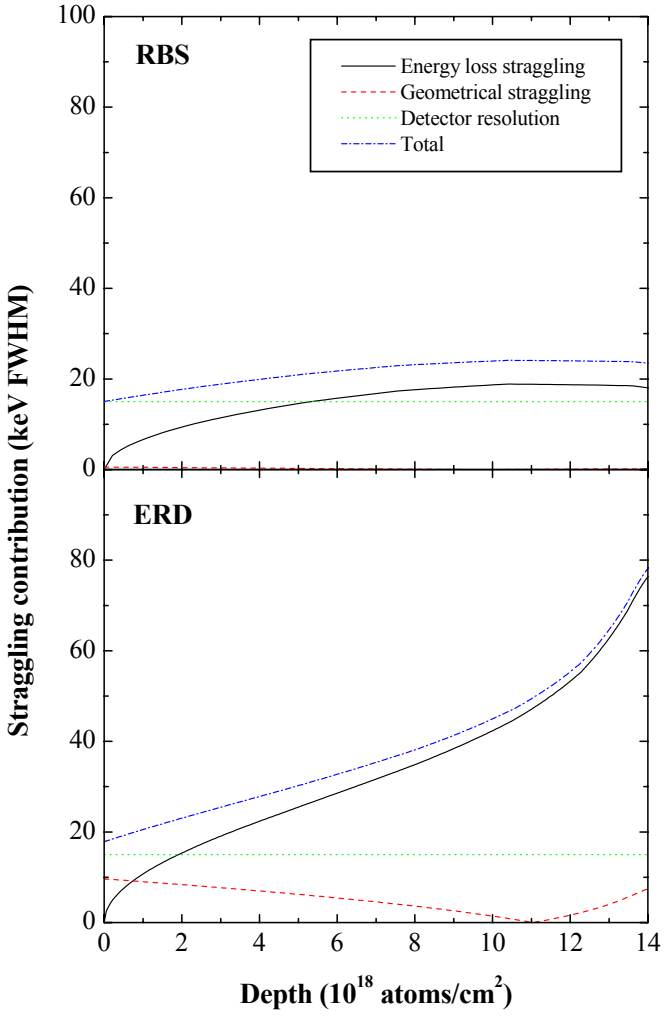

Figure 4.11.: Contributions of electronic energy loss straggling, geometrical straggling and detector resolution to the total energy straggling at the sample surface for 2.6 MeV ^{4}He incident on $C_{0.99}D_{0.01}$. Beam diameter 0.5 mm, aperture width 0.5 mm, distance sample-detector aperture 100 mm, detector resolution 15 keV FWHM.
Top: RBS geometry with $\theta = 165°$, $\alpha = 0°$, $\beta = 15°$ for ^{4}He backscattered from ^{12}C.
Bottom: ERDA geometry with $\theta = 30°$, $\alpha = 75°$, $\beta = 75°$ for the deuterium recoils.

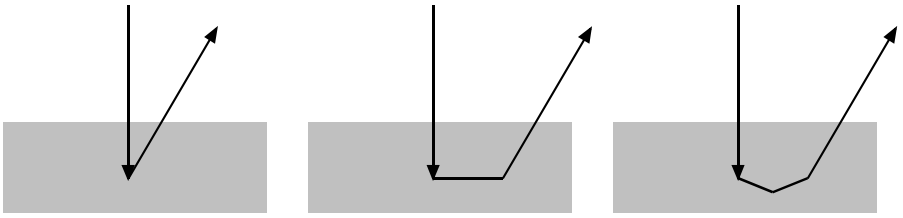

Figure 4.12.: Examples of ion trajectories with one, two and three scattering events.

4.9. Multiple and plural scattering

4.9.1. Overview

SIMNRA uses straight lines as trajectories for the ingoing and outgoing particles, with one single scattering event connecting the trajectories of the particles, see Figure 4.12 left. This is only an approximation to physical reality, because the particles on the ingoing and outgoing path suffer many small angle deflections with small scattering angles (this has been called multiple scattering) and additionally may perform more than one scattering event with large scattering angle (see Figure 4.12 middle and right), before they are scattered towards the detector. This has been called plural scattering.

Multiple scattering has been reviewed by Szilágyi *et al.* [39] and Amsel *et al.* [54]. Multiple scattering results in an angular spread of the particles and therefore in a spread of path lengths. Due to the path length differences, we get an energy spread of the particles in a given depth.

Plural scattering with 2, 3, 4, ... scattering events is responsible for the background behind the low energy edge of high Z elements on top of low Z elements and the steeper increase of the spectra towards low energies than calculated with single scattering [55, 56, 57, 58, 59]. SIMNRA is able to calculate dual scattering, i. e. all particle trajectories with two scattering events.

4.9.2. Multiple (small angle) scattering

Angular and lateral spread due to multiple collisions with small deflection angles was treated analytically and numerically by Sigmund *et al.* [60, 61] for realistic screened interaction potentials of the Thomas-Fermi and Lenz-Jensen type. However, their theory is only valid for

1. Single elemental targets
2. The stopping of ions is neglected.

Due to these two assumptions the original Sigmund theory is only of limited practical use.

Szilagyi *et al.* [39] and Amsel *et al.* [54] have proposed a method how to extend the original Sigmund theory to multi-elemental targets with stopping, thus yielding the angular spread

distribution for realistic cases. They also proposed an approximation, how to obtain the energy spread distribution from the angular spread distribution via the chord angle.

Angular spread and energy spread are strongly correlated [54, Section 4]. This correlation is taken into account in the calculation of the energy of backscattered or recoiled particles.

The Szilagyi/Amsel theory was initially implemented in the DEPTH code [39, 62], which is primarily intended for depth-resolution calculations. SIMNRA contains an independent implementation of the Szilagyi/Amsel theory[7]. A comparison of DEPTH, SIMNRA, Monte-Carlo calculations in binary collision approximation, and molecular dynamics calculations, can be found in [63].

When using multiple scattering calculations, it should be kept in mind that SIMNRA uses the following approximations:

1. Multiple scattering energy spread distributions are approximated by Gaussian functions. In reality, these distributions have stronger wings, which are underestimated by SIMNRA.

2. Multiple scattering distributions are assumed to be symmetric around a mean value. This is never fulfilled exactly, and most strongly violated at normal incidence and at grazing incidence.

3. Energy transfer to target atoms (i.e. nuclear stopping and straggling) results in low-energy tails. These tails are neglected.

4.9.3. Plural (large angle) scattering

Plural large angle scattering cannot be treated analytically. SIMNRA approximates plural scattering effects by calculating all particle trajectories with two scattering events (dual scattering), see Figure 4.12. The contribution of trajectories with more than two large angle deflections is neglected. Plural (large angle) and multiple (small angle) scattering may be combined in the calculations.

SIMNRA performs the calculation of dual scattering in the following way: During each step of the incident ion particles are scattered into the whole sphere of 4π. We introduce the polar system with the polar angles ψ, φ, see Figure 4.13: ψ is the altitude, and φ the azimuth angle. After the first scattering event the scattered particles have the direction ψ, φ. The scattering angle θ_1 of the first scattering event is given by

$$\cos\theta_1 = \sin\alpha \sin\psi \sin\varphi - \cos\alpha \cos\psi$$

[7] The full Szilagyi/Amsel theory is implemented in SIMNRA 5.76 and higher. Earlier versions of SIMNRA treated the correlation between angular and energy spread only approximately, thus resulting in somewhat different results.

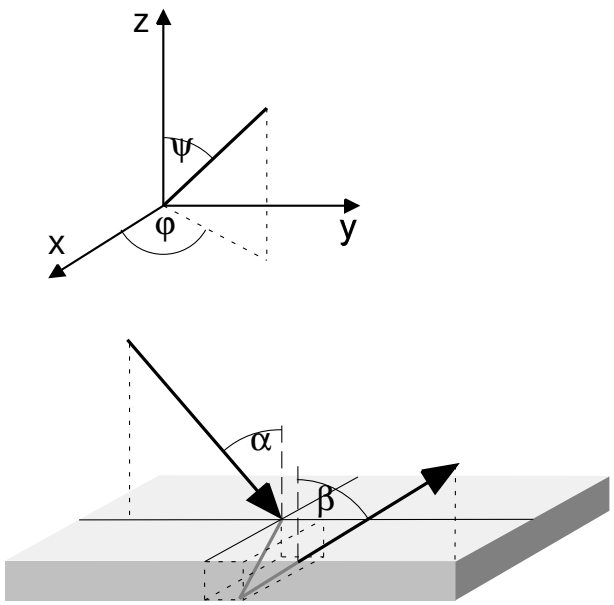

Figure 4.13.: Geometry used for the calculation of dual scattering, with the altitude angle ψ and azimuth angle φ.

SIMNRA uses the Rutherford cross-section for the calculation of the number of scattered particles in the first scattering event. The new angle α' of the particles after the first scattering is

$$\alpha' = 180° - \psi$$

The scattering angle θ_2 of the second scattering event is given by[8]

$$\cos\theta_2 = \sin\beta\,\cos\varphi_\beta\,\sin\psi\,\cos\varphi + \sin\beta\,\sin\varphi_\beta\,\sin\psi\,\sin\varphi + \cos\beta\,\cos\psi, \tag{4.77}$$

with φ_β the azimuth angle of the exit vector $\overrightarrow{\beta}$. SIMNRA subdivides the whole sphere of 4π into 10 ψ-intervals and 12 φ-intervals, resulting in 120 solid angle intervals. SIMNRA considers only trajectories with scattering angles $\theta_1, \theta_2 > 20°$ for dual scattering. Trajectories with smaller scattering angles are very similar to single scattering trajectories. For each solid angle interval a full backscattering spectrum with the starting depth of the particles equal to the depth of the incident ions and the new incident angle α' and the new scattering angle θ_2 is calculated.

Figure 4.14 compares the simulated spectra with single and dual scattering for 500 keV ^{4}He ions incident on a 100 nm gold layer on top of silicon with experimental data. With the inclusion of dual scattering the experimental results are much better approximated. Dual scattering gives the background between the low energy edge of Au and the Si edge, and the steeper increase

[8] Equation 4.77 is valid in general geometry. SIMNRA version 6.03 and earlier used an equation which was only valid in IBM geometry.

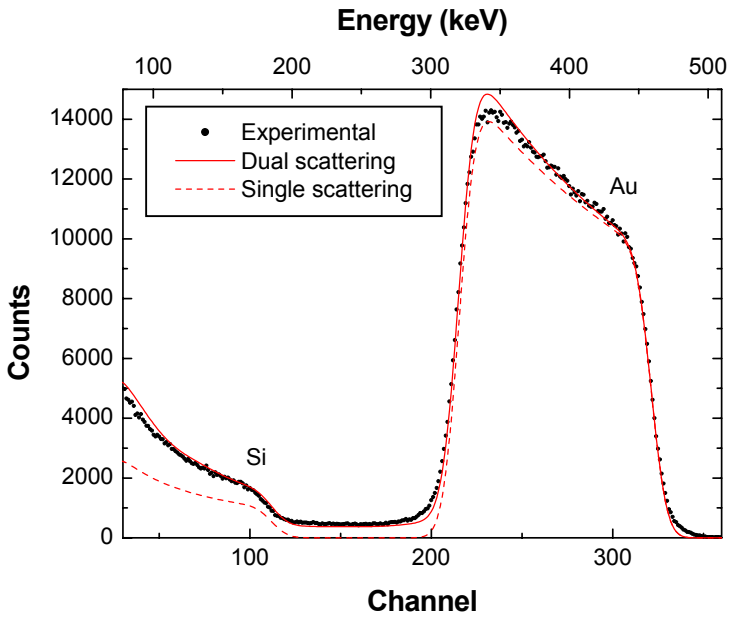

Figure 4.14.: 500 keV ^{4}He ions incident on 100 nm Au on top of Si, scattering angle 165°. Circles: experimental data points, dashed line: simulation with one scattering event, solid line: simulation with two scattering events.

of the gold spectrum is better described. The results with dual scattering are slightly lower than the experimental results. This is due to trajectories with more than two scattering events which are not calculated.

4.10. Surface roughness

The quantitative application of ion beam analysis methods is usually restricted to laterally homogeneous and smooth films. The experimentalist is often confronted with rough surfaces. The effects of rough surfaces of *thick* targets on RBS were investigated in some detail by Edge and Bill [64], Knudson [65], Bird *et al.* [66], and Hobbs *et al.* [67]. Wüest and Bochsler [68] and Yesil *et al.* [69, 70] attacked the problem by means of a Monte-Carlo computer simulation, taking into account correlation effects of the surface roughness and multiple surface crossings of the incident and emerging ions. It turned out that effects of rough surfaces of *thick* targets occur only for grazing angles of the incident or emerging ions. This is especially the case in ERDA on thick, rough targets, as was shown by Yesil *et al.* [69, 70] and Kitamura *et al.* [71]. Hydrogen depth profiling on rough surfaces by ERDA was studied experimentally by Behrisch *et al.* [72].

Astonishingly, the effects of rough *thin films* were studied much more scarcely. For RBS, rough films on a smooth substrate were investigated by Shorin and Sosnin [73] and Metzner *et al.* [74, 75]. Shorin and Sosnin [73] used a Monte-Carlo computer simulation. The Monte-Carlo approach suffers from long computing times of the order of hours [70], rendering these codes impractical for evaluation of experimental spectra. Moreover, the Shorin/Sosnin code treats only RBS with Rutherford cross-sections, neglecting non-Rutherford scattering, NRA and ERDA. The theoretical approach of Metzner *et al.* [74, 75] allows to extract the thickness distribution of rough films from a measured spectrum. However, this approach is only valid for RBS with Rutherford cross sections, a scattering angle of exactly 180° and constant stopping power, thus severely limiting the practical applicability of this work. The computer code RUMP [17, 18] allows to fuzz the interface between two layers by roughening the top layer. However, this is intended only for small roughness amplitudes, and the roughness distribution function is not documented.

Moreover, all work done so far treats only the case of a rough film on a smooth substrate. But in practice also the case of a film deposited on a rough substrate (Figure 4.15(b)) is sometimes encountered. This section describes the algorithms used for the description of rough surfaces and compares results of code calculations with experimental data. The limitations of the used approximations are discussed.

4.10.1. Rough film on a smooth substrate

A rough film on a smooth substrate is shown schematically in Figure 4.15(a). The substrate can be considered to be smooth, if its roughness is much smaller than the mean thickness $\bar{d}$ of the film. The film thickness distribution is described by a distribution function $p(d)$, with the film thickness d measured perpendicular to the substrate, see Figure 4.15(a) and $d \geq 0$. In the literature, usually a Gaussian distribution centered at $\bar{d}$ with variance σ^2 and cut-off at zero is used for $p(d)$ [74, 75]. However, a more natural choice of a distribution function with only

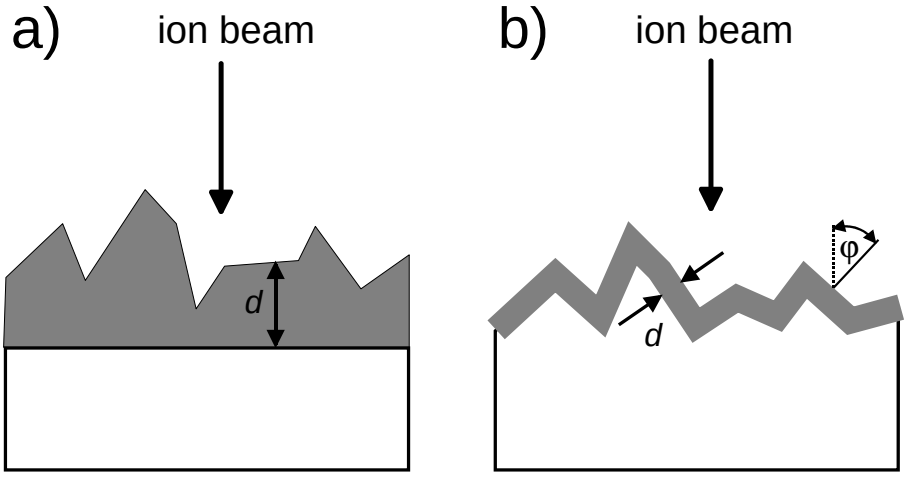

Figure 4.15.: Schematic representation of a rough film on a smooth substrate (a), and of a smooth film on a rough substrate (b).

positive values $d \geq 0$ is the Gamma distribution, which is also fully described by its mean value $\bar{d}$ and standard deviation σ. The Gamma distribution is defined by

$$p(d) = \frac{\beta^\alpha}{\Gamma(\alpha)} d^{\alpha-1} e^{-\beta d}, d > 0 \tag{4.78}$$

with $\alpha = \bar{d}^2/\sigma^2$ and $\beta = \bar{d}/\sigma^2$. $\Gamma(\alpha)$ is the Gamma function. The Gamma distribution is shown in Figure 4.16 for $\bar{d} = 1$ and different standard deviations σ. The corresponding Gaussian distributions centered at 1 and identical σ are shown for comparison. If $\sigma \ll \bar{d}$, i.e. if the width of the distribution is small compared to its mean value, Gaussian and Gamma distributions are nearly identical, see the curves for $\sigma = 0.1$ in Figure 4.16. With increasing σ the two distributions get more and more different (see the curves for $\sigma = 0.3$ and 0.7 in Figure 4.16). For $\sigma = \bar{d}$ the Gamma distribution decreases exponentially with $p(d) = e^{-d}$, and for $\sigma > \bar{d}$ an integrable singularity develops at $d = 0$.

A RBS, NRA or ERDA spectrum of a rough film is approximated by a superposition of N spectra with different layer thicknesses d_i. N can be adjusted by the *Number of thickness steps* in the *Setup: Calculation...* menu, see subsection 3.6.3. Typically about $N = 20$ sub-spectra are necessary to obtain a smooth superposition, though N has to be increased to about $N = 50$ for broad distributions with $\sigma \geq \bar{d}$. The weight w_i of each sub-spectrum is determined according to the thickness distribution function. For each sub-spectrum the layer is treated to be smooth with thickness d_i. Correlation effects, such as incidence through a hump and emergence through a valley or multiple surface crossings, are neglected. This is only correct for backscattering at a scattering angle of exactly 180° and for transmission geometries. However, for scattering

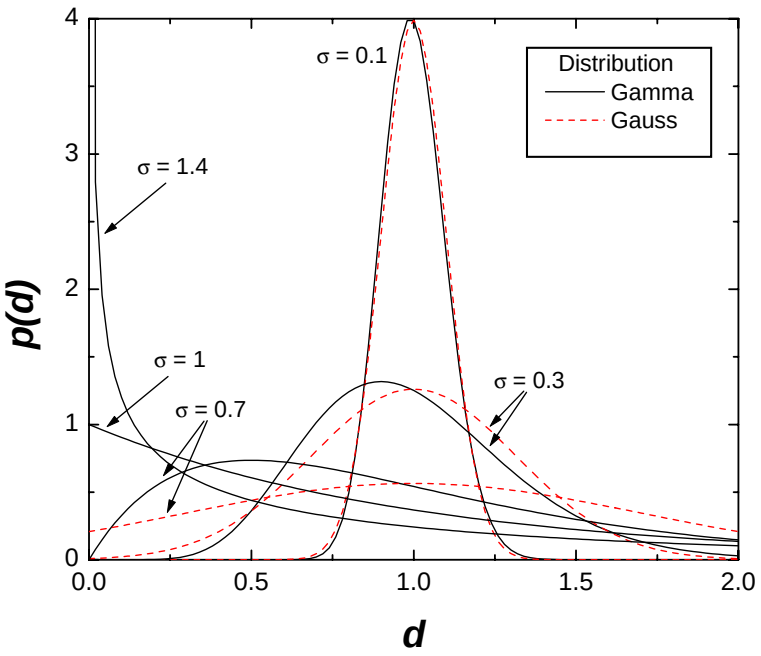

Figure 4.16.: Comparison of Gaussian distribution functions centered at 1 (dashed lines) and Gamma distribution functions (solid lines) with mean value $\bar{d} = 1$ and different standard deviations σ.

angles in the range 150°–180° and non-grazing incidence and emergence angles, as are used in many RBS and NRA setups, correlation effects still play only a minor role and can be neglected without severe loss of accuracy. But it should be kept in mind that the used approximation gets invalid for grazing incidence or exit angles, as is the case in ERDA - in these cases correlation effects may be dominant and can change the shape of the spectra considerably.

The effect of layer roughness on the shape of RBS spectra is shown in Figure 4.17 for incident ^{4}He ions backscattered from a gold layer at a scattering angle of 165°. The film thickness distributions are described by the Gamma distributions shown in Figure 4.16. If the thickness variation is much smaller than the mean film thickness ($\sigma/\bar{d} = 0.1$), only the low energy edge of the film is affected by the roughness and gets broader. With increasing roughness the broadening of the low energy edge increases, until at $\sigma/\bar{d} \approx 0.6$ the high energy edge begins to decrease. The energy $E_{1/2}$, at which the low energy edge has decreased to its half height, remains fairly constant until large roughness amplitudes of the order $\sigma/\bar{d} \approx 0.6$, i.e. until the high energy edge begins to decrease. For sufficiently thick films, i.e. if the film is completely resolved, this energy is therefore a rather robust measure of the mean film thickness even for large roughnesses, as long as the high energy edge is not affected.

The energy spectrum of 1.5 MeV ^{4}He backscattered from a rough Ni-film deposited on polycrystalline carbon is shown in Figure 4.18. The measured spectrum is well reproduced

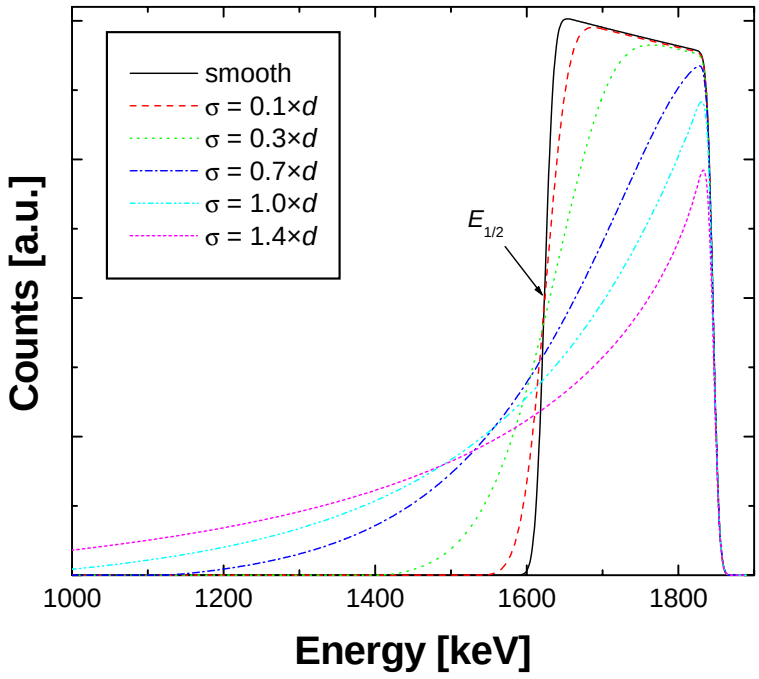

Figure 4.17.: Calculated energy spectra for 2 MeV ^{4}He backscattered from a smooth and rough gold layers with mean thickness $\bar{d} = 1 \times 10^{18}$ Au-atoms/cm^2 and different roughnesses with standard deviation σ. The film thickness distributions are shown in Figure 4.16. Incident angle $\alpha = 0°$, scattering angle 165°. $E_{1/2}$ marks the energy, at which the low energy edge has decreased to its half height.

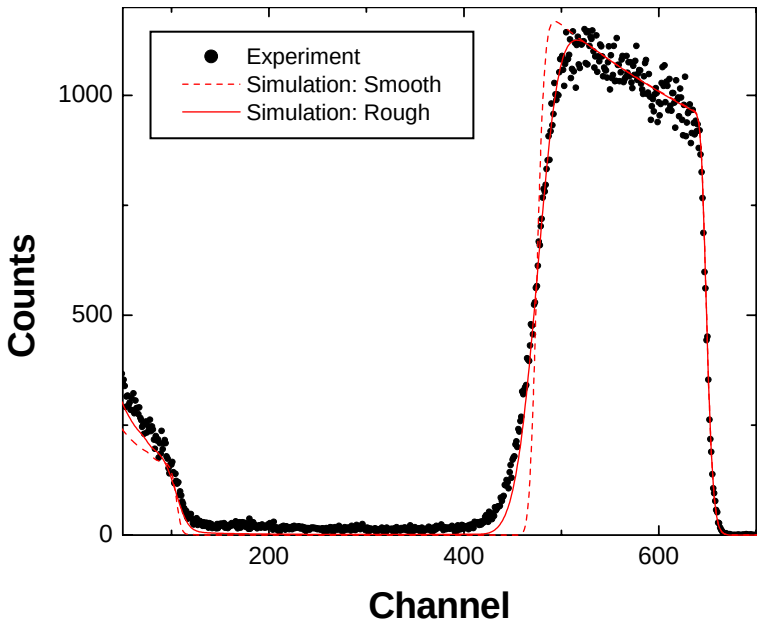

Figure 4.18.: 1.5 MeV ^{4}He backscattered at 165° from a rough Ni-film with a mean thickness of 2.17×10^{18} Ni-atoms/cm^2 on carbon substrate. Dots: Experimental data; Dashed line: Simulation assuming a smooth Ni layer; Solid line: Simulation assuming a rough Ni layer with roughness $\sigma = 2.12 \times 10^{17}$ Ni-atoms/cm^2.

in the simulation by a mean Ni layer thickness of 2.17×10^{18} Ni-atoms/cm^2 (238 nm) and a roughness with standard deviation $\sigma = 2.12 \times 10^{17}$ Ni-atoms/cm^2 (23 nm) (solid line). The experimental data are not well reproduced by the spectrum of a smooth Ni layer (dashed line). The roughness of the Ni film was determined from line scans with a profiler. The roughness distribution, i.e. the deviation of the actual surface from the leveled one, was approximately Gaussian: For small values of $\sigma/\bar{d}$ a Gaussian and a Gamma distribution cannot be distinguished, see Figure 4.16. The carbon substrate was already rough with a standard deviation $\sigma_C = 18.2$ nm. The roughness of the Ni film on the substrate was $\sigma_{C+Ni} = 26.5$ nm. This roughness is made up by the roughness of the carbon substrate plus the roughness of the Ni film σ_{Ni}. By assuming the two roughnesses to be independent, i.e. $\sigma^2_{C+Ni} = \sigma^2_C + \sigma^2_{Ni}$, the roughness of the Ni film alone is about 19.3 nm, in good agreement with the result from He backscattering of 23 nm.

The energy spectrum of 2.0 MeV ^{4}He backscattered from a rough oxidised aluminum film on polycrystalline carbon is shown in Figure 4.19. The carbon substrate was well polished and had a mean roughness < 25 nm [76]. The film was exposed for about 8 months as erosion monitor at the vessel wall of the nuclear fusion tokamak experiment JET [77, 76], the wall temperature was about 300°C. The initial Al layer thickness was 3.16×10^{18} atoms/cm^2 (525 nm), but

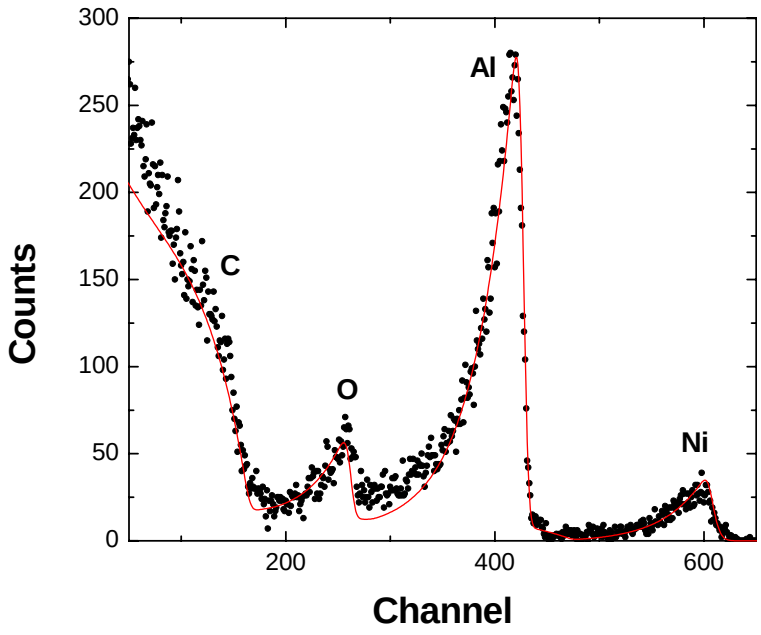

Figure 4.19.: 2 MeV ^{4}He backscattered at 165° from a rough oxidised aluminum film on carbon. The film was used as long term sample in the tokamak JET and was strongly eroded by plasma impact. Additionally some Ni was deposited from the plasma. Dots: Experimental data; Solid line: Simulation with a mean film thickness of 1.11×10^{18} atoms/cm^2 and roughness $\sigma = 1.06 \times 10^{18}$ atoms/cm^2. Film composition 68% Al, 30% O, 2% Ni.

decreased due to sputtering by bombardment with energetic hydrogen atoms from the nuclear fusion plasma to 7.5×10^{17} Al-atoms/cm^2. At the same time the Al film was oxidised and some nickel, which was initially eroded at an erosion dominated area of the JET vessel wall [9], was redeposited on the Al film and incorporated. The observed spectrum with the tails at the low energy sides of the O, Al and Ni peaks cannot be reproduced by assuming a smooth layer. But it is fairly well reproduced by a rough layer with a mean film thickness of 1.11×10^{18} atoms/cm^2, roughness $\sigma = 1.06 \times 10^{18}$ atoms/cm^2, and composition 68% Al, 30% O, 2% Ni (solid line in Figure 4.19). The shape of the film thickness distribution is close to the curve with $\sigma = 1$ in Figure 4.16. This example shows clearly, that non-Gaussian distributions of layer thicknesses are observed in practice and can be described by a Gamma distribution.

4.10.2. Smooth film on a rough substrate

A film with homogeneous thickness d on a rough substrate is shown schematically in Figure 4.15b. The substrate is considered to be rough, if its roughness amplitude is much larger

[9] The JET vessel walls consist of Inconel, a stainless steel with high nickel content.

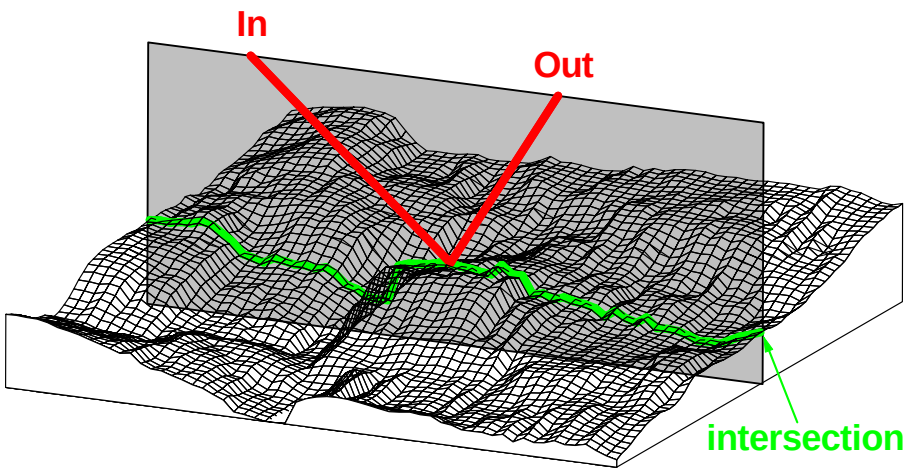

Figure 4.20.: Schematic representation of a rough surface. In: Direction of the incident beam; Out: Direction of the outgoing beam; Light gray: Plane spanned by the incident and outgoing beams; Intersection: Intersection of this plane with the rough surface.

than the thickness d of the film. We assume a rough substrate to consist of inclined line segments with local inclination angle φ (see Figure 4.15b and Figure 4.21), and the film thickness d is measured parallel to the local surface normal. Such a rough surface is described by a distribution of local tilt angles $p(\varphi)$. The concept of a local tilt angle was already used by Küstner *et al.* for the calculation of the sputtering yield of rough surfaces by ion bombardment in the energy range 100 eV to several keV [78]. In Küstner's work the rough surface was treated as a fully 3-dimensional object, which was necessary due to the 3-dimensional nature of the collision cascades created by keV ions. In MeV ion beam analysis the trajectories of the incident and emerging ions can be approximated with good accuracy by straight lines, and we have to consider only the intersection of the plane, which is formed by the directions of the incident and emerging ions, and the target surface, see Figure 4.20: This is only a 2-dimensional line profile as the one shown in Figure 4.15b.

The tilt angle distribution is given by $p(\varphi)$. This distribution describes the frequency of occurence of a line segment inclined by φ. A rough surface without preferential orientation has a mean tilt angle

$$\bar{\varphi} = \int_{-90^\circ}^{90^\circ} \varphi\, p(\varphi)\, d\varphi = 0^\circ. \tag{4.79}$$

The probability distribution $\tilde{p}(\varphi)$ of hitting a surface tilted by φ by an incident ion is given by

$$\tilde{p}(\varphi) = p(\varphi)\cos(\alpha - \varphi), \tag{4.80}$$

with the incident angle α of the ion. α is measured towards the surface normal of a non-inclined surface. The factor $\cos(\alpha - \varphi)$ is due to the projection of the line segment into the

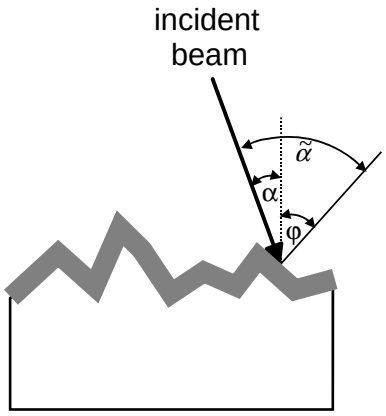

Figure 4.21.: Schematic representation of the incident angle α, local inclination angle φ, and local incident angle $\tilde{\alpha}$.

plane perpendicular to the incident ion trajectory: It is more likely to hit a segment which is perpendicular to the incident trajectory than an inclined segment - and obviously it is impossible to hit a segment which is tilted parallel to the incident beam. It is important to note that a profiler or a scanning tunneling microscope (STM), which samples the surface at a constant step width parallel to the surface, measures the distribution $\tilde{p}(\varphi)$ rather than $p(\varphi)$: Large tilt angles are under-represented, and tilt angles of 90° cannot be measured at all.

RBS, NRA and ERDA spectra of a smooth film on a rough substrate are approximated by a superposition of M spectra with different local incident angles $\tilde{\alpha}$, where

$$\tilde{\alpha} = |\alpha - \varphi| \tag{4.81}$$

and local exit angles $\tilde{\beta}$. The choice of $\tilde{\beta}$ is discussed below. M can be adjusted by the *Number of angular steps* in the *Setup: Calculation...* menu, see subsection 3.6.3. The weight of each sub-spectrum is determined according to the distribution function $\tilde{p}(\varphi)$. For each sub-spectrum the substrate is treated to be smooth, i.e. a spectrum for a smooth layer, but with angles $\tilde{\alpha}$ and $\tilde{\beta}$ is calculated. Incident angles $\tilde{\alpha} > 90°$ are excluded: This represents a line segment which cannot be hit by the incident beam. As in the case of a rough film on a smooth substrate, surface correlation effects like shadowing of one line segment by another, and multiple surface crossings are neglected.

In IBM geometry (with $\alpha + \beta + \theta = 180°$) , the local exit angle $\tilde{\beta}$ for a given inclination angle φ is given by

$$\tilde{\beta} = |\beta + \varphi| \tag{4.82}$$

This relation was used by SIMNRA 4.70–4.90 and ref. [79]. But this choice of β is only valid in IBM geometry and results in unrealistic spectra if a rough surface is bombarded at non-normal incidence in non-IBM geometry. SIMNRA 5.00–5.20 used a more general approach, where the

correct relation between the angles in any geometry and even the 3-dimensional nature of a rough surface were taken into account by rotating the inclined line segments and calculating an averaged β. Although more accurate than Equation 4.82, it turned out that this approach suffered from numerical instabilities at non-normal incident angles $\alpha > 30°$ and non-IBM geometry. In SIMNRA 5.25 the choice of $\tilde{\beta}$ was changed again and is calculated in the following way:

1. For each inclination angle the local angle of incidence $\tilde{\alpha}$ is calculated according to Equation 4.81.

2. The azimuth angle ψ between the incident and exit beams is calculated from

$$\sin\psi = \frac{\cos\beta + \cos\theta\cos\alpha}{\sin\theta\sin\alpha}. \tag{4.83}$$

3. As scattering angle θ and azimuth angle ψ are constant for a given geometry, the local exit angle $\tilde{\beta}$ can be calculated for a given local incident angle $\tilde{\alpha}$ from

$$\cos\tilde{\beta} = \sin\psi\sin\theta\sin\tilde{\alpha} - \cos\theta\cos\tilde{\alpha}. \tag{4.84}$$

Equation 4.84 is valid for any geometry.

For a given local tilt angle φ, the calculation of the local incident and exit angles $\tilde{\alpha}$ and $\tilde{\beta}$ depends on the setting of the *Dimension of substrate roughness* switch, see section 3.6.3.

- *2-dimensional*: In the 2-dimensional model the local incident and exit angles $\tilde{\alpha}$ and $\tilde{\beta}$ are calculated according to Equation 4.81 and Equation 4.84.

- *2.5-dimensional*: In the 2.5-dimensional model it is assumed, that the surface consists of small planes, which are tilted by a local tilt angle φ, and rotated by an angle ω along the surface normal. In a fully 3-dimensional surface model, the local incident and exit angles $\tilde{\alpha}$ and $\tilde{\beta}$ depend on φ and ω, and it would be necessary to calculate spectra for each possible combination of φ and ω. In order to keep computing times short, this is not done. Instead, for each tilt angle the average angles $\tilde{\alpha}$ and $\tilde{\beta}$ are used, averaged over ω. Therefore the 2.5-dimensional model uses only one set $\tilde{\alpha}, \tilde{\beta}$ for each φ (as would be the case in the 2-dimensional case), but this set is obtained by averaging a 3-dimensional surface model. The accuracy of the 2.5-dimensional model is therefore somewhere in between a 2-dimensional and a fully 3-dimensional model.

Which distribution has to be used as tilt angle distribution? A line profile of the surface of a carbon fibre composite (CFC) material manufactured by Dunlop is shown in Figure 4.22 (top). Due to its high thermal conductivity this material is used for high heat flux components in the tokamak experiment JET. The standard deviation of the surface roughness is about $\sigma = 8.2\ \mu$m.

A histogram of the tilt angle distribution $\tilde{p}(\varphi)$, obtained with a profiler from several line scans in different sample directions, is shown in Figure 4.22 (bottom). Tilt angles larger than about 60° are not observed due to the apex angle of the profiler tip. The tilt angle distribution is fairly well described by a Lorentz distribution for the tilt angles $p(\varphi)$ (dashed line), while a Gaussian distribution underestimates strongly the wings of the distribution (dotted line). The full width at half maximum (FWHM) of the Lorentz distribution is 26.6°.

Calculated backscattering spectra for incident ^{4}He ions backscattered from a gold layer with thickness 1×10^{18} atoms/cm^2 at a scattering angle of 165° are shown in Figure 4.23 for a smooth and rough substrates. The rough substrates are described by a Lorentz distribution of tilt angles with different FWHM w. On a rough substrate the low energy edge gets a tail, which increases with increasing roughness. This tail extends to energies close to zero. With increasing roughness the Au peak also gets broader, and the energy $E_{1/2}$, at which the low energy edge has decreased to its half height, is no good measure for the film thickness: It depends on the roughness of the substrate. The high energy edge and the plateau are only slightly affected by substrate roughness and decrease only little at large roughnesses due to shadowing: The backscattered particles do not reach the detector any more, because the exit angle β points inside the layer. For $w = \infty$ the local tilt angles are equipartitioned, and the corresponding spectrum represents the case of maximum roughness.

A measured spectrum for 2.5 MeV protons backscattered from a tungsten layer on top of a rough carbon substrate is shown in Figure 4.24. The non-Rutherford elastic scattering data from [80] were used for the C(p,p)C cross section. The substrate is the same CFC material, which surface is shown in Figure 4.22. The mean W layer thickness was about 3.5 μm, while the standard deviation of the substrate roughness was about 8.2 μm, i.e. the substrate roughness was considerably larger than the thickness of the W layer. The dotted line in Figure 4.24 is the calculated spectrum for a smooth W layer on a smooth carbon substrate. Plural scattering in the W layer was included in dual scattering approximation, see subsection 4.9.3. Plural scattering results for example in the small background visible between the carbon and tungsten signals in channels 500–650. This spectrum has only minor resemblance with the experimental curve, and requires a slightly thicker W layer (3.6 μm) for best fit. The dashed line is calculated for a rough W layer, characterized by a Gamma-distribution of layer thicknesses with a mean thickness of 3.5 μm and standard deviation $\sigma = 0.3$ μm on a rough carbon substrate, characterized by a Lorentz distribution of tilt angles with FWHM = 20°. The roughnesses of the layer and the substrate are assumed to be independent, and plural scattering is not taken into account. The W peak (channels > 650) is already well described, but the low energy tail below the peak is underestimated. The solid line uses the same roughness parameters, but takes additionally plural scattering into account. Now the whole experimental spectrum is reproduced well. Compared to the smooth layer the contribution of plural scattering has increased strongly, which is due to an enhancement of plural scattering at inclined incidence. The height and shape of the low energy tail below the W-peak in channels < 650 are determined by the wings of the tilt angle distribution with inclination angles > ±45°. The observed tilt angle distribution, see

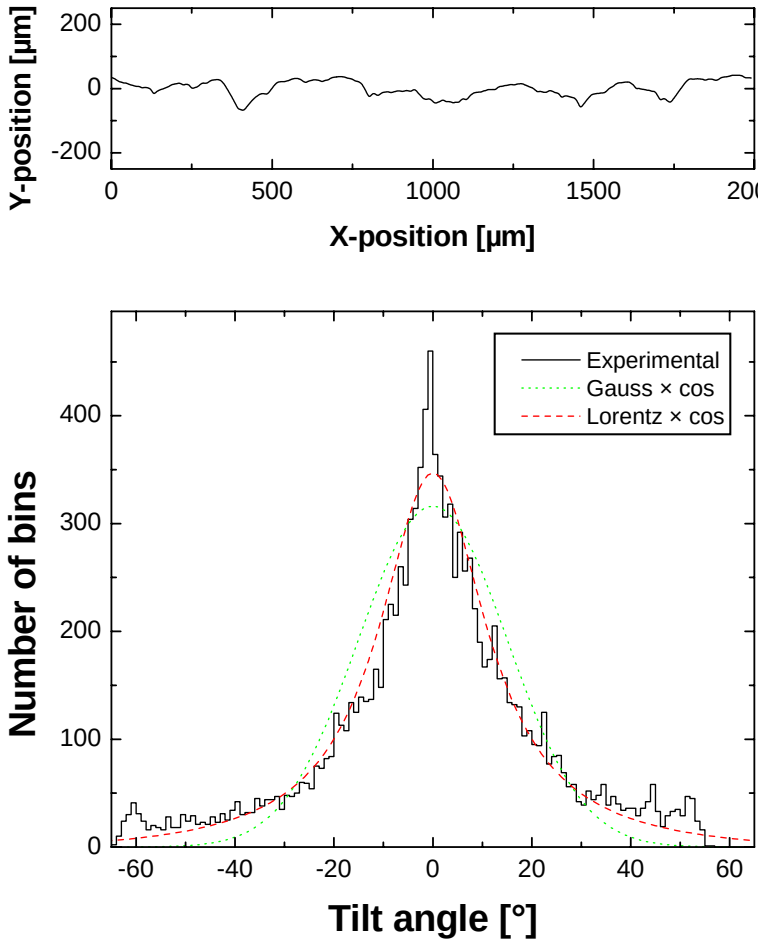

Figure 4.22.: Top: Line profile of a carbon fibre composite (CFC) surface. Bottom: Histogram of the local tilt angle distribution of the CFC surface. Solid line: Experimental data; Dashed line: Lorentz distribution times cosine of the tilt angle; Dotted line: Gaussian distribution times cosine of the tilt angle.

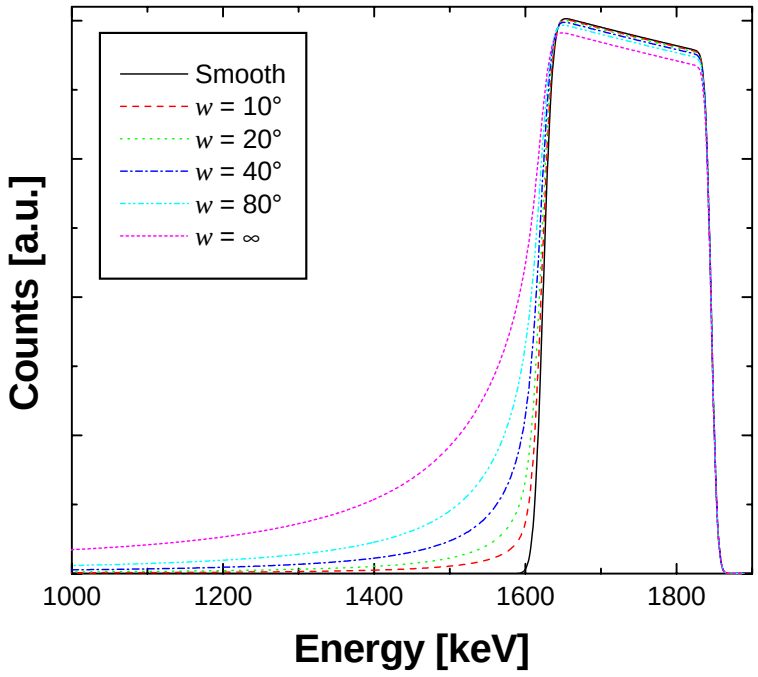

Figure 4.23.: Calculated energy spectra for 2 MeV ^{4}He backscattered from a gold layer with thickness 1×10^{18} Au-atoms/cm^2 on a rough substrate with different roughnesses. The roughness is described by a Lorentz distribution of tilt angles with FWHM w. $w = \infty$ is an equipartition of tilt angles. Incident angle $\alpha = 0°$, scattering angle $165°$.

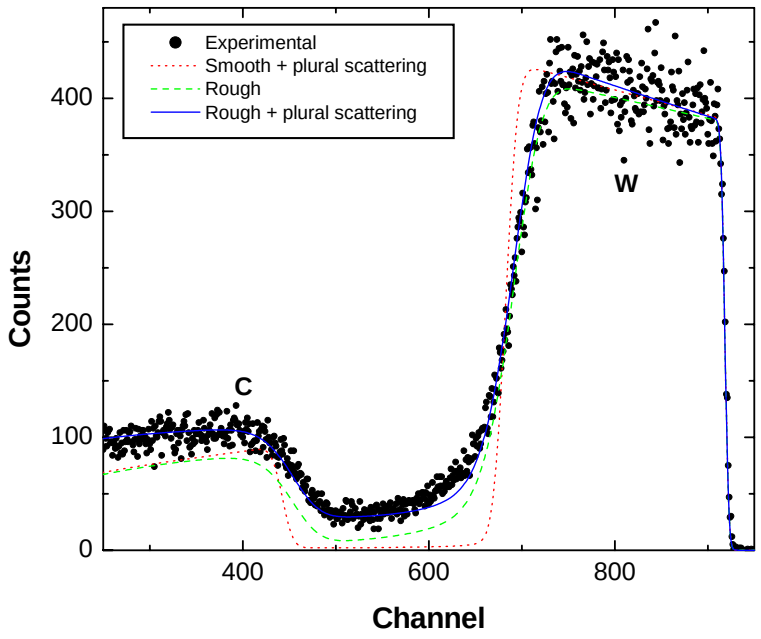

Figure 4.24.: 2.5 MeV protons backscattered from 3.5 μm W on a rough carbon substrate, scattering angle 165°. Dots: Experimental data; Dotted line: Calculated spectrum for a smooth W layer (3.6 μm) on a smooth C substrate including plural scattering; Dashed line: Calculated spectrum for a rough W layer (3.5 μm, $\sigma = 0.30$ μm) on a rough substrate (FWHM 20°); Solid line: As dashed line, but including plural scattering.

Figure 4.22, is best described by a FWHM of 26.6°, while the best fit to the measured spectrum yields a FWHM of about 20°. It is assumed that inaccuracies in the measurement of the tilt angle distribution at high inclinations due to the apex angle of the profiler tip and the constant step width, together with uncertainties in the calculation of the plural scattering background, are the reason for this small discrepancy. Additionally it should be kept in mind that the used model of inclined line segments, see Figure 4.15(b), is only an approximation to physical reality, and the real surface has an additional fine structure.

The influence of the different roughnesses on the shape of the RBS spectrum is shown in more detail in Figure 4.25. The experimental data (black dots) and the solid line in the top and bottom figures are the same as in Figure 4.24. The substrate roughness is kept constant in Figure 4.25 (top), and the roughness of the W layer is varied from smooth to 0.6 μm. The roughness of the W-layer influences mainly the low energy edge of the W peak, best fit is obtained for $\sigma = 0.3$ μm. The bottom part shows the influence of the carbon substrate roughness for constant W-layer roughness. Substrate roughness influences mainly the low energy tail below the W-peak, while the low energy edge of the W-peak is less affected by substrate roughness. Best fit is obtained for about 20° FWHM. Due to the different effects of the

two roughnesses on the shape of RBS spectra the two roughnesses can be easily distinguished.

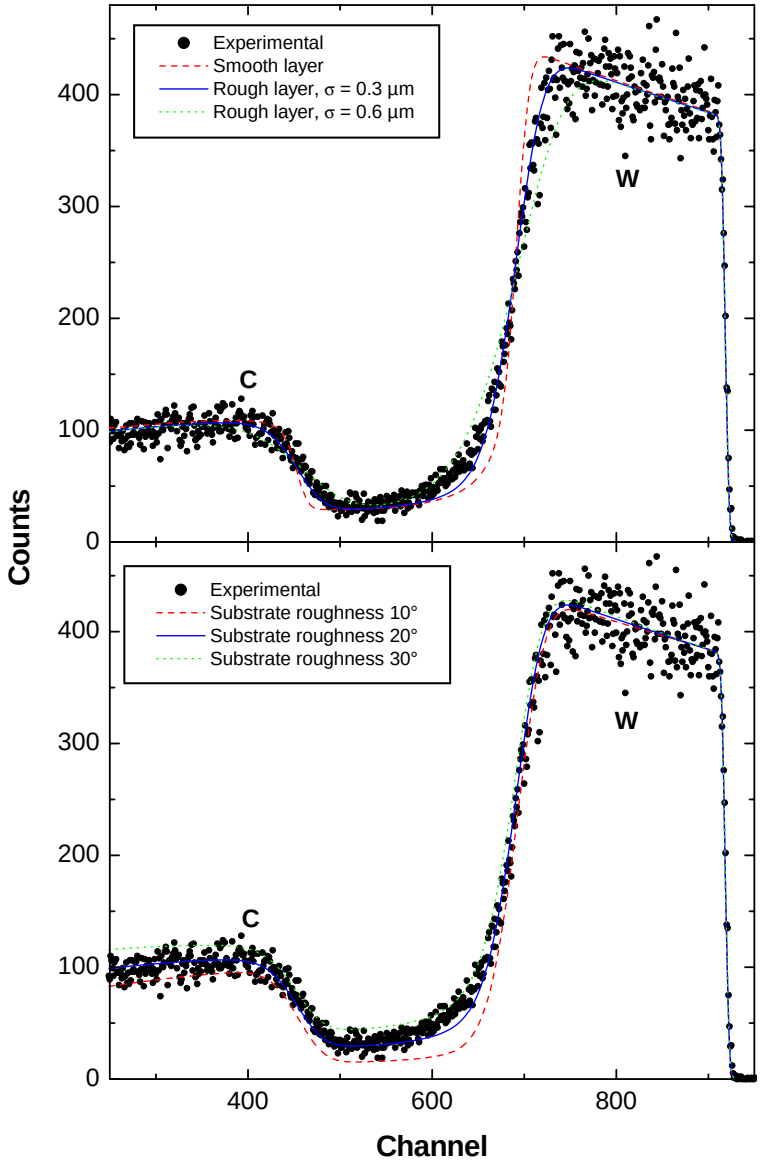

Figure 4.25.: Same experimental data as in Figure 4.24, compared to simulation calculations with different roughness parameters. Top: Calculations for a rough carbon substrate (FWHM 20°) and different W-layer roughnesses, characterized by a Gamma-distribution with standard deviation σ; Bottom: Calculations for a rough W layer (σ = 0.3 μm) and different substrate roughnesses, characterized by a Lorentz-distribution of tilt angles with different FWHM's. Mean W-layer thickness 3.5 μm, plural scattering included.

4.11. Live time and pile-up

Nuclear spectroscopy systems are unavoidable sources of spectral distortions due to the finite pulse widths of the generated electronic signals and the paralyzable nature of the electronic system, which is not able to accept a second pulse while the previous is still being processed. Due to the finite pulse width there is always a probability of pulses to overlap, resulting in pulse pile-up, while the paralyzation of the system results in dead time losses of incident pulses. These distortions of the spectra can be minimized by decreasing the incident count rate (by decreasing the incident beam current or the detector solid angle), but they are usually clearly visible at higher count rates. These are often desirable due to the shorter measuring times.

This section describes how SIMNRA can take these effects into account in simulation calculations.

4.11.1. Live time correction

An Analog-Digital-Converter (ADC) requires a certain time to digitize an incident analog pulse. While the pulse is being processed, the ADC is not able to accept another pulse – this pulse is rejected. The time during which the electronics is busy (and unable to accept a pulse) is called *dead time* T_{Dead} . The *live time* T_{Live} is the time during which the electronics is able to accept pulses, while the *real time* of a measurement is called T_{Real}. These times are connected through the relation

$$T_{Real} = T_{Live} + T_{Dead}.$$

A pile-up rejector, which rejects overlapping pulses, is an additional source of system dead time.

The probability of a pulse to be detected is given by

$$P_{Live} = \frac{T_{Live}}{T_{Real}}, \tag{4.85}$$

because it is accepted only if it arrives during the system live time interval.

If a live-time correction is applied to simulated spectra (by checking *Apply live-time correction* in the *Live-time and pile-up* form, section 3.6.2), then the initial number of simulated counts n_k^0 in channel k is multiplied by the probability, that the counts actually are detected, to give the final number of simulated counts n_k:

$$n_k = P_{Live}\, n_k^0. \tag{4.86}$$

n_k^0 is the number of counts, which would be detected for an indefinitely small incident count rate (or an indefinitely fast ADC). Note that the live-time correction is applied to simulated spectra and *not* to experimental data – SIMNRA does not modify experimental spectra.

4.11.2. Calculation of pile-up

Due to the finite width of the electronic pulses there is always a probability of pulses to overlap. This phenomenon is called *pulse pile-up*. Pile-up can be minimized by decreasing the incident count rate (by decreasing the incident beam current or the detector solid angle), and by reducing the width of the electronic pulses. Gaussian shaping with a peaking times of 0.5 μs is still long enough to preserve the optimal energy resolution of most semiconductor detectors used for RBS. A pile-up rejector can additionally decrease the pile-up level, which, however, can never achieve a complete elimination of pile-up effects.

SIMNRA offers two different models for calculating pile up. See subsection 3.6.3 on how to select the different models, and for some remarks about computing times.

- *Accurate* model: This model is close to physical reality. Pulse shape effects and overlap of pulses according to their arrival-time distribution are taken into account correctly. The influence of a pile-up rejector circuit is modelled realistically. Major disadvantage of this model is its long computing time, especially for spectra with many channels.
- *Fast* model: This model is less accurate than the previous one, but can be calculated much faster.

The selection of the pile-up model depends on the use of a pile-up rejector circuit, the pulse shaping time, the desired level of accuracy, and the available computer power. In many cases, the *Fast* model already gives good results, especially if a pile-up rejector is used and the pulse rise time is larger than about 1 μs. The *Accurate* model should be used only if necessary.

Accurate model

The effect of pulse pile-up is shown schematically in Figure 4.26. Two overlapping pulses with heights i and j may be interpreted by the analyzing system as corresponding to a fictitious event with height k, and the ADC assigns to it an erroneous energy value. We will treat only double-pulse pile-up (i.e. the pile-up of exactly two pulses), while triple and other multiple pulse pile-up will be not considered – under realistic conditions for RBS or NRA other than double pulse pile-up is not observed [81].

The effect of pile-up on a single peak is shown schematically in Figure 4.27. Two pulses arriving (almost) simultaneously result in a sum pulse with (almost) double height. Increasing time lag between the two pulses give sum pulses with heights between the original and the double height, resulting in a pile-up spectrum which extends from the original peak to the doubled channel number.

The mathematical models for pile-up calculations were already developed in the Seventies, and we adopt the model by Wielopolski and Gardner [82]. This model was initially developed for Gaussian shaped pulses, which are used by analog amplifiers. The model is also valid

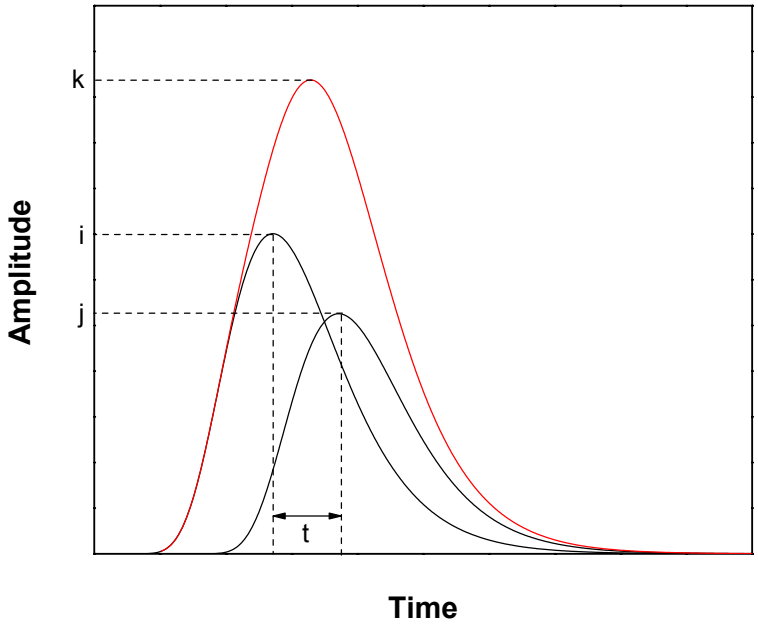

Figure 4.26.: Pile-up of a pulse with height i and a subsequent pulse with height j to a sum pulse of height k. t is the time interval between the two pulses.

for modern Digital-Signal-Processors (DSP's), with the only difference that DSP's use digital filtering, corresponding to trapezoidal pulse shaping instead of analog Gaussian shaping.

Identifying pulse height with channel number (i.e. assuming linearity of the electronic system and no ADC offset), then the probability P_i of a pulse of height i in channel i is given by

$$P_i = \frac{n_i}{N},$$

where

$$N = \sum_{i=1}^{m} n_i,$$

with n_i the number of count in channel i, m the total number of channels, and N the total number of counts in the spectrum. P_i is obtained from a simulated spectrum neglecting pile-up effects, or can be obtained from a low counting rate experiment in which the pile-up probability is negligible.

The time lag between any two pulses is distributed according to the interval probability distribution, which is derived from the Poisson probability distribution. The probability P_{ijk} is the probability, that a pulse of height i combines with a following pulse of height j to a pulse of height k, Figure 4.26. In order to obtain a sum pulse of height k the second pulse j must arrive within a certain time interval $[t, t + dt]$. The probability P_{ijk} can be obtained as the product of the probabilities that

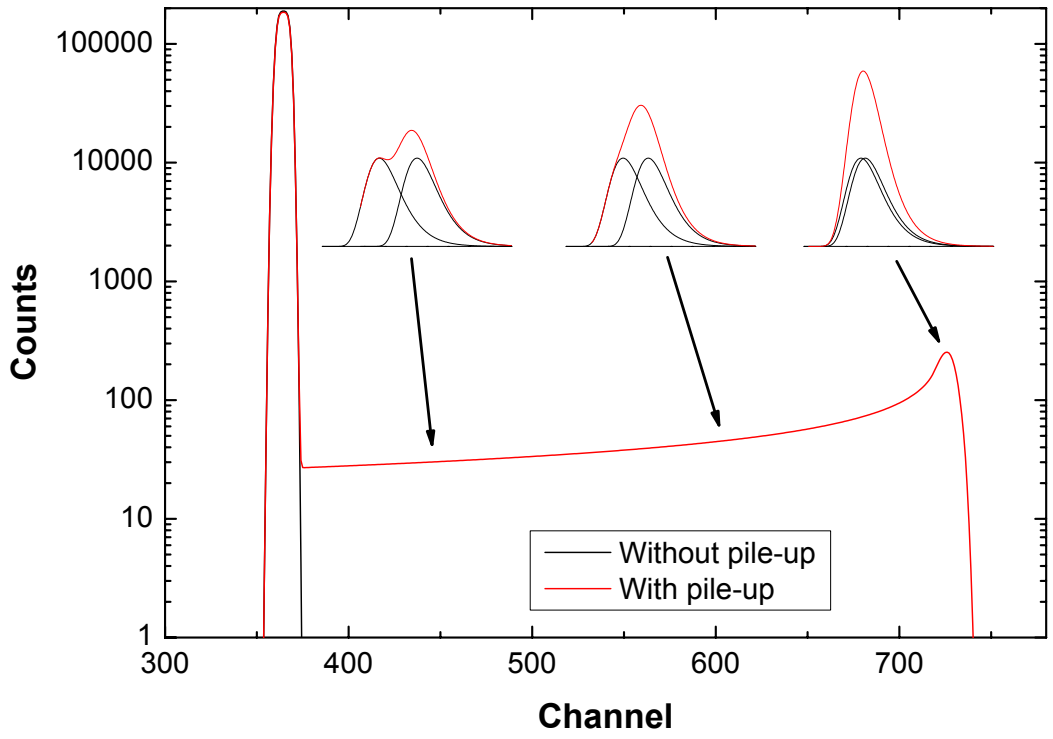

Figure 4.27.: Effect of pile-up on a single peak. The inset shows the individual and the sum pulses, which give the pile-up spectrum.

1. There is no pulse between time zero (when the initial pulse occured) and time t:

$$P_1 = e^{-\alpha t}.$$

2. There is one pulse between time t and time $t + dt$.

$$P_2 = \alpha\, dt$$

3. There are zero pulses between time $t + dt$ and the end of the first pulse T_w.

$$P_3 = e^{-\alpha(T_w - t)}$$

For details see [82]. The differential P_{ijk} is the product of these probabilities:

$$dP_{ijk} = \alpha\, e^{-\alpha T_w}\, dt$$

A pulse-height analyzer is only capable to analyze pulses into discrete channels (multi-channel analyzer). The P_{ijk} is obtained by integrating the differential probability over the time period that will give a pulse of size k. This time interval is from $t_1(i, j, k)$ to $t_2(i, j, k + 1)$, so that

$$\begin{aligned} P_{ijk} &= \int_{t_1}^{t_2} \frac{dP_{ijk}}{dt} dt && (4.87)\\ &= \alpha\, e^{-\alpha T_w} (t_2 - t_1) && (4.88)\\ &= \alpha\, e^{-\alpha T_w}\, \Delta t_{ijk} && (4.89) \end{aligned}$$

The probability P_{ijk} is proportional to the time increment Δt_{ijk} between the two pulses.

Unfortunately, the time increment Δt_{ijk} can be calculated analytically only for very simple pulse shapes. Wielopolski and Gardner [82] approximated the true pulse shapes by parabolic pulses, see Figure 4.28 and Figure 4.29. In that approximation, Δt_{ijk} is obtained from

$$\Delta t_{ijk} = T_p \left(\left[\frac{(i + j - k + 1)(i + j)}{ij} \right]^{1/2} - \left[\frac{(i + j - k)(i + j)}{ij} \right]^{1/2} \right), \text{for } l \le k \le i + j, \quad (4.90)$$

where T_p is the pulse rise time (i.e. the time to reach the maximum value, see Figure 3.5), and l is whichever is largest of i and j. For parabolic pulses, we can use $T_w = T_p$. Other approximations (including the true pulse shape by numerical integration)can be found in [83].

Pile-up results in losses and gains of pulses in each channel k. Losses in channel k are due to pile-up with pulses j into channel i, where the pulses k may pile up with a following pulse j , or may pile up with a preceding pulse j. The losses from channel k are given by

$$L_k = N P_k \sum_{j=1}^{m} P_j \sum_{i=a}^{j+k} \left(P_{kji} + P_{jki} \right), \quad (4.91)$$

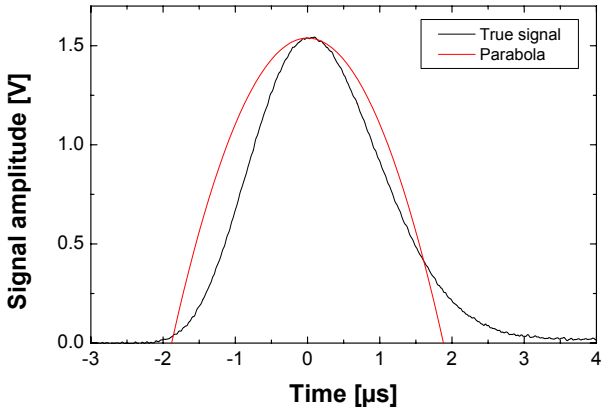

Figure 4.28.: Comparison of a real pulse (Ortec 672 spectroscopy amplifier, Gaussian shaping, shaping time 1 μs) with the parabolic pulse approximation, pulse rise time $T_p = 1.9$ μs according to Table 3.1.

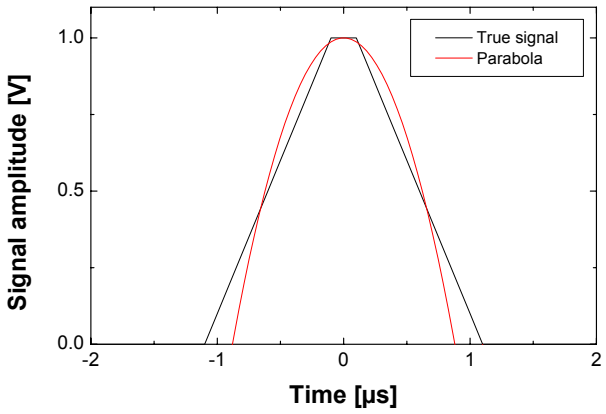

Figure 4.29.: Comparison of a trapezoidal pulse shape, as used by digital signal processors (DSP filter rise time 1 μs, DSP flat top duration 0.2 μs), with the parabolic pulse approximation, pulse rise time $T_p = 0.9$ μs according to Table 3.1.

where a is the largest of k and j.

The gain in channel k is due to pile-up of pulses i and j:

$$G_k = N \sum_{i=1}^{k-1} \sum_{j=p}^{k-1} P_i P_j P_{ijk}, \tag{4.92}$$

where $p = k - i$.

The content of each channel of the spectrum with pile-up n_k^{PU} is then given by

$$\begin{aligned} n_k^{PU} &= n_k - L_k + G_k & (4.93)\\ &= n_k - N P_k \sum_{j=1}^{m} P_j \sum_{i=a}^{j+k} \left(P_{kji} + P_{jki} \right) + N \sum_{i=1}^{k-1} \sum_{j=p}^{k-1} P_i P_j P_{ijk}, & (4.94) \end{aligned}$$

with the channel content of the undistorted spectrum without pile-up n_k.

The total number of counts lost due to pile-up $L = \sum_{k=1}^{m} L_k$, and the total number of gained pulses $G = \sum_{k=1}^{m} G_k$ are connected through $L = 2G$, i.e. the total number of lost pulses is twice the number of gains.

Effect of a pile-up rejector A pile-up rejector (PUR) rejects pulse pairs, if their time lag t is larger than the pile-up rejector pair resolution time τ_2 . Pulses arriving almost simultaneously (i.e. with a time lag smaller than τ_2) are *not* rejected – A pile-up rejector therefore can only reduce the amount of pile-up, but is unable to eliminate it completely. The PUR pair resolution time can be found in the technical specifications of the spectroscopy amplifier and is usually ≤ 0.5 μs, with typical values of 0.3–0.5 μs.

A pile-up rejector is modelled in the following way: If the pile-up rejector is on, then pile-up occurs only, if the time lag t between the two pulses is smaller than τ_2, i.e.

$$P_{ijk} = \begin{cases} \alpha\, e^{-\alpha T_w} (t_2 - t_1) & \text{if } t_1, t_2 \leq \tau_2 \\ 0 & \text{otherwise} \end{cases}$$

see Equation 4.88.

The effect of a pile-up rejector on pile-up from a single peak is shown in Figure 4.30. Pulse pairs arriving almost simultaneously are not influenced by the pile-up rejector, resulting in a pile-up peak at twice the channel number than the original peak. Pile-up of pulses with a time lag larger than the pair resolution time (which gives the pile-up signal between the two peaks, see Figure 4.27) is eliminated.

Fast model

Major disadvantage of the *Accurate* model (section 4.11.2) is its long computing time. A much faster (but also less accurate) model for pile-up calculations was proposed by Jeynes [84]. In

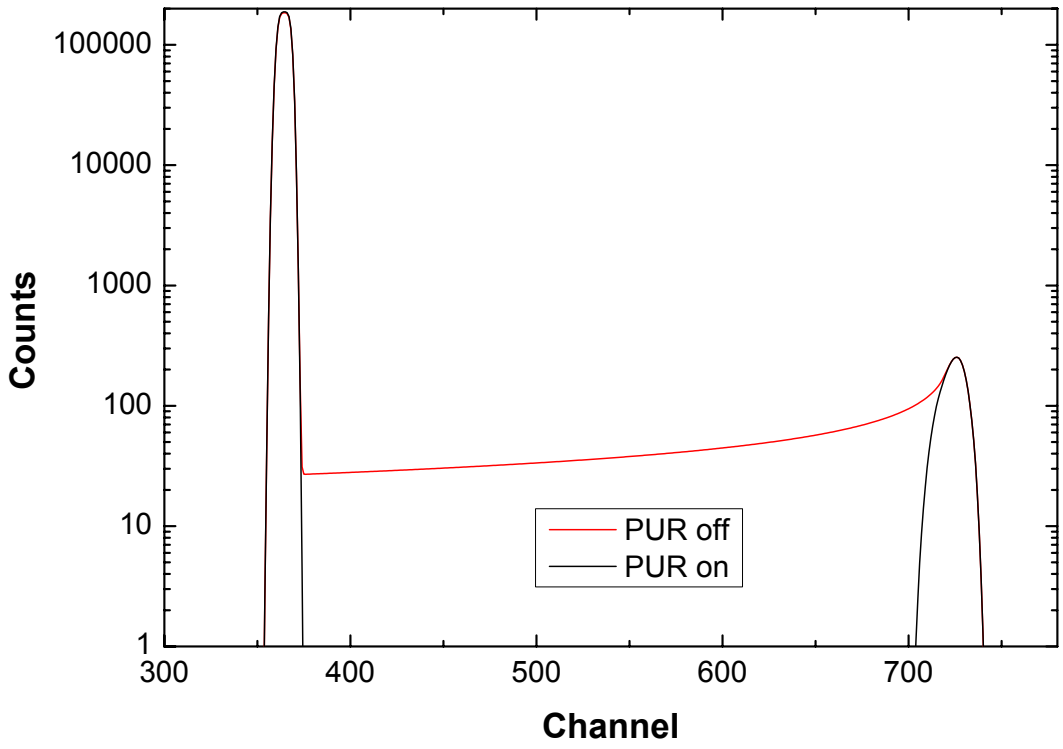

Figure 4.30.: Effect of a pile-up rejector (PUR) on pile-up from a single peak. The pile-up with a pile-up rejector switched off and on is shown. Pulse rise time 1 μs, pair resolution time 0.3 μs. The curve with PUR off is the same as in Figure 4.27.

the Jeynes model (which is selected by the *Fast* pile-up model in SIMNRA) two pulses i and j always pile up to a pulse k with $k = i + j$. I.e., in the Jeynes model two pulses always arrive simultaneously, and

$$\Delta t_{ijk} = \begin{cases} T_f & \text{if } i+j=k \\ 0 & \text{otherwise} \end{cases}$$

where T_f is a fudge factor without physical meaning and the dimension of a time.

The losses L_k and gains G_k in each channel k then can be written as

$$L_k = 2AN\,n_k$$
$$G_k = A\sum_{i=1}^{k-1} n_i\,n_{k-i},$$

with a fudge factor A

$$A = \frac{T_f}{T_{Real}} e^{-\alpha T_f}.$$

The content of each channel of the spectrum with pile-up n_k^{PU} is then given by

$$n_k^{PU} = n_k - L_k + G_k \tag{4.95}$$
$$= n_k - 2AN\,n_k + A\sum_{i=1}^{k-1} n_i\,n_{k-i}, \tag{4.96}$$

with the channel content of the undistorted spectrum without pile-up n_k. The factor A (or T_f) can be freely adjusted to obtain best fit to a measured spectrum.

The *Accurate* and *Fast* models are compared in Figure 4.31. The *Fast* model cannot reproduce the pile-up contribution which occurs without a pile-up rejector, because it assumes that two pulses always arrive simultaneously, which is generally not the case. However, the *Fast* model is not too bad if a pile-up rejector is used and the pulse rise time is larger than the pair resolution time of the pile-up rejector: In this case, only pulses which arrive almost simultaneously are registered, and two pulses with heights i and j add up to a sum pulse of height $k \approx i + j$, as is assumed in the *Fast* model. The fudge parameter T_f then is identical to the pair resolution time τ_2 of the pile-up rejector.

The comparison of the *Accurate* and *Fast* models can be summarized as follows:

1. The *Fast* model can be applied, if a pile-up rejector is used and the pulse rise time T_p is larger than the pair resolution time τ_2 of the pile-up rejector. Because $\tau_2 \leq 0.5\ \mu s$, this means that $T_p \geq 1\ \mu s$.

2. The *Accurate* model has to be used, if the measurement was done without a pile-up rejector, or if short pulses are used, i.e. if the pulse rise time $T_p < 1\ \mu s$.

The *Accurate* and *Fast* models are compared in Figure 4.32 to an experimental RBS spectrum. Both models describe the experimental pile-up quite well, although the *Accurate* model gives a slightly better approximation to the experimental spectrum.

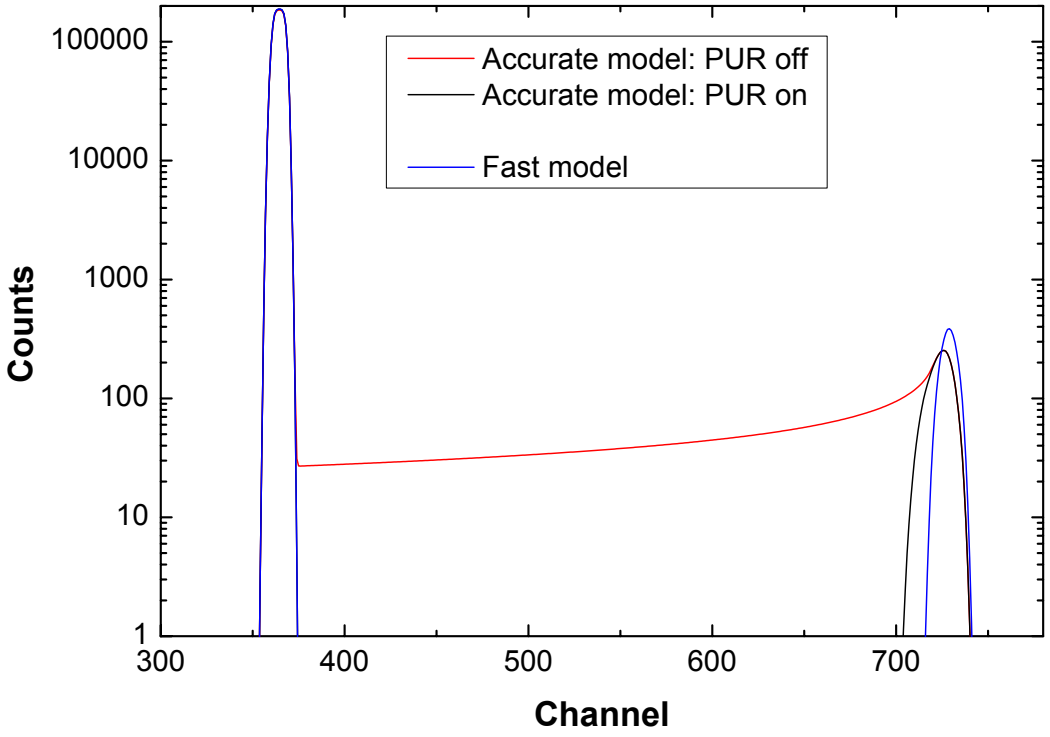

Figure 4.31.: Comparison of the *Accurate* and *Fast* models for pile-up from a single peak. *Accurate* model with pile-up rejector (PUR) on and off. Pulse rise time 1 μs, pair resolution time 0.3 μs, *Fast* model fudge time 0.3 μs.

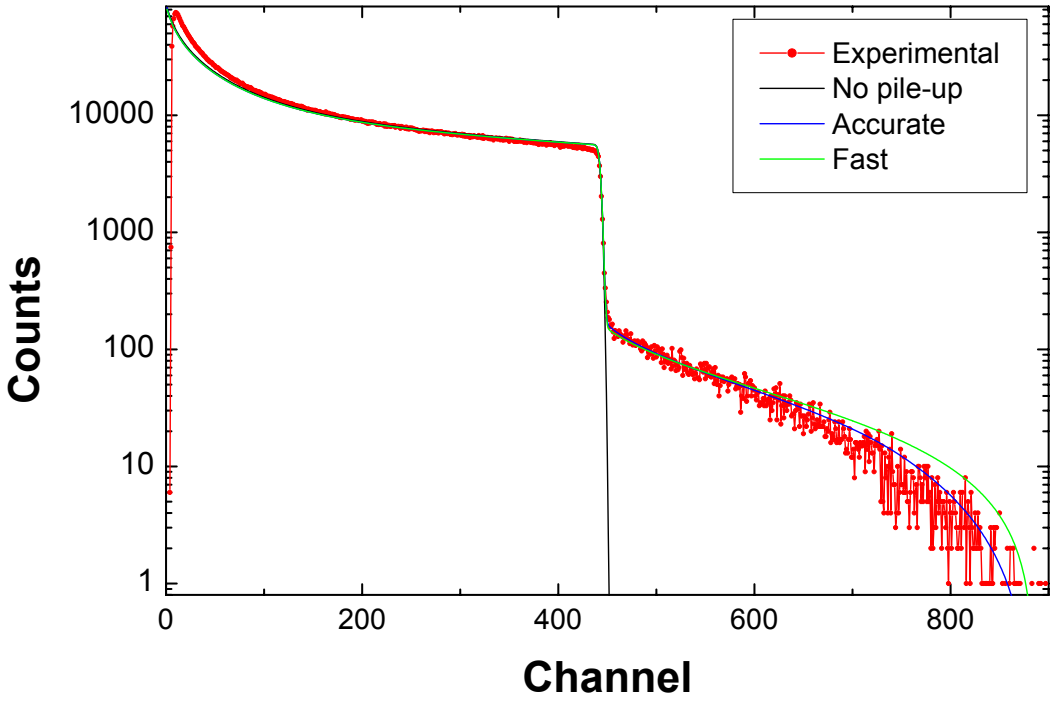

Figure 4.32.: 2 MeV ^{4}He backscattered from Au, $\theta = 165°$. The experimental spectrum was measured with a Canberra 9660 DSP, filter rise time 0.5 μs, filter flat top 0.1 μs, pile-up rejector enabled, 6.5% dead time. Simulated spectra without pile-up; accurate model with 0.44 μs rise time (according to Table 3.1) and 0.35 μs PUR pair resolution time; fast model with $T_f = 0.32$ μs.

5. Examples

This chapter gives several examples for the abilities of SIMNRA. All backscattering spectra were measured at the IPP Garching at a scattering angle $\theta = 165°$. The solid angle of the detector was 1.08×10^{-3} sr. A standard surface barrier detector with a nominal energy resolution of 15 keV FWHM was used.

5.1. RBS: Rutherford cross-sections

Figure 5.1 shows the measured and simulated spectra for 1.0 MeV ^{4}He incident ions on a gold layer with a thickness of about 100 nm on top of silicon. The simulated spectrum fits the measured data very well. The low background between the Si edge and the low energy Au edge is due to plural scattering (this means the backscattered particles have suffered more than one scattering event with large scattering angle) [57, 58, 59], which was not simulated for this example. The deviation between experiment and simulation at low energies in the Si spectrum is due to the same reason.

Figure 5.2 compares simulated spectra with single and dual scattering for 500 keV ^{4}He ions incident on a 100 nm gold layer on top of silicon with experimental data. At this low energy plural scattering is important. With the inclusion of dual scattering the experimental results are much better approximated. Dual scattering gives the background between the low energy edge of Au and the Si edge, and the steeper increase of the gold spectrum is better described. The results with dual scattering are slightly lower than the experimental results. This is due to trajectories with more than two scattering events, which are not calculated.

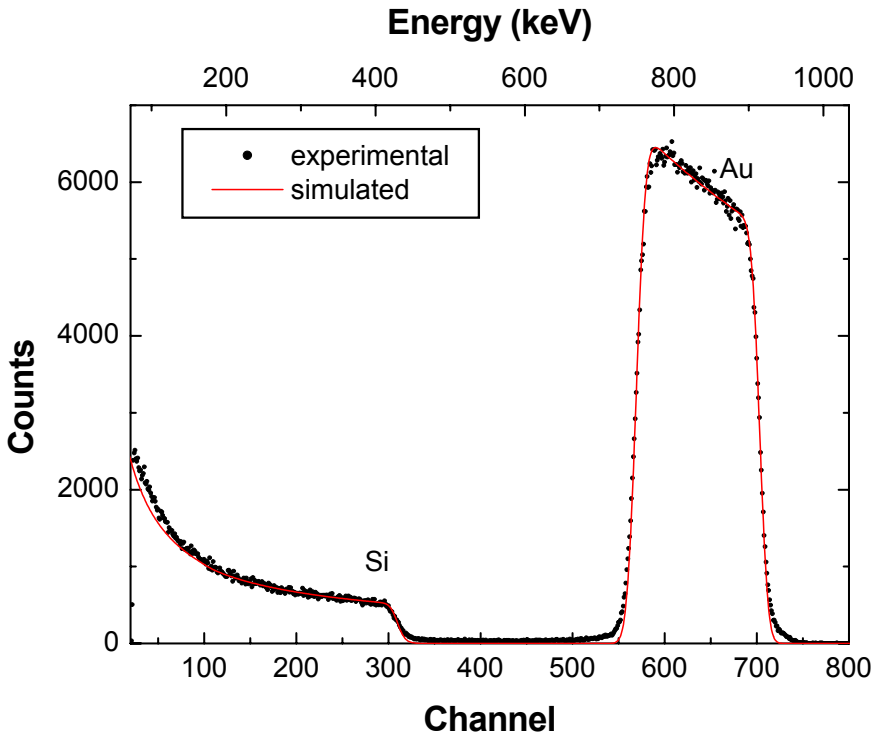

Figure 5.1.: 1000 keV ^{4}He incident on Au on top of silicon, $\theta = 165°$.

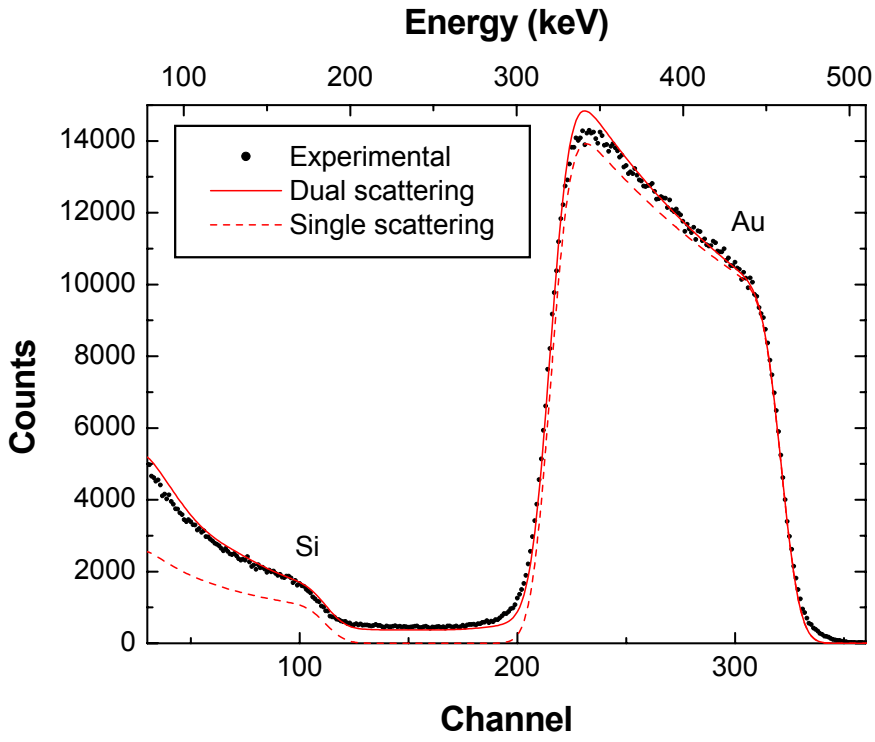

Figure 5.2.: 500 keV ^{4}He ions incident on 100 nm Au on top of Si, scattering angle 165°. Circles: experimental data points, dashed line: simulation with one scattering event, solid line: simulation with two scattering events.

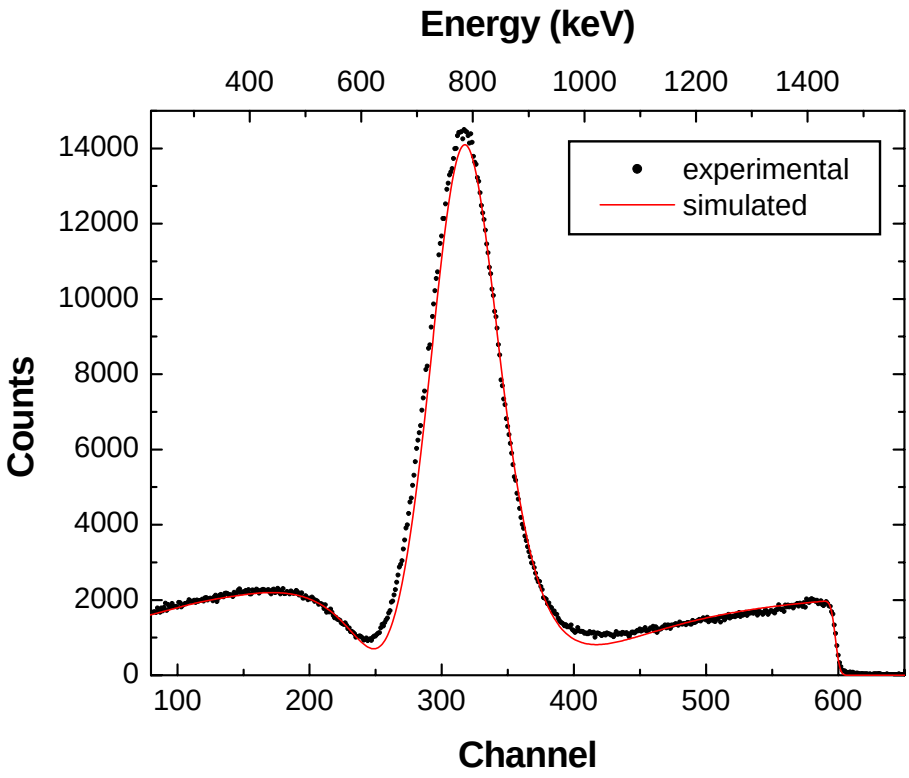

Figure 5.3.: 2000 keV protons on carbon (HOPG), $\alpha = 5°$, $\theta = 165°$.

5.2. RBS: Non-Rutherford cross-sections

Figure 5.3 shows the measured and simulated spectra for 2.0 MeV protons incident on highly oriented pyrolytic graphite (HOPG). To avoid channelling the incident angle α was 5°. The cross-section is non-Rutherford, and the cross-section data of Amirikas *et. al.* [80] were used for the simulation. The pronounced peak in the spectrum is due to the resonance in the ^{12}C(p,p)^{12}C cross-section at 1732 keV. The measured and simulated spectra agree very well.

Figure 5.4 shows the measured and simulated spectra for 2.0 MeV protons incident on silicon. To avoid channelling the incident angle α was 5°. The cross-section is non-Rutherford, and the cross-section data of Vorona *et. al.* [85] were used for the simulation. As in the case of carbon the measured and simulated spectra agree very well. The structures in the simulated spectrum between channel 500 and 700 are due to the experimentally determined cross-section data, which contain these structures.

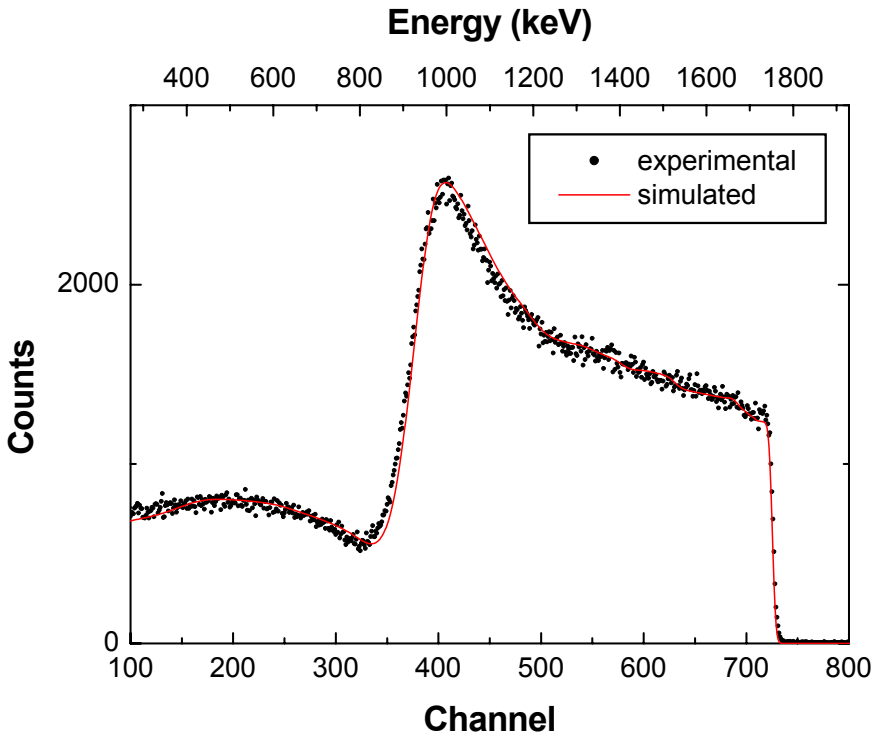

Figure 5.4.: 2000 keV protons backscattered from silicon, $\alpha = 5°$, $\theta = 165°$.

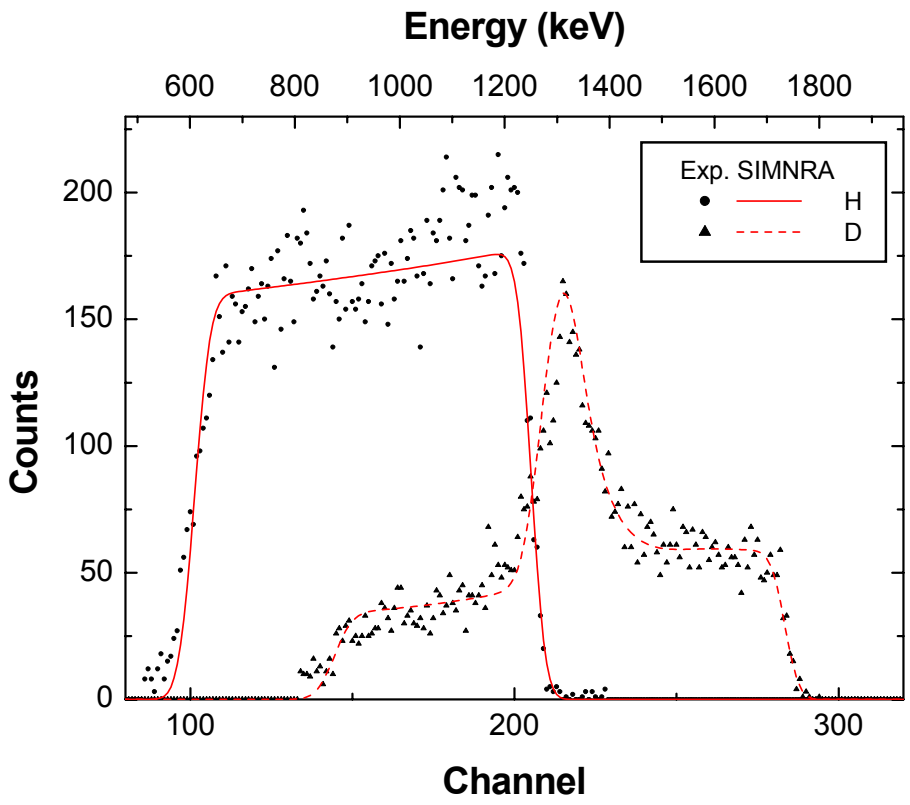

Figure 5.5.: ERDA with 2.6 MeV ^{4}He ions incident on a soft amorphous hydrocarbon layer (a:C-H layer) containing both H and D. The recoiling H and D atoms were separated with a ΔE-E telescope detector, the backscattered ^{4}He ions are not shown. $\alpha = \beta = 75°$, $\theta = 30°$.

5.3. ERDA: Non-Rutherford cross-sections

Figure 5.5 shows the measured and simulated spectra for ERDA with 2.6 MeV incident ^{4}He ions on a soft amorphous hydrocarbon layer (a:C-H layer) containing both H and D. The recoiling H and D atoms were separated with a ΔE-E telescope detector [86]. Both recoil cross-sections are non-Rutherford. The cross-section data of Baglin *et al.* [87] for H(^{4}He,H)^{4}He and of Besenbacher *et al.* [88] for D(^{4}He,D)^{4}He were used for the simulation. The peak in the deuterium spectrum is due to a resonance at a ^{4}He energy of 2130 keV. The measured and simulated data agree very well.

6. Acknowledgements

Many cross-section data files included with SIMNRA have been taken from SigmaBase (http://ibaserver.physics.isu.edu/sigmabase), which is maintained by I. Vickridge. See the file http://ibaserver.physics.isu.edu/sigmabase/newuser.html for more information about SigmaBase.

The stopping power data and subroutines for Ziegler-Biersack stopping have been taken from Ziegler's SRIM 97 program, but were translated from BASIC to PASCAL.

The routines for reading RUMP's RBS file format were obtained from Peter Revesz, Cornell University, USA. They were translated from C to PASCAL.

The graphics subsystem for SIMNRA versions prior to 4.5 was developed by Achim von Keudell, Max-Planck-Institut für Plasmaphysik, Garching, Germany.

Valuable input and bug reports were obtained from Joachim Roth, Hans Maier, Karl Krieger, Thomas Köck, and Karl Ertl (Max-Planck-Institut für Plasmaphysik, Garching, Germany), Jörg Röhrich and Swen Lindner (Hahn Meitner Institut, Berlin, Germany), Günther Dollinger (Technische Universität, München, Germany), Peter Revesz (Cornell University, USA), Andreas Gabrielsen (Norway), Caroline Raepsaet (Centre d'études de Saclay, France), and Alexander Gurbich (Institute of Physics and Power Engineering, Obninsk, Russia).

Additional cross section data were obtained from Iva Bogdanović Radović (Rudjer Bošković Institute, Zagreb, Croatia), B. Diaz-Herrera (Max-Planck-Institut für Plasmaphysik, Garching, Germany), L.Y. Kim (Max-Planck-Institut für Plasmaphysik, Garching, Germany), Beata Tyburska (Max-Planck-Institut für Plasmaphysik, Garching, Germany), Herbert Kulinski (Max-Planck-Institut für Plasmaphysik, Garching, Germany), Massimo Chiari (I.N.F.N. - Sezione di Firenze, Italy), Ana Rita Lopes Ramos (Nuclear and Technological Institute, Sacavém, Portugal), Alexander Gurbich (Institute of Physics and Power Engineering, Obninsk, Russia), and Jari Likonen (VTT, Espoo, Finland).

SIMNRA was developed at the Max-Planck-Institut für Plasmaphysik, Garching, Germany.

The R33 file format and the R33Manager were developed by Ian Vickridge, Université Paris, France. The text of Appendix was written by I. Vickridge and has been taken from the file R33Help.htm.

Starting from version 5.84, SIMNRA uses Inno Setup for creating the setup program.

6. Acknowledgements

SIMNRA uses libxml2 for reading and writing xml files.

A. OLE automation reference

This section describes OLE 2.0 automation support in SIMNRA. SIMNRA is an OLE automation server, which allows other applications to control SIMNRA. This is useful for batch processing of a large number of spectra and the like. A short overview of the OLE objects and methods is given below, for a complete description of the parameters associated with OLE automation methods see Appendix A. Some sample programs can be found in section A.10.

Objects

SIMNRA exports the following OLE automation objects:

- *Simnra.App* — The application itself.
- *Simnra.Setup* — Experimental setup.
- *Simnra.Calc* — Parameters for calculation.
- *Simnra.Target* — Target with layers and elements.
- *Simnra.Fit* — Fit parameters.
- *Simnra.Spectrum* — Experimental and simulated spectra; Plot properties.
- *Simnra.Stopping* — Stopping powers, energy loss and straggling in elements and layers.

Properties and methods

SIMNRA exports the following OLE automation properties and methods, grouped by object:

Simnra.App

- *Active* — Specifies whether SIMNRA is active and has focus.
- *BringToFront* — Brings SIMNRA to the front above all other applications.
- *CalculateSpectrum* — Calculates a simulated spectrum.
- *CalculateSpectrumToDepth* — Calculates a simulated spectrum until a specified depth.

- *CalculatingSpectrum* — Indicates if a spectrum is being calculated.
- *CopySpectrumData* — Copies experimental and simulated spectra in ASCII format to the Windows clipboard.
- *DeleteSpectrumOnCalculate* — Specifies whether the current simulated spectrum is deleted if a new calculation is performed.
- *FileName* — Name of the nra-file.
- *FitSpectrum* — Fits a spectrum.
- *Height* — Height of the form, in pixels.
- *Hide* — Hides SIMNRA.
- *LastMessage* — Text of the last error message or warning.
- *Left* — Left side of the form, relative to the screen in pixels.
- *Maximize* — Maximizes SIMNRA to fill the whole screen.
- *Minimize* — Minimizes SIMNRA to the Windows task bar.
- *Open* — Opens a NRA-file.
- *ReadSpectrumData* — Imports experimental data in different data formats.
- *Restore* — Restores the minimized application to its normal size.
- *SaveAs* — Saves a NRA-file.
- *Show* — Shows SIMNRA, if it was hidden.
- *ShowMessages* — Specifies if error messages are shown.
- *SpectrumChanged* — Indicates if the calculated spectrum has changed, i.e. was re-calculated.
- *Top* — Top side of the form, relative to the screen in pixels.
- *Width* — Width of the form, in pixels.
- *WriteSpectrumData* — Writes all spectra (experimental, simulated) in ASCII-format to a file.

Simnra.Setup

- *Alpha* — Incident angle [deg].
- *Beamspread* — Energy spread of incident beam [keV FWHM].
- *Beta* — Exit angle [deg].
- *CalibrationLinear* — Linear calibration term B for energy calibration, see Equation 3.1 [keV/channel].
- *CalibrationOffset* — Calibration offset A for energy calibration, see Equation 3.1 [keV].
- *CalibrationQuadratic* — Quadratic calibration term C for energy calibration, see Equation 3.1 [keV/channel^2].
- *DetectorResolution* — Detector resolution [keV FWHM].
- *DetectorType* — Type of detector (solid state, time-of-flight,...).
- *Energy* — Energy of incident ions [keV].
- *LiveTime* — Live time of a measurement [s].
- *LTCorrection* — Specifies if a live time correction is applied.
- *ParticlesSr* — Number of incident particles times solid angle [sr].
- *PUCalculation* — Specifies if pile-up is calculated.
- *PUROn* — Pile-up rejector on or off.
- *PURResolution* — Pile-up rejector pair-resolution time [μs].
- *RealTime* — Real time of a measurement [s].
- *RiseTime* — Rise time of the amplified pulse from zero to its maximum value [μs].
- *SetBeta* — Sets the exit angle β as function of incident angle α and scattering angle θ for IBM and Cornell geometries.
- *Theta* — Scattering angle [deg].

Simnra.Calc

- *AutoStepwidthIn* — Specifies if automatic step width control for incident ions is used.
- *AutoStepwidthOut* — Specifies if automatic step width control for outgoing ions is used.
- *CreateSpectrum* — Specifies if a spectrum is calculated.
- *dEin* — Stepwidth incident ions [keV].
- *dEout* — Stepwidth outgoing ions [keV].
- *DualScattering* — Specifies if dual scattering is calculated.
- *ElementSpectra* — Specifies if individual spectra for each element in the target are calculated.
- *EMin* — Cutoff energy [keV].
- *HighEnergyStopping* — Selects high energy stopping (Andersen-Ziegler only).
- *Isotopes* — Specifies if isotopes are taken into account.
- *IsotopeSpectra* — Specifies if individual spectra for each isotope in the target are calculated.
- *LogFile* — Specifies if a log file (SIMNRA.LOG) is created.
- *MultipleScattering* — Specifies if multiple scattering is calculated.
- *NumberOfAngleVariations* — Number of angle steps in the calculation of rough substrates.
- *NumberOfDVariations* — Number of thickness steps in the calculation of rough layers.
- *PUModel* — Selects the pile-up model.
- *ScreeningModel* — Selects the electronic screening model to the Rutherford cross section.
- *Straggling* — Specifies if energy loss and geometrical straggling are taken into account.
- *StragglingModel* — Selects the electronic energy-loss straggling model.
- *SubstrateRoughnessDimension* — Dimensionality of substrate roughness.
- *ZBStopping* — Selects Ziegler-Biersack or Andersen-Ziegler stopping.

Simnra.Target

- *AddElement* — Adds an element to a layer.
- *AddLayer* — Adds a layer to the target.
- *DeleteElement* — Deletes an element from a layer.
- *DeleteLayer* — Deletes a layer from the target.
- *ElementConcentration* — Concentration of an element in a layer.
- *ElementName* — Name of an element in a layer.
- *HasLayerRoughness* — Specifies if a layer is rough.
- *HasSubstrateRoughness* — Specifies if the substrate is rough.
- *InsertLayer* — Inserts a layer.
- *LayerRoughness* — FWHM of the roughness of a layer [10^{15} atoms/cm^2].
- *LayerThickness* — Thickness of a layer [10^{15} atoms/cm^2].
- *NumberOfElements* — Number of different elements in a layer.
- *NumberOfLayers* — Total number of layers in the target.
- *ReadTarget* — Read a target description from file.
- *SaveTargetAs* — Save a target description to file.
- *SubstrateRoughness* — FWHM of the substrate roughness [deg].
- *SubstrateRoughnessDistribution* — Distribution function of the substrate roughness.

Simnra.Fit

- *Accuracy* — Desired accuracy of the fit.
- *Chi2* — Quadratic deviation χ^2 between the simulated and measured data points.
- *Chi2Evaluation* — Method of χ^2 evaluation.
- *EnergyCalibration* — Specifies if the energy calibration is fitted.
- *LayerComposition* — Specifies if the composition of a layer is fitted.
- *LayerNr* — Specifies which layer is fitted.

- *LayerRoughness* — Specifies if the roughness of a layer is fitted.
- *LayerThickness* — Specifies if the thickness of a layer is fitted.
- *MaxIterations* — Maximum number of fit iterations.
- *NumberOfRegions* — Number of different fit regions.
- *ParticlesSr* — Specifies if the number of incident particles times solid angle is fitted.
- *RegionMaxChannel* — Upper channels of fit regions.
- *RegionMinChannel* — Lower channels of fit regions.

Simnra.Spectrum

- *AutoScale* — Specifies if the plot is scaled automatically.
- *BottomAxisMax* — Bottom axis maximum.
- *BottomAxisMin* — Bottom axis minimum.
- *Data* — Data in a specific channel.
- *Integrate* — Integrates a spectrum.
- *LeftAxisMax* — Left axis maximum.
- *LeftAxisMin* — Left axis minimum.
- *NumberOfChannels* — Number of channels in a spectrum.

Simnra.Stopping

- *EnergylossInLayer* — Energy loss in a target or foil layer [keV].
- *StoppingInElement* — Stopping power in an element [keV/10^{15} atoms/cm^2].
- *StoppingInLayer* — Stopping power in a target or foil layer [keV/10^{15} atoms/cm^2].
- *StragglingInLayer* — FWHM of energy loss straggling in a target or foil layer [keV].

A.1. Data types

SIMNRA is written in Borland Delphi and uses only automation compatible data types. The data types used by Delphi, the corresponding types in Microsoft's Interface Definition Language IDL, and the corresponding types used in Variants are summarized below.

Delphi type	IDL type	Variant type	Description
Boolean	VARIANT_BOOL	VT_BOOL	True = -1, False = 0
Double	double	VT_R8	8-byte real
Integer	long	VT_I4	4-byte signed integer
WideString	BSTR	VT_BSTR	binary string

A.2. Simnra.App

The *Simnra.App* object represents the application itself.

A.2.1. Properties

Active

[Get] Property Active : Boolean;

Description

Specifies whether SIMNRA is active and has focus. *Active* is True while SIMNRA is active and False if it is not. SIMNRA is active if it has focus, and becomes inactive when a window from a different application is about to become activated. *Active* is readonly.

Related Properties and Methods

App.BringToFront 156
App.Minimize 160
App.Restore 162

CalculatingSpectrum

[Get] Property CalculatingSpectrum : Boolean;

Description

Indicates if a spectrum is currently being calculated. *CalculatingSpectrum* is True while a spectrum is being calculated (by clicking *Calculate Spectrum* or *Calculate Spectrum Fast*), and False after the calculation has been finished. *CalculatingSpectrum* can be used for synchronizing SIMNRA with OLE clients. *CalculatingSpectrum* is readonly.

Related Properties and Methods

App.SpectrumChanged 155

DeleteSpectrumOnCalculate

[Get/Set] Property DeleteSpectrumOnCalculate : Boolean;

Default Value

true

Description

If *DeleteSpectrumOnCalculate* is *true*, the current simulated spectrum is deleted before a new spectrum is calculated. If *false*, the current simulated spectrum is conserved, and the new spectrum is added to the current one. Default is *true*. Example:

```
'  Spectrum for scattering angle 160°
Setup.Theta = 160
App.CalculateSpectrum

' Spectrum for scattering angle 170° is now added
' to the previous spectrum
App.DeleteSpectrumOnCalculate = false
Setup.Theta = 170
App.CalculateSpectrum
```

Related Properties and Methods

App.CalculateSpectrum 156

FileName

[Get] Property FileName : WideString;

Description

Name of the currently used nra-file including full path. *FileName* is readonly. If you want to change *FileName*, you have to open or save an nra-file.

Related Properties and Methods

App.Open 161
App.SaveAs 163

Height

[Get/Set] Property Height : Integer;

Description

Height of the main form, in pixels.

Related Properties and Methods

App.Left 154
App.Top 155
App.Width 155

LastMessage

[Get] Property LastMessage : WideString;

Description

Text of the last error message or warning. *LastMessage* is retained until a new error or warning is issued or it is read with *LastMessage*. *LastMessage* is readonly. See section A.9 for more details about error handling.

Related Properties and Methods

App.ShowMessages 154

Left

[Get/Set] Property Left : Integer;

Description

Position of the left side of the form, relative to the screen in pixels.

Related Properties and Methods

App.Height 153
App.Top 155
App.Width 155

ShowMessages

[Get/Set] Property ShowMessages : Boolean;

Default Value

false

Description

Specifies if error messages are shown or suppressed. If *ShowMessages* is *true*, program execution is stopped if an error is encountered, and a message box with an error description or warning is shown. Program execution is resumed after pressing the *OK* button. If *ShowMessages* is *false*, the message box is suppressed and program execution continues. The routine which produced the error, like *App.Open* or *App.CalculateSpectrum*, returns an error flag. The text of the error message can be retrieved with *LastMessage*. See section A.9 for more details about error handling.

Related Properties and Methods

App.LastMessage 153

SpectrumChanged

[Get/Set] Property SpectrumChanged : Boolean;

Description

Indicated if the calculated spectrum has changed due to a new calculation. SIMNRA will set *SpectrumChanged* to true, if a new spectrum has been calculated. But note that SIMNRA will never set *SpectrumChanged* to false – this has to be done by the OLE client. *SpectrumChanged* can be used to inform OLE clients that the calculated spectrum has changed. The client should set *SpectrumChanged* to false after having obtained the spectrum.

Related Properties and Methods

App.CalculatingSpectrum 151

Top

[Get/Set] Property Top : Integer;

Description

Position of the top of the form, relative to the screen in pixels.

Related Properties and Methods

App.Height 153
App.Left 154
App.Width 155

Width

[Get/Set] Property Width : Integer;

Description

Width of the main form, in pixels.

Related Properties and Methods

App.Height 153
App.Left 154
App.Top 155

A.2.2. Methods

BringToFront

Procedure BringToFront;

Description

Brings SIMNRA to the front above all other applications.

Parameters

None

Return Value

None

Related Properties and Methods

App.Active 151
App.Minimize 160
App.Restore 162

CalculateSpectrum

Function CalculateSpectrum : Boolean;

Description

Calculates a simulated spectrum. See section 3.9 for details and differences to *App.CalculateSpectrumFast*.

Parameters

None

Return Value

Returns *true* if the calculation succeeded.

Related Properties and Methods

App.CalculateSpectrumToDepth 157
App.CalculateSpectrumFast 157
App.DeleteSpectrumOnCalculate 152

CalculateSpectrumFast

Function CalculateSpectrumFast : Boolean;

Description

Calculates a fast simulated spectrum. See section 3.9 for details and differences to *App.CalculateSpectrum*.

Parameters

None

Return Value

Returns *true* if the calculation succeeded.

Related Properties and Methods

App.CalculateSpectrum 156
App.CalculateSpectrumToDepth 157
App.DeleteSpectrumOnCalculate 152

CalculateSpectrumToDepth

Function CalculateSpectrumToDepth(Depth : Double) : Boolean;

Description

Calculates a simulated spectrum until a specified depth. The calculation is finished when the specified depth is reached. *CalculateSpectrumToDepth* is identical to *CalculateSpectrum*, but it is considerably faster for small values of *Depth*. *CalculateSpectrumToDepth* should not be used for spectrum simulation, but can be used for depth-resolution calculations and the like.

Parameters

Depth Maximum depth of calculation [10^{15} atoms/cm^2].

Return Value

Returns *true* if the calculation succeeded.

Related Properties and Methods

App.CalculateSpectrum 156
App.CalculateSpectrumFast 157
App.DeleteSpectrumOnCalculate 152

CopySpectrumData

Procedure CopySpectrumData;

Description

Copies experimental and simulated spectra in ASCII format to the Windows clipboard. See *Edit: Copy Data* in section 3.5 for a description of the format.

Parameters

None

Return Value

None

Related Properties and Methods

App.WriteSpectrumData 164

FitSpectrum

Function FitSpectrum : Boolean;

Description

Fits a spectrum. You have to adjust the fit parameters in the *Simnra.Fit* (see page 186) object first, before the fit can be performed with *FitSpectrum*.

Parameters

None

Return Value

Returns *true* if the fit succeeded.

Hide

Procedure Hide;

Description

Hides SIMNRA. The program is still running, but not visible.

Parameters

None

Return Value

None

Related Properties and Methods

App.Minimize 160
App.Show 163

Maximize

Procedure Maximize;

Description

Maximizes SIMNRA to fill the whole screen. SIMNRA must be visible, i.e. not minimized or hidden, otherwise *Maximize* has no effect.

Parameters

None

Return Value

None

Related Properties and Methods

App.Minimize 160

Minimize

Procedure Minimize;

Description

Minimizes SIMNRA to the Windows task bar.

Parameters

None

Return Value

None

Related Properties and Methods

App.Maximize 160
App.Restore 162
App.Active 151
App.BringToFront 156

Open

Function Open(FileName : WideString; FileType : Integer = -1) : Boolean;

Description

Opens a NRA-file.

Parameters

FileName	The name of the NRA-file including path.
FileType	Format of the file. Allowed values for *FileType* are: -1: Unknown file format. 0: NRA file format. 1: IBA data format (IDF) file. 2: XNRA file format. See section 3.4 for more details about the file formats. *FileType* is optional and can be omitted. If *FileType* is omitted (or if *FileType* = *-1*), then the file type is determined automatically from the file extension.

Return Value

Returns *true* if the file was opened successfully.

Related Properties and Methods

App.SaveAs 163

ReadSpectrumData

Function ReadSpectrumData(FileName : WideString; Format : Integer) : Boolean;

Description

Imports experimental data in different formats.

Parameters

FileName	The name of the spectrum data file including path.

Format	Format of the spectrum data file. Allowed values for *Format* are: 1: Data in ASCII file format 2: Data in Canberra's CAM file format 4: Data in RUMP's RBS file format 5: Data in user defined format. Requires a used supplied dll. See section 3.15 for more details.

Return Value

Returns *true* if the file was imported successfully.

Related Properties and Methods

App.WriteSpectrumData 164

Restore

Procedure Restore;

Description

Restores the minimized application to its normal size.

Parameters

None

Return Value

None

Related Properties and Methods

App.Active 151
App.BringToFront 156
App.Minimize 160

SaveAs

Function SaveAs(FileName : WideString; FileType : Integer = 0) : Boolean;

Description

Save a NRA-file.

Parameters

FileName	The name of the NRA-file including path. If the file already exists it will be overwritten.
FileType	Format of the file. Allowed values for *FileType* are: 0: NRA file format. 1: IBA data format (IDF) file. 2: XNRA file format. See section 3.4 for more details about the file formats. *FileType* is optional and can be omitted. If *FileType* is omitted, then a file in NRA file format is written.

Return Value

Returns *true* if the file was saved successfully.

Related Properties and Methods

App.Open 161

Show

Procedure Show;

Description

Shows SIMNRA, if it was hidden.

Parameters

None

Return Value

None

Related Properties and Methods

App.Hide 159

WriteSpectrumData

Function WriteSpectrumData(FileName : WideString) : Boolean;

Description

Writes all spectra (experimental, simulated) in ASCII-format to a file. See *File: Write Spectrum Data...* in section 3.4 for a description of the file format.

Parameters

FileName	The name of the data file including path. If the file already exists it will be overwritten.

Return Value

Returns *true* if the file was written successfully.

Related Properties and Methods

App.ReadSpectrumData 161
App.CopySpectrumData 158

A.3. Simnra.Setup

The *Simnra.Setup* object represents the experimental setup.

A.3.1. Properties

Alpha

[Get/Set] Property Alpha : Double;

Description

Incident angle α [deg].

Related Properties and Methods

Setup.Beta 165
Setup.Theta 170

Beamspread

[Get/Set] Property Beamspread : Double;

Description

Energy spread of incident beam [keV FWHM].

Related Properties and Methods

Setup.Energy 167

Beta

[Get/Set] Property Beta : Double;

Description

Exit angle β [deg].

Related Properties and Methods

Setup.Alpha 164
Setup.Theta 170
Setup.SetBeta 171

CalibrationLinear

[Get/Set] Property CalibrationLinear : Double;

Description

Linear calibration term B for energy calibration, see Equation 3.1 [keV/channel].

Related Properties and Methods

Setup.CalibrationOffset 166
Setup.CalibrationQuadratic 166

CalibrationOffset

[Get/Set] Property CalibrationOffset : Double;

Description

Calibration offset *A* for energy calibration, see Equation 3.1 [keV].

Related Properties and Methods

Setup.CalibrationLinear 165
Setup.CalibrationQuadratic 166

CalibrationQuadratic

[Get/Set] Property CalibrationQuadratic : Double;

Description

Quadratic calibration term *C* for energy calibration, see Equation 3.1 [keV/channel^2].

Related Properties and Methods

Setup.CalibrationLinear 165
Setup.CalibrationOffset 166

DetectorResolution

[Get/Set] Property DetectorResolution : Double;

Description

Detector resolution [keV FWHM].

DetectorType

[Get/Set] Property DetectorType : Integer;

Description

Type of detector. Allowed values are:
0 : Solid-state detector.
1 : Time-of-flight detector.
2 : Electrostatic detector.

Related Properties and Methods

Setup.DetectorResolution 166

Energy

[Get/Set] Property Energy : Double;

Description

Energy of incident ions [keV].

Related Properties and Methods

Setup.Beamspread 165

LiveTime

[Get/Set] Property LiveTime : Double;

Description

Live time of a measurement [s].

Related Properties and Methods

Setup.LTCorrection 168
Setup.RealTime 169

LTCorrection

[Get/Set] Property LTCorrection : Boolean;

Description

True if a live time correction is applied, else *False*.

Related Properties and Methods

Setup.LiveTime 167
Setup.RealTime 169

ParticlesSr

[Get/Set] Property ParticlesSr : Double;

Description

Number of incident particles times solid angle [sr].

PUCalculation

[Get/Set] Property PUCalculation : Boolean;

Description

True if pile-up is calculated, else *False*.

Related Properties and Methods

Setup.PUROn 169
Setup.PURResolution 169
Setup.RiseTime 170

PUROn

[Get/Set] Property PUROn : Boolean;

Description

True if a pile-up rejector was used, else *False*. See section 3.6.2 for details.

Related Properties and Methods

Setup.PUCalculation 168
Setup.PURResolution 169
Setup.RiseTime 170

PURResolution

[Get/Set] Property PURResolution : Double;

Description

Pile-up rejector pair-resolution time [μs]. See section 3.6.2 for details.

Related Properties and Methods

Setup.PUCalculation 168
Setup.PUROn 169
Setup.RiseTime 170

RealTime

[Get/Set] Property RealTime : Double;

Description

Real time of a measurement [s].

Related Properties and Methods

Setup.LiveTime 167
Setup.LTCorrection 168

RiseTime

[Get/Set] Property RiseTime : Double;

Description

Rise time of the amplified pulse from zero to its maximum value [μs]. See section 3.6.2 for details.

Related Properties and Methods

Setup.PUCalculation 168
Setup.PURResolution 169

Theta

[Get/Set] Property Theta : Double;

Description

Scattering angle θ [deg].

Related Properties and Methods

Setup.Alpha 164
Setup.Beta 165

TOFLength

[Get/Set] Property TOFLength : Double;

Description

Length of the flight path for a time-of-flight detector [m]. This value is only used, if *Setup.DetectorType* is set to time-of-flight detector.

Related Properties and Methods

Setup.DetectorType 167
Setup.TOFTimeResolution 171

TOFTimeResolution

[Get/Set] Property TOFTimeResolution : Double;

Description

Time resolution of a time-of-flight detector [ps]. The full width at half maximum (FWHM) has to be used. This value is only used, if *Setup.DetectorType* is set to time-of-flight detector.

Related Properties and Methods

Setup.DetectorType 167
Setup.TOFLength 170

A.3.2. Methods

SetBeta

Function SetBeta(Geometry : Integer) : Double;

Description

Sets the exit angle β as function of incident angle α and scattering angle θ for IBM and Cornell geometries. α and θ must be defined first with *Setup.Alpha* and *Setup.Theta*.

Parameters

Geometry — IBM or Cornell geometry. Possible values for *Geometry* are:
0: IBM geometry.
1: Cornell geometry.
Any other value for *Geometry* is ignored.

Return Value

Returns the exit angle β [°].

Related Properties and Methods

Setup.Beta 165

A.4. Simnra.Calc

The *Simnra.Calc* object represents the parameters of the calculation.

A.4.1. Properties

AutoStepwidthIn

[Get/Set] Property AutoStepwidthIn : Boolean;

Description

Specifies if automatic step width control for incident ions is used.

Related Properties and Methods

Calc.AutoStepwidthOut 172

AutoStepwidthOut

[Get/Set] Property AutoStepwidthOut : Boolean;

Description

Specifies if automatic step width control for outgoing ions is used.

Related Properties and Methods

Calc.AutoStepwidthIn 172

CreateSpectrum

[Get/Set] Property CreateSpectrum : Boolean;

Description

Specifies if a spectrum is calculated or not. This parameter is always *True*, and should not be changed.

dEin

[Get/Set] Property dEin : Double;

Description

Stepwidth incident ions [keV].

Related Properties and Methods

Calc.dEout 173

dEout

[Get/Set] Property dEout : Double;

Description

Stepwidth outgoing ions [keV].

Related Properties and Methods

Calc.dEin 173

DualScattering

[Get/Set] Property DualScattering : Boolean;

Description

Specifies if dual scattering is calculated.

ElementSpectra

[Get/Set] Property ElementSpectra : Boolean;

Description

Specifies if individual spectra for each element in the target are calculated.

Related Properties and Methods

Calc.IsotopeSpectra 175

EMin

[Get/Set] Property EMin : Double;

Description

Cutoff energy [keV].

HighEnergyStopping

[Get/Set] Property HighEnergyStopping : Boolean;

Description

Selects if high energy stopping power data are used or not. This switch is only used together with the stopping power data by Andersen-Ziegler and has no influence if Ziegler-Biersack stopping is selected. See subsection 3.6.3 for more details.

Related Properties and Methods

Calc.ZBStopping 178

Isotopes

[Get/Set] Property Isotopes : Boolean;

Description

Specifies if isotopes are taken into account.

IsotopeSpectra

[Get/Set] Property IsotopeSpectra : Boolean;

Description

Specifies if individual spectra for each isotope in the target are calculated.

Related Properties and Methods

Calc.ElementSpectra 174

LogFile

[Get/Set] Property LogFile : Boolean;

Description

Specifies if a log file (SIMNRA.LOG) with additional information about the calculation is created.

MultipleScattering

[Get/Set] Property MultipleScattering : Boolean;

Description

Specifies if multiple scattering is calculated.

NumberOfAngleVariations

[Get/Set] Property NumberOfAngleVariations : Integer;

Description

Number of angle steps in the calculation of rough substrates.

Related Properties and Methods

Calc.NumberOfDVariations 176

NumberOfDVariations

[Get/Set] Property NumberOfDVariations : Integer;

Description

Number of thickness steps in the calculation of rough layers.

Related Properties and Methods

Calc.NumberOfAngleVariations 175

PUModel

[Get/Set] Property PUModel : Integer;

Description

Selects the pile-up model, see subsection 3.6.3. Allowed values are:
0 : *Accurate* model
1 : *Fast* model.

Straggling

[Get/Set] Property Straggling : Boolean;

Description

Specifies if energy loss and geometrical straggling are taken into account.

Related Properties and Methods

Calc.StragglingModel 177

ScreeningModel

[Get/Set] Property ScreeningModel : Integer;

Description

Selects the screening function to the Rutherford cross-section due to partial screening of the nuclear charges by the electron shells surrounding both nuclei, see section 4.4. Allowed values are:
0 : Rutherford cross-section without screening (Equation 4.15)
1 : Andersen's screening function (Equation 4.17).
Rutherford cross-section without screening should be used only for test purposes. Andersen's screening function is highly recommended and the program default.

StragglingModel

[Get/Set] Property StragglingModel : Integer;

Description

Selects the electronic energy-loss straggling model. Allowed values are:
1 : Bohr's theory.
2 : Chu's theory.
See subsection 4.8.2 for more details about straggling models.

Related Properties and Methods

Calc.Straggling 176

SubstrateRoughnessDimension

[Get/Set] Property SubstrateRoughnessDimension : Integer;

Description

Dimensionality of substrate roughness. Allowed values are:
0: Dimension 2.0 1: Dimension 2.5

ZBStopping

[Get/Set] Property ZBStopping : Boolean;

Description

Selects Ziegler-Biersack or Andersen-Ziegler stopping. If *ZBStopping* is *true*, Ziegler-Biersack stopping is used, while Andersen-Ziegler is selected if *ZBStopping* is set to *false*. See subsection 3.6.3 for more details about stopping power data.

Related Properties and Methods

Calc.HighEnergyStopping 174

A.5. Simnra.Target

The *Simnra.Target* object represents the target with all layers and elements.

A.5.1. Properties

ElementAmount

[Get/Set] Property ElementAmount[lay, el : Integer] : Double;

Description

Amount of element number *el* in layer number *lay* [10^{15} atoms/cm^2].

Parameters

lay	Number of the layer, with $1 \leq lay \leq NumberOfLayers$.
el	Number of the element, with $1 \leq el \leq NumberOfElements[lay]$.

Related Properties and Methods

Target.ElementConcentration 179
Target.LayerThickness 181

ElementConcentration

[Get/Set] Property ElementConcentration[lay, el : Integer] : Double;

Description

Concentration of element number *el* in layer number *lay*. The sum of concentrations of all elements in a layer must be equal to 1. This is not checked by SIMNRA. If *ElementConcentration* is changed, it is the responsibility of the programmer to assure that the sum of the concentrations is equal to 1.

Parameters

lay Number of the layer, with $1 \leq lay \leq NumberOfLayers$.

el Number of the element, with $1 \leq el \leq NumberOfElements[lay]$.

ElementName

[Get/Set] Property ElementName[lay, el : Integer] : WideString;

Description

Name of element number *el* in layer number *lay*. Returns *'XX'* if the element is unknown.
Attention: Do not use *ElementName* to add new elements to the target: The element should already be present in at least one layer. If you add new elements, they will have undefined cross sections.

Parameters

lay Number of the layer, with $1 \leq lay \leq NumberOfLayers$.

el Number of the element, with $1 \leq el \leq NumberOfElements[lay]$.

HasLayerRoughness

[Get/Set] Property HasLayerRoughness[lay : Integer] : Boolean;

Description

Specifies if the layer number *lay* is rough or not. The FWHM of the roughness is specified by *Target.LayerRoughness*. If *HasLayerRoughness* is *false*, the layer is treated as smooth, and *Target.LayerRoughness* is ignored.

Parameters

lay Number of the layer, with $1 \leq lay \leq NumberOfLayers$.

Related Properties and Methods

Target.LayerRougness 181

HasSubstrateRoughness

[Get/Set] Property HasSubstrateRoughness : Boolean;

Description

Returns *true* if the substrate is rough, and *false* if substrate roughness is switched off, i.e. the substrate is smooth. Substrate roughness can be switched off by setting *HasSubstrateRoughness* to *false*. If *HasSubstrateRoughness* is set to *true*, Lorentzian substrate roughness is selected. The FWHM of the roughness is specified by *Target.SubstrateRoughness*. If *HasSubstrateRoughness* is *false* then *Target.SubstrateRoughness* is ignored.
Note: This function is obsolete and maintained only for backward compatibility to earlier versions of SIMNRA. Use *Target.SubstrateRoughnessDistribution* instead.

Related Properties and Methods

Target.SubstrateRougness 182
Target.SubstrateRoughnessDistribution 182

LayerRoughness

[Get/Set] Property LayerRoughness[lay : Integer] : Double;

Description

FWHM of the roughness of layer number *lay* [10^{15} atoms/cm^2]. *Target.HasLayerRoughness[lay]* must be *true*, otherwise *LayerRoughness* has no effect.

Parameters

lay Number of the layer, with $1 \leq lay \leq NumberOfLayers$.

Related Properties and Methods

Target.HasLayerRougness 180

LayerThickness

[Get/Set] Property LayerThickness[lay : Integer] : Double;

Description

Thickness of layer number *lay* [10^{15} atoms/cm^2].

Parameters

lay Number of the layer, with $1 \leq lay \leq NumberOfLayers$.

NumberOfElements

[Get] Property NumberOfElements[lay : Integer] : Integer;

Description

Number of different elements in layer number *lay*. *NumberOfElements* is readonly.

Parameters

lay Number of the layer, with $1 \leq lay \leq NumberOfLayers$.

NumberOfLayers

[Get] Property NumberOfLayers : Integer;

Description

Total number of layers in the target. *NumberOfLayers* is readonly.

SubstrateRoughness

[Get/Set] Property SubstrateRoughness : Double;

Description

FWHM of the substrate roughness [deg]. *Target.SubstrateRoughnessDistribution* must be $\neq 0$ (or *Target.HasSubstrateRoughness* must be *true*), otherwise *SubstrateRoughness* has no effect.

Related Properties and Methods

Target.HasSubstrateRougness 180
Target.SubstrateRoughnessDistribution 182

SubstrateRoughnessDistribution

[Get/Set] Property SubstrateRoughnessDistribution : Integer;

Description

Distribution function of the substrate roughness. Allowed values are:

0: Smooth substrate. Substrate roughness is switched off. Same as *Target.HasSubstrateRoughness := false*.
1: Lorentzian roughness distribution. Same as *Target.HasSubstrateRoughness := true*
2: Gaussian roughness distribution.

The FWHM of the substrate roughness is set with *Target.SubstrateRoughness*.

Related Properties and Methods

Target.HasSubstrateRougness 180
Target.SubstrateRoughness 182

A.5.2. Methods

AddElement

Function AddElement(lay : Integer): Boolean;

Description

Adds an element to layer number *lay*. The element has no name and zero concentration. After adding the elements properties have to be set with *ElementName* and *ElementConcentration*.
Attention: Do not use *AddElement* to add new elements to the target. See *ElementName* for details.

Parameters

lay	Number of the layer, with $1 \leq lay \leq NumberOfLayers$.

Return Value

Returns *true* if the element was added successfully.

Related Properties and Methods

Target.AddLayer 183
Target.ElementConcentration 179
Target.ElementName 179

AddLayer

Function AddLayer : Boolean;

Description

Adds a new layer. The layer is the last layer in the stack, has zero thickness and contains no elements. After adding a layer at least one element has to be added with *AddElement* and layer properties like thickness, roughness etc. have to be set.

Parameters

None

Return Value

Returns *true* if the layer was added successfully.

Related Properties and Methods

Target.AddElement 183
Target.InsertLayer 185

DeleteElement

Function DeleteElement(lay, el : Integer) : Boolean;

Description

Deletes element number *el* in layer number *lay*.

Parameters

lay	Number of the layer, with $1 \leq lay \leq NumberOfLayers$.
el	Number of the element, with $1 \leq el \leq NumberOfElements[lay]$.

Return Value

Returns *true* if the element was deleted successfully.

Related Properties and Methods

Target.DeleteLayer 185

DeleteLayer

Function DeleteLayer(lay : Integer) : Boolean;

Description

Deletes layer number *lay*.

Parameters

lay Number of the layer to delete, with $1 \leq lay \leq NumberOfLayers$.

Return Value

Returns *true* if the layer was deleted successfully.

Related Properties and Methods

Target.DeleteElement 184

InsertLayer

Function InsertLayer(lay : Integer) : Boolean;

Description

Inserts a new layer in front of layer number *lay*. The layer has zero thickness and contains no elements. After inserting a layer at least one element has to be added with *AddElement* and layer properties like thickness, roughness etc. have to be set.

Parameters

lay Number of the layer, with $1 \leq lay \leq NumberOfLayers$.

Return Value

Returns *true* if the layer was inserted successfully.

Related Properties and Methods

Target.AddLayer 183

ReadTarget

Procedure ReadTarget(FileName : WideString);

Description

Reads a target description from file *FileName*. The current target is replaced by the content of *FileName*. *FileName* must be either a valid nra or target description file.

Parameters

FileName	Name of the file including path.

Related Properties and Methods

Target.SaveTargetAs 186

SaveTargetAs

Procedure SaveTargetAs(FileName : WideString);

Description

Saves the target description to file *FileName*.

Parameters

FileName	Name of the file including path.

Related Properties and Methods

Target.ReadTarget 186

A.6. Simnra.Fit

The *Simnra.Fit* object represents the fit parameters, i.e. what to fit, number of fit regions, maximum number of iterations etc. You have to adjust the fit parameters in the *Simnra.Fit* object first, before the fit can be performed with the *App.FitSpectrum* 159 method.

A.6.1. Properties

Accuracy

[Get/Set] Property Accuracy : Double;

Default Value

0.01

Description

Desired accuracy of the fit, see subsection 3.9.1. Fitting will be performed until the desired accuracy is obtained or the maximum number of iterations is reached.

Related Properties and Methods

Fit.MaxIterations 190

Chi2Evaluation

[Get/Set] Property Chi2Evaluation: Integer;

Default Value

0

Description

Determines how χ^2 is determined, see page 50 for details. Allowed values are:
0: Channels.
1: Integrals.

EnergyCalibration

[Get/Set] Property EnergyCalibration : Boolean;

Default Value

false

Description

Specifies if the energy calibration (offset and linear term) is fitted. The energy calibration is fitted, if *EnergyCalibration* is *true*.

LayerComposition

[Get/Set] Property LayerComposition : Boolean;

Default Value

false

Description

Specifies if the composition and thickness of a target layer is fitted. The number of the layer is specified by the *LayerNr* property. The composition of layer number *LayerNr* is fitted, if *LayerComposition* is *true*. Only one layer can be fitted at the same time.

Related Properties and Methods

Fit.LayerNr 188
Fit.LayerThickness 189

LayerNr

[Get/Set] Property LayerNr : Integer;

Default Value

1

Description

Specifies the number of the target layer, which thickness or composition is fitted. Only one layer can be fitted at the same time. *Fit.LayerComposition* and/or *Fit.LayerThickness* must be *true*, otherwise *layerNr* has no effect.

Related Properties and Methods

Fit.LayerComposition 188
Fit.LayerThickness 189

LayerRoughness

[Get/Set] Property LayerRoughness : Boolean;

Default Value

false

Description

Specifies if the roughness of a target layer is fitted. The number of the layer is specified by the *LayerNr* property. The roughness of layer number *LayerNr* is fitted, if *LayerRoughness* is *true*. Only one layer can be fitted at the same time.

Related Properties and Methods

Fit.LayerNr 188
Fit.LayerComposition 188

LayerThickness

[Get/Set] Property LayerThickness : Boolean;

Default Value

false

Description

Identical to *Fit.LayerComposition*, see 188. Only used for backward compatibility with previous versions. This method should not be used for new developments.

Related Properties and Methods

Fit.LayerNr 188
Fit.LayerComposition 188

MaxIterations

[Get/Set] Property MaxIterations : Integer;

Default Value

20

Description

Maximum number of fit iterations. Fitting will be performed until the desired accuracy is obtained or the maximum number of iterations is reached.

Related Properties and Methods

Fit.Accuracy 187

NumberOfRegions

[Get/Set] Property NumberOfRegions : Integer;

Default Value

1

Description

Number of different regions where χ^2 is calculated, see subsection 3.9.1. At least one region must exist, and the regions should not overlap. The lower and upper channels of the regions are specified by the *Fit.RegionMinChannel* and *Fit.RegionMaxChannel* properties.

Related Properties and Methods

Fit.RegionMaxChannel 191
Fit.RegionMinChannel 191

ParticlesSr

[Get/Set] Property ParticlesSr : Boolean;

Default Value

false

Description

Specifies if the number of incident particles times solid angle is fitted. The number of incident particles times solid angle is fitted, if *ParticlesSr* is *true*.

RegionMaxChannel

[Get/Set] Property RegionMaxChannel[reg : Integer] : Integer;

Default Value

8192

Description

Upper channel of fit region number *reg*.

Related Properties and Methods

Fit.NumberOfRegions 190
Fit.RegionMinChannel 191

RegionMinChannel

[Get/Set] Property RegionMinChannel[reg : Integer] : Integer;

Default Value

1

Description

Lower channel of fit region number *reg*.

Related Properties and Methods

Fit.NumberOfRegions 190
Fit.RegionMaxChannel 191

A.6.2. Methods

Chi2

Function Chi2 : Double;

Description

Quadratic deviation χ^2 between the simulated and measured data points, see subsection 3.9.1. χ^2 is weighted with the statistical error of the experimental data. χ^2 is calculated only in the fit regions defined by *NumberOfRegions*, *RegionMaxChannel* and *RegionMinChannel*. *Chi2* can be used to develop your own fit algorithms.

Parameters

None

Return Value

Returns χ^2.

Related Properties and Methods

Fit.NumberOfRegion 190
Fit.RegionMaxChannel 191
Fit.RegionMinChannel 191

A.7. Simnra.Spectrum

The *Simnra.Spectrum* object represents experimental and simulated spectra, and allows to change plot parameters.

A.7.1. Input parameter

The properties and methods of *Simnra.Spectrum* require the input parameter *spID*, which specifies if the experimental or simulated spectrum is accessed. The possible values for *spID* are:

spID	Selected spectrum
1	Experimental data
2	Simulated data

Other values are not allowed.

A.7.2. Properties

AutoScale

[Get/Set] Property AutoScale : Boolean;

Default Value

true

Description

If *AutoScale* is *true* the plot is scaled automatically, if experimental data are imported or a new calculation is performed. If *false*, the axis scales remain fixed.

BottomAxisMax

[Get/Set] Property BottomAxisMax : Double;

Description

Bottom axis maximum.

Related Properties and Methods

BottomAxisMin 193

BottomAxisMin

[Get/Set] Property BottomAxisMin : Double;

Description

Bottom axis minimum.

Related Properties and Methods

BottomAxisMax 193

LeftAxisMax

[Get/Set] Property LeftAxisMax : Double;

Description

Left axis maximum.

Related Properties and Methods

LeftAxisMin 194

LeftAxisMin

[Get/Set] Property LeftAxisMin : Double;

Description

Left axis minimum.

Related Properties and Methods

LeftAxisMax 194

NumberOfChannels

[Get] Property NumberOfChannels[spID : Integer] : Integer;

Description

Number of channels in the experimental or simulated spectrum. *NumberOfChannels* is readonly.

Related Properties and Methods

spID 192

A.7.3. Methods

Data

Function Data(spID, chan : Integer) : Double;

Description

Value of experimental or simulated data in channel *chan*.

Parameters

spID	Selects the experimental or simulated spectrum.
chan	Channel number, with $0 \leq chan \leq NumberOfChannels$.

Return Value

Returns the value in channel *chan*.

Related Properties and Methods

spID 192

Integrate

Function Integrate(spID, lowChannel, upChannel : Integer) : Double;

Description

Sum of counts of the experimental or simulated spectrum in the range from *lowChannel* to *upChannel*.

Parameters

spID	Selects the experimental or simulated spectrum.
lowChannel	Lower channel, with $0 \leq lowChannel \leq NumberOfChannels$.

upChannel Upper channel, with $0 \leq upChannel \leq NumberOfChannels$.

Return Value

Returns the sum of counts.

Related Properties and Methods

spID 192

A.8. Simnra.Stopping

The *Simnra.Stopping* object allows to calculate stopping powers, energy losses and energy loss straggling in elements, target and foil layers.

A.8.1. Input parameter

The methods of *Simnra.Stopping* require the input parameter *TargetID*, which specifies if a layer is in the target or foil. The possible values for *TargetID* are:

TargetID	
1	Target
2	Foil

Other values are not allowed.

A.8.2. Methods

EnergylossInLayer

Function EnergylossInLayer(Z1 : Integer; M1 : Double; E : Double; TargetID : Integer; lay : Integer) : Double;

Description

Energy loss of an ion *Z1* in a target or foil layer. The layer is traversed perpendicularly, incident angle α and exit angle β are ignored. The stopping power model is selected with *Calc.ZBStopping* (page 178) and *Calc.HighEnergyStopping* (page 174), and may be additionally modified by a correction factor to the stopping power, see section 3.7. The accuracy of the energy loss calculation is influenced by the settings of *Calc.AutoStepwidthOut* (page 172) and *Calc.dEOut* (page 173).

Parameters

Z1	Nuclear charge of the ion.
M1	Mass of the ion [amu].
E	Incident energy [keV].
TargetID	Selects target or foil.
lay	Number of the target or foil layer.

Return Value

Returns the energy loss in the layer [keV].

Related Properties and Methods

TargetID 196
Stopping.StoppingInLayer 198

StoppingInElement

Function StoppingInElement(Z1 : Integer; M1 : Double; E : Double; Z2 : Integer) : Double;

Description

Stopping power of an ion *Z1* in element *Z2*. The stopping power model is selected with *Calc.ZBStopping* (page 178) and *Calc.HighEnergyStopping* (page 174).

Parameters

Z1 Nuclear charge of the ion.

M1 Mass of the ion [amu].

E Incident energy [keV].

Z2 Nuclear charge of the target element.

Return Value

Returns the stopping power in element *Z2* [keV/10^{15} atoms/cm^2].

Related Properties and Methods

Calc.ZBStopping 178
Calc.HighEnergyStopping 174

StoppingInLayer

Function StoppingInLayer(Z1 : Integer; M1 : Double; E : Double; TargetID : Integer; lay : Integer) : Double;

Description

Stopping power of an ion *Z1* in a target or foil layer. The stopping power model is selected with *Calc.ZBStopping* (page 178) and *Calc.HighEnergyStopping* (page 174), and may be additionally modified by a correction factor to the stopping power, see section 3.7.

Parameters

Z1 Nuclear charge of the ion.

M1 Mass of the ion [amu].

E Incident energy [keV].

TargetID Selects target or foil.

lay Number of the target or foil layer.

Return Value

Returns the stopping power in the layer [keV/10^{15} atoms/cm^2].

Related Properties and Methods

TargetID 196
Stopping.EnergyLossInLayer 196

StragglingInLayer

Function StragglingInLayer(Z1 : Integer; M1 : Double; E : Double; TargetID : Integer; lay : Integer) : Double;

Description

Energy loss straggling of an ion *Z1* in a target or foil layer. The layer is traversed perpendicularly, incident angle α and exit angle β are ignored. The electronic energy-loss straggling model is selected with *Calc.StragglingModel*. See *Stopping.EnergylossInLayer* for a list of additional switches, which influence the straggling calculation.

Parameters

Z1 Nuclear charge of the ion.

M1	Mass of the ion [amu].
E	Incident energy [keV].
TargetID	Selects target or foil.
lay	Number of the target or foil layer.

Return Value

Returns the full width at half maximum (FWHM) of the energy loss straggling in the layer [keV].

Related Properties and Methods

TargetID 196
Stopping.EnergylossInLayer 196
Calc.StragglingModel 177

A.9. Error handling

If SIMNRA is run as stand alone application, i.e. not as OLE server, it reports errors by showing message boxes with error messages or warnings, and program execution is stopped until the *OK* button of the message box is pressed by the user. This behaviour is reasonable for an interactive application, but it is not wishful for an OLE server: The server is controlled by another application or script, and the display of a message box to a script is useless. Therefore, if SIMNRA is running as server, it handles errors in a different way: Message boxes are suppressed and program execution continues, even if an error is encountered. The error is reported by an error flag as return value of the routine which produced it. The text of the last error message can be retrieved with *App.LastMessage*.

This behaviour can be changed by setting *App.ShowMessages* = *true*: In this case error messages will be shown as message boxes, and program execution is stopped until the *OK* button of the box is pressed. SIMNRA is able to detect if it is running as stand alone application or as server, and *App.ShowMessages* is set to *false* automatically, if invoked as server.

The following code in Visual Basic Script shows the use of the error handling routines:

```
' Create the application object
Set App = CreateObject("Simnra.App")

' Wait 1000 ms: May be necessary for the server to start
WScript.Sleep 1000

' Open a NRA-file
Success = App.Open("c:\temp\test.nra")

' Some error reported by App.Open: Display last error message and exit
If Not Success Then
WScript.Echo App.LastMessage
Exit
End If

' Calculate a spectrum
Success = App.CalculateSpectrum
```

A.10. Programming examples

Sample program in Borland Delphi showing the use of the OLE automation objects.

```
Var App : Variant;
Result : Boolean;
Begin
{ Create the application object }
App := CreateOLEObject('Simnra.App');

{ Wait 1000 ms: May be necessary for the server to start }
Sleep(1000);

{ Open a NRA-file }
Result := App.Open('c:\temp\test.nra');

{ Calculate a spectrum }
Result := App.CalculateSpectrum;

{ Save the NRA-file }
Result := App.SaveAs('c:\temp\test.nra');
End;
```

Sample program in Visual Basic Script showing the use of the OLE automation objects.

```
' Create the application object
Set App = CreateObject("Simnra.App")

' Wait 1000 ms: May be necessary for the server to start
WScript.Sleep 1000

' Open a NRA-file
Result = App.Open("c:\temp\test.nra")

' Calculate a spectrum
Result = App.CalculateSpectrum

' Save the NRA-file
Result = App.SaveAs("c:\temp\test.nra")
```

Sample program in Visual Basic Script showing the use of the Fit object.

```
' Create the application object
Set App = CreateObject("Simnra.App")

' Create the fit object
Set Fit = CreateObject("Simnra.Fit")

' Wait 1000 ms: May be necessary for the server to start
WScript.Sleep 1000

' Open a NRA-file
Result = App.Open("c:\temp\test.nra")

' Fit thickness and composition of layer number 2
Fit.LayerNr = 2
Fit.LayerThickness = True
Fit.LayerComposition = True

' One fit region from channel 100 to 200
Fit.NumberOfRegions = 1
Fit.RegionMinChannel(1) = 100
Fit.RegionMaxChannel(1) = 200

' Perform the fit
Result = App.FitSpectrum
```

Sample program in Visual Basic Script showing how to add layers and elements.

```
' Create the application object
Set App = CreateObject("Simnra.App")

' Create the target object
Set Target = CreateObject("Simnra.Target")

' Wait 1000 ms: May be necessary for the server to start
WScript.Sleep 1000

' Open a NRA-file
Result = App.Open("c:\temp\test.nra")

' Add an empty layer: Will be the last layer
Target.AddLayer
lay = Target.NumberOfLayers

' Set the layer thickness to 1000 × 10^15 atoms/cm^2
Target.LayerThickness(lay) = 1000

' Add one element: Will be the last element
Target.AddElement(lay)
el = Target.NumberOfElements(lay)

' Set the element properties
' Attention: Au already has to be present in an already existing layer!
Target.ElementName(lay, el) = "Au"
Target.ElementConcentration(lay, el) = 1.0

' Calculate the spectrum
Result = App.CalculateSpectrum
```

B. The R33 cross section file format

The R33 cross section file format
April 2002
By I. C. Vickridge
Groupe de Physique des Solides, UMR 7588 du CNRS
Tour 23, Universités de Paris 7 et 6
2, Place Jussieu
75251 Paris

B.1. Introduction

In September 1991, in response to the workshop on cross sections for Ion Beam Analysis (IBA) held in Namur (July 1991, Nuclear Instruments and Methods B66(1992)), a simple ascii format was proposed to facilitate transfer and collation of nuclear reaction cross section data for Ion Beam Analysis (IBA) and especially for Nuclear Reaction Analysis (NRA). Although intended only as a discussion document, the ascii format - referred to as the R33 (DSIR Report 33) format - has become a de facto standard. In the decade since this first proposal there have been spectacular advances in computing power and in software usability, however the simplicity and cross-platform compatibility of the ascii character set has ensured that the need for an ascii format remains.

Nuclear reaction cross section data for Nuclear Reaction analysis has been collected and archived on the Sigmabase websites (google : Sigmabase) for about the last 7 years. This data has largely been entered in the R33 format, although there is a series of elastic cross sections that are expressed as the ratio to the corresponding Rutherford cross sections that have been entered in a format referred to as RTR (ratio to Rutherford). During this time the R33 format has been modified and added to - firstly to take into account angular distributions, which were not catered for in the first proposal, and more recently to cater for elastic cross sections expressed as the ratio-to-Rutherford, which it is useful to have for some elastic scattering programs. It is thus timely to formally update the R33 format.

There exists also the large nuclear cross section data collections of the Nuclear Data Network - the OECD NEA Nuclear data section, the IAEA Nuclear data section, and the Brookhaven

National Laboratory National Nuclear Data Centre amongst others. The R33 format is proposed to become a legal computational format for the Nuclear Data Network ('Nuclear Data Needs in Ion Beam Analysis'. I.C. Vickridge. In ŞLong Term Needs for Nuclear Data DevelopmentŤ, Report INDC(NDS)-428, August 2001, International Atomic Energy Agency, Vienna.). It is thus also necessary to provide an updated formal definition of the R33 format in order to provide the necessary specification for adoption of R33 as an accepted computational format.

Guiding considerations. In defining the updated R33 format I have required that previous valid R33 files should also conform to the updated format. This is so that R33 reading programs that conform to the updated specification will be able to read the existing R33 files - providing backward compatibility. There is also some redundancy in the format. This is partly from intellectual laziness, but also provides some checking of internal consistency to weed out errors.

B.2. The new R33 Format definition.

An R33 data file contains one cross section either as a function of (laboratory) incident energy, or as a function of (laboratory) detection angle. The file is made up of entries, and the data section. Each entry consists of a legal keyword followed by a colon followed by a space, followed by data in Ascii format. The keyword may be in any mixture of upper and lower case characters. Legal separators for numerical data are space, comma, colon, and semi-colon characters. Decimal points are represented only by full stops, and not by commas (as can be the case in some European countries). The legal ascii character set for the purposes of R33 files is ascii 0 to ascii FF. Apart from the 'Comment' entry and the optional 'Version' entry, entries may be in any order. Each entry ends with a carriage-return line-feed sequence. Some entries are optional [O], most are required [R], and some are mutually exclusive [Mx] where all entries for which the value of x is the same are mutually exclusive. See below for special conditions that apply to the keywords 'Comment', 'Nvalues', and 'Data', and 'EndData'. Default values are suggested for R33 reading routines, so that if an optional entry is omitted, or if a required entry is unreadable or missing illegally, the value of the corresponding variable in the reader is well-defined. All energies are expressed for the laboratory frame in keV and all angles in the laboratory frame in degrees. English is the preferred language.

Special note on data entry order: The original R33 specification called for data to be listed as x, y, xerrror, yerror, however the R33 files originally generated for the Sigmabase contained data entries in the order : x, xerror, y, yerror. The original specification was intended to allow for files containing no error information to be smaller, since the two final entries could simply be omitted. However given that the Sigmabase data fits easily on a single floppy, without compression, the file size arguments are not compelling and insisting on following the original specification will involve disrupting several existing readers, as well as introducing

confusion through the existence of two families of R33 files since copies of the erroneous files will probably lie around for years in different places. So, the new specification legalises the previous erroneous usage.

B.2.1. Syntax of an R33 Entry

The syntax for the list of legal keywords and the associated data is :

Keyword: [Mx, O/R] (Default) <data type>
Note: Additional notes and guidelines concerning use of the entry. Data type may be:

string (an arbitrary series of ascii characters)

n (integer) a series of ascii characters without decimal point representing a signed integer number

r (real) a series of ascii characters that represent a signed real number. Format is fairly flexible - but only decimal points (and NOT decimal commas) are accepted. Any format that can be read in a Borland Pascal readln(r) statement is acceptable.

B.2.2. List of legal entries

Comment: [R] ('None') <String>
Note: An unlimited number of ascii characters, including single CR LF sequences, but terminating by a double CR LF sequence. There is no requirement to embed CR LF sequences within the Comment, however it is recommended to place CR LF sequences at convenient places at least every 80 characters so that if the file is printed, the comment field is printed on successive lines that are not longer than 80 characters. The double CR LF sequence that signals the end of the comment is simply a blank line. It is not felt necessary to specify an upper limit to the size of the comment, however it is expected that a useful comment would not be longer than a few tens of lines - or a few thousand characters. Note that Unix systems place only a LF character to signal an end-of-line. This is illegal for R33 files. There are freeware and shareware utilities that can add the necessary CR characters if R33 files are generated under Unix.

Version: [O] ('R33') <String>

Note: Allowed values are (case-insensitive) 'R33' and ' R33a'. This entry can be used to signal that the file conforms to the special subset of R33 files proposed by M. O. Thompson for elastic scattering cross sections for use in RUMP. Sigmabase files will always be DSIR R33, but the 'R33a' variant is detailed here for completeness. All R33a files are legal R33 files, but R33a files have the following additional conditions:
1) The Version entry is required, and must be the first entry after the Comment.
2) Only elastic cross sections can be in valid R33a files.
3) Nvalues must either not be present (so that Data and EndData entries are used), or have a value of less-than-or-equal-to zero.

Source: [R]('Unknown')<String>
Note: A concise bibliographic source (preferable) or another indication of where the data has come from (avoid if possible). This field should contain the most authoritative original source for the data. This will usually be the original publication, or thesis reference. In some cases data has been input by experimenters before or without publication. In this case this entry should contain something like 'Measured and input by D. Withrington'. It should be kept small - an upper limit of 256 characters is suggested, but not required. It would be expected that further details pertaining to Mrs Withrington would be found in the Comment.

Name: [R]('unknown')<String>
Note: The name of person or institution responsible for creating the R33 file. For R33 files automatically created from Exfor files, this would be IAEA, or NNDC, or International Nuclear Data Network or whatever. No provision is made here for including update histories, however this may be accommodated in the Comment field.

Address1: [O] (' ')<String>
⋮
Address9: [O] (' ') <String>
Note: The address of the person or institution responsible for creating the R33 file. Up to nine lines of address information may be included. This can include telephone numbers, emails and so on.

Serial Number: [R] (0) <n>
Note: The serial number will be a number providing a unique link back to the Exfor dataset from which the R33 file was generated. The default value of zero means that this number has not been assigned.

Reaction: [R] (' ') <String>

Note: the reaction string is written in a standard format that can be parsed without too much difficulty. It conforms to the usual notation of:

target nucleus(incident ion, light product)product nucleus

Nuclei are specified by their chemical symbol preceded by A : e.g. 28Si, or 6Li. The mass number is required. Some common light species may also be represented by shorthand notation, with lower case being required.

n=neutron
p=proton
d=deuterium
t=triton
a=alpha particle
h=3He
x=x-ray
g=gamma

The light product may correspond to a particular energy level of the product nucleus. This is signaled by a 'postfix' on the light product. For example, 16O(d,p1)17O is the (d,p) reaction which leaves the residual 17 oxygen in the 1st excited state. Some cross sections may be sums of several particle groups corresponding to different excited states of the compound or product nucleus. Usually such a cross section would be used when the particle groups are not resolved by the detection method employed. In this case, the postfix lists the states concerned, separated by plus signs. E.g. 14N(d,p5+6)15N. Some elastic cross sections correspond to targets having several isotopes. In this case, it is necessary to use the 'composition' keyword.

Masses: [R] (1,1,1,1)] <r,r,r,r>

Note: Four mass values in amu corresponding to the four nuclei specified in the reaction string, separated by legal separators. The order is m1, m2, m3, m4 for a reaction in which m1+m2->m3+m4. The specification of which of the two initial and final masses are m1 and m3 respectively is given by the reaction string in which we always have : m2(m1,m3,)m4, so that m1 corresponds to the projectile and m3 to the light product. At present there is no intention to cater for the few cases in which there are three or more products - for example 11B(p,a)2a. In principle the masses could be deduced directly from the reaction string, however in the interests of simplicity it seems worthwhile adding them to the R33 file to avoid having to write a reaction string parser in R33 readers. In the special case where the ŚcompositionŠ keyword is used, the values there override any contained in the ŚMassesŠ entry.

Zeds: [R] (1,1,1,1) <n,n,n,n>

Note: Four integers representing the atomic number of the four nuclei specified in the reaction string, in the same order as the mass entries. The Zs could also be deduced directly from the reaction string, but see the comment in the Masses entry.

Composition: [O] ('Natural') <string, r, string, r,Ě>
Note: This entry caters for elastic cross sections measured from targets that contain a mixture of isotopes from which the elastically particles are not resolved. It consists of a list of isotopes and atom-proportions, or the value 'natural' (case insensitive) which means that a target of naturally occurring isotopic composition has been used. Isotopes are specified as for the reaction string, without shorthand notation. Example:

Target: 12C, 23.0, 13C, 26.0

If the proportions do not sum to 100, then it is assumed that they are relative amounts. In the example given, 23/49 of the atoms are 12C, and 26/49 are 13C. If the 'Composition' entry exists and has a legal value, then the values in the 'masses' entry should correspond to the appropriate weighted sum indicated in the 'composition' keyword. For example, if the target for an elastic cross section is natural silicon, then the mass given should be 28.086 - the weighted sum of stable Si isotopes in natural abundance.

Qvalue: [R] (0.0) <r, r, r, r, r>
Note: A list of up to five Q values, expressed in keV, separated by legal separators. As explained in the Reaction entry, some cross sections are for multiple particle groups, for example when the groups are not resolved experimentally. In this case a Q value is required for each particle contributing to the cross section.

Distribution: [R] ('Energy') <String>
Note: Allowed values are 'Energy', and 'Angle' . This entry says whether the data contained in this file are for a cross-section as a function of laboratory energy ('Energy') or laboratory angle ('Angle').

Theta: [M1, R] (0.0) <r>

Energy: [M1,R](1.0) <r>
Note: Theta gives the laboratory angle with respect to the incident beam, so that backscattering would be 180ř. Energy gives the laboratory energy of the incident beam. If both entries are present (an illegal condition Ě) then only the entry corresponding to the keyword in the 'Distribution' entry will be used.

Sigfactors: [O] (1.0, 0.0) <r,r>
Note: Scale conversion factor and its associated error common to all the cross section data. See original R33 publication in Appendix 1 for discussion.

Units: [O] ('mb') <String>
Note: Valid values are 'mb', 'rr' and 'tot'. R33 files are always in mb/sr, or units proportional to mb/sr for differential cross sections, and mb for total cross sections. The constant of proportionality given in the enfactors entry is independent of energy. Some users find it preferable to have elastic scattering cross sections relative to the Rutherford cross section. Since the conversion factor is no longer energy-independent, the enfactors entry can no longer cater for this. In this case, the units entry should specify 'rr' for ratio to Rutherford. Nevertheless, it is recommended that elastic cross sections be stored as cross sections just like the inelastic scattering cross sections - i.e. in mb/sr. The value 'tot' indicates that the cross section is integrated over all angles, and is expressed as a function of energy. Thus if 'tot' is used as a unit then the distribution must be 'energy' and the value of theta has no meaning. Nevertheless, it is suggested that a valid real number be given for theta so that reading routines don't have to cater for non-numerical values for theta (such as 'Theta: irrelevant'!).

Enfactors: [O] (1.0, 0.0, 0.0, 0.0) <r,r,r,r>
Note: Scale conversion factors and associated errors common to all the energy or angle data. See original R33 publication in Appendix 1 for discussion.

Nvalues: [M2,R] (0)<n>

Data: [M2,R]

Enddata: [O]
Note: two methods are allowed for representing the data. The first corresponds to the original R33 specification. The data immediately following the 'Nvalues' entry consists of the cross section data, one point per line, and each point represented by four values (X, dX, Y, dY):
energy(or angle), energy(or angle) random error, sigma, sigma random error
The data ends after Nvalues lines of data.
Alternatively (and recommended), the data may be bracketed by 'Data' and 'Enddata' entries. An entry of 'Nvalues: 0' is equivalent to a 'Data' entry. The data immediately follow the Data entry, one point per line as for the Nvalues option, and the file terminates with the end of the file, or with the optional EndData entry. Nvalues is maintained for backward compatibility, but in practice most routines will simply read and count the number of lines read until the end of the file or an EndData entry is reached, so this is the preferred option. The use of the Enddata entry simply allows a check that all of the data values are contained in the file and have been read. Data entries must be arranged in order of increasing energy or angle. Duplicate energy or angle values are not allowed (the cross section must be single-valued).

Bibliography

[1] N.P. Barradas, M. Mayer, and M. Thompson. Nucl. Instr. Meth. B 268 (2010) 1824. 7

[2] EG&G ORTEC. Model 672 spectroscopy amplifier operating manual. Tech. rep., EG&G ORTEC, Oak Ridge, U.S.A. 18

[3] H.H. Andersen and J.F. Ziegler. *Hydrogen - Stopping Powers and Ranges in All Elements*, vol. 3 of *The Stopping and Ranges of Ions in Matter*. Pergamon Press, New York, 1977. 22, 24, 85, 88

[4] J.F. Ziegler. *Helium - Stopping Powers and Ranges in All Elements*, vol. 4 of *The Stopping and Ranges of Ions in Matter*. Pergamon Press, New York, 1977. 22, 86

[5] J.F. Ziegler, J.P. Biersack, and U. Littmark. *The Stopping and Range of Ions in Solids*, vol. 1 of *The Stopping and Ranges of Ions in Matter*. Pergamon Press, New York, 1985. 22, 87, 88, 89, 97

[6] J.F. Ziegler. private communication. 1997. 22

[7] G. Konac, S. Kalbitzer, Ch. Klatt, D. Niemann, and R. Stoll. Nucl. Instr. Meth. B 136-138 (1998) 159. 22, 90

[8] G. Konac, Ch. Klatt, and S. Kalbitzer. Nucl. Instr. Meth. B 146 (1998) 106. 22, 90

[9] J.R. Tesmer and M. Nastasi, Eds. *Handbook of Modern Ion Beam Materials Analysis*, first ed. Materials Research Society, Pittsburgh, Pennsylvania, 1995. 34, 78

[10] J.A. Nelder and R. Mead. Computer Journal 7 (1965) 308. 49

[11] M.S. Caceci and W.P. Cacheris. Byte, 5 (1984) 340. 49

[12] W.H. Press, B.P. Flannery, S.A. Teukolsky, and W.T. Vetterling. *Numerical Recipes*. Cambridge University Press, Cambridge, New York, 1988. 49, 51, 82, 83

[13] L. Cliche, S.C. Gujrathi, and L.A. Hamel. Nucl. Instr. Meth. B 45 (1990) 270. 69

[14] W. Hösler and R. Darji. Nucl. Instr. Meth. B 85 (1994) 602. 69

[15] E. Steinbauer, P. Bauer, M. Geretschläger, G. Bortels, J.P. Biersack, and P. Burger. Nucl. Instr. Meth. B 85 (1994) 642. 69

[16] M. J. F. Healy, M. Torres, and J. D. Painter. Nucl. Instr. Meth. B 249 (2006) 789. 70

[17] R. Doolittle. Nucl. Instr. Meth. B 9 (1985) 344. 71, 82, 111

[18] R. Doolittle. Nucl. Instr. Meth. B 15 (1986) 227. 71, 111

[19] G. Audi and A.H. Wapstra. Nucl. Phys. A595 (1995) 409. 73

[20] P. De Bievre and P.D.P. Tylor. Int. J. Mass. Spectrom. Ion Phys. 123 (1993) 149. 73

[21] J. L'Ecuyer, J.A. Davies, and N. Matsunami. Nucl. Instr. Meth. 160 (1979) 337. 78

[22] M. Hautala and M. Luomajärvi. Rad. Effects 45 (1980) 159. 78

[23] H.H. Andersen, F. Besenbacher, P. Loftager, and W. Möller. Phys. Rev. A21, 6 (1980) 1891. 78

[24] S.R. Lee and R.R. Hart. Nucl. Instr. Meth. B 79 (1993) 463. 78

[25] M. Bozoian, K.M. Hubbard, and M. Nastasi. Nucl. Instr. Meth. B 51 (1990) 311. 80

[26] M. Bozoian. Nucl. Instr. Meth. B 58 (1991) 127. 80

[27] M. Bozoian. Nucl. Instr. Meth. B 82 (1993) 602. 80

[28] D.A. Bromley, J.A. Kuehner, and E. Almqvist. Phys. Rev. Lett. 4, 7 (1960) 365. 80

[29] D.A. Bromley, J.A. Kuehner, and E. Almqvist. Phys. Rev. 123, 3 (1961) 878. 80, 81

[30] J. Liu, Z. Zheng, and W.K. Chu. Nucl. Instr. Meth. B 118 (1996) 24. 85

[31] J.F. Ziegler. Nucl. Instr. Meth. B 136-138 (1998) 141. 85

[32] H. Paul, A. Schinner, and P. Sigmund. Nucl. Instr. Meth. B 164-165 (2000) 212. 85

[33] H. Paul. http://www.exphys.uni-linz.ac.at/stopping/. 85

[34] J.F. Ziegler. *Stopping Cross-Sections for Energetic Ions in all Elements*, vol. 5 of *The Stopping and Ranges of Ions in Matter*. Pergamon Press, New York, 1980. 86

[35] J.F. Ziegler and J.M. Manoyan. Nucl. Instr. Meth. B 35 (1988) 215. 87, 88, 89, 90

[36] W.H. Bragg and R. Kleeman. Philos. Mag. 10 (1905) 318. 90

[37] D. Boutard, W. Möller, and B.M.U. Scherzer. Phys. Rev. B38, 5 (1988) 2988. 90

[38] D.I. Thwaites. Nucl. Instr. Meth. B 27 (1987) 293. 90

[39] E. Szilágyi, F. Pászti, and G. Amsel. Nucl. Instr. Meth. B 100 (1995) 103. 93, 94, 96, 104, 107, 108

[40] E. Szilágyi. Nucl. Instr. Meth. B 161-163 (2000) 37. 93

[41] M.A. Kumakhov and F.F. Komarov. *Energy Loss and Ion Ranges in Solids*. Gordon and Breach Science Publishers, New York, London, Paris, 1981. 94

[42] J.R. Bird and J.S. Williams, Eds. *Ion Beams for Materials Analysis*. Academic Press, Sydney, New York, Tokyo, 1989. 94

[43] J. Tirira, Y. Serruys, and P. Trocellier. *Forward Recoil Spectrometry*. Plenum Press, New York, London, 1996. 94

[44] P.V. Vavilov. Soviet Physics J.E.T.P. 5 (1957) 749. 94

[45] N. Bohr. Mat. Fys. Medd. Dan. Vid. Selsk. 18, 8 (1948) . 94, 95

[46] J.W. Mayer and E. Rimini. *Ion Handbook for Material Analysis*. Academic Press, New York, San Francisco, London, 1977. 94, 95, 96, 103

[47] M.G. Payne. Phys. Rev. 185, 2 (1969) 611. 94

[48] C. Tschalär. Nucl. Instr. Meth. 61 (1968) 141. 94

[49] C. Tschalär. Nucl. Instr. Meth. 64 (1968) 237. 94

[50] W.K. Chu. Phys. Rev. 13 (1976) 2057. 95, 96

[51] Q. Yang, D.J. O'Connor, and Z. Wang. Nucl. Instr. Meth. B 61 (1991) 149. 96

[52] O. Schmelmer, G. Dollinger, C.M. Frey, A. Bergmaier, and S. Karsch. Nucl. Instr. Meth. B 145 (1998) 261. 103

[53] D. Dieumegard, D. Dubreuil, and G. Amsel. Nucl. Instr. Meth. 166 (1979) 431. 104

[54] G. Amsel, G. Battistig, and A. L'Hoir. Nucl. Instr. Meth. B 201 (2003) 325. 107, 108

[55] A. Weber, H. Mommsen, W. Sarter, and A. Weller. Nucl. Instr. Meth. 198 (1982) 527. 107

[56] A. Weber and H. Mommsen. Nucl. Instr. Meth. 204 (1983) 559. 107

[57] E. Steinbauer, P. Bauer, and J.P. Biersack. Nucl. Instr. Meth. B 45 (1990) 171. 107, 137

[58] P.Bauer, E. Steinbauer, and J.P. Biersack. Nucl. Instr. Meth. B 79 (1993) 443. 107, 137

[59] W. Eckstein and M. Mayer. Nucl. Instr. Meth. B 153 (1999) 337. 107, 137

[60] P. Sigmund and K.B. Winterbon. Nucl. Instr. Meth. 119 (1974) 541. 107

[61] A.D. Marwick and P. Sigmund. Nucl. Instr. Meth. 126 (1975) 317. 107

[62] E. Szilágyi. DEPTH for targets containing multilayers. http://www.kfki.hu/∼ionhp/doc/prog/mdepth.htm. 108

[63] M. Mayer, K. Arstila, K. Nordlund, E. Edelmann, and J. Keinonen. Nucl. Instr. Meth. B 249 (2006) 823. 108

[64] R.D. Edge and U. Bill. Nucl. Instr. Meth. 168 (1980) 157. 111

[65] A.R. Knudson. Nucl. Instr. Meth. 168 (1980) 163. 111

[66] J.R. Bird, P. Duerden, D.D. Cohen, G.B. Smith, and P. Hillery. Nucl. Instr. Meth. 218 (1983) 53. 111

[67] C.P. Hobbs, J.W. McMillan, and D.W. Palmer. Nucl. Instr. Meth. B 30 (1988) 342. 111

[68] M. Wüest and P. Bochsler. Nucl. Instr. Meth. B 71 (1992) 314. 111

[69] I.M. Yesil. Einfluß der Oberflächenrauhigkeit auf ERDA-Tiefen-Profile. Master's thesis, Ludwig Maximilian Universität, München, 1995. In german. 111

[70] I.M. Yesil, W. Assmann, H. Huber, and K.E.G. Löbner. Nucl. Instr. Meth. B 136-138 (1998) 623. 111

[71] A. Kitamura, T. Tamai, A. Taniike, Y. Furuyama, T. Maeda, N. Ogiwara, and M. Saidoh. Nucl. Instr. Meth. B 134 (1998) 98. 111

[72] R. Behrisch, S. Grigull, U. Kreissig, and R. Grötschel. Nucl. Instr. Meth. B 136-138 (1998) 628. 111

[73] V.S. Shorin and A.N. Sosnin. Nucl. Instr. Meth. B 72 (1992) 452. 111

[74] H. Metzner, M. Gossla, and Th. Hahn. Nucl. Instr. Meth. B 124 (1997) 567. 111

[75] H. Metzner, Th. Hahn, M. Gossla, J. Conrad, and J.-H. Bremer. Nucl. Instr. Meth. B 134 (1998) 249. 111

[76] M. Mayer, R. Behrisch, C. Gowers, P. Andrew, and A.T. Peacock. Change of the optical reflectivity of mirror surfaces exposed to JET plasmas. In *Diagnostics for Experimental Thermonuclear Fusion Reactors 2*, P. Stott, G. Gorini, P. Prandoni, and E. Sindoni, Eds. Plenum Press, New York, London, 1998, p. 279. 115

[77] M. Mayer, R. Behrisch, P. Andrew, and A.T. Peacock. J. Nucl. Mater. 241-243 (1997) 469. 115

[78] M. Küstner, W. Eckstein, E. Hechtl, and J. Roth. J. Nucl. Mater. 265 (1999) 22. 117

[79] M. Mayer. Nucl. Instr. Meth. B 194 (2002) 177. 118

[80] R. Amirikas, D.N. Jamieson, and S.P. Dooley. Nucl. Instr. Meth. B 77 (1993) 110. 120, 140

[81] G. Amsel, E. Girard, G. Vizkelethy, G. Battistig, Y. Girard, and E. Szilágyi. Nucl. Instr. Meth. B, 64 (1992) 811. 127

[82] L. Wielopolski and R.P. Gardner. Nucl. Instr. Meth., 133 (1976) 303. 127, 130

[83] D. Cano-Ott, J.L. Tain, A. Gadea, B. Rubio, L. Batist, M. Karny, and E. Roeckl. Nucl. Instr. Meth. A, 430 (1999) 488. 130

[84] C. Jeynes, Z.H. Jafri, R.P. Webb, A.C. Kimber, and M.J. Ashwin. Surface and Interface Analysis 25 (1997) 254. 132

[85] J. Vorona, J.W. Olness, W. Haeberli, and H.W. Lewis. Phys. Rev. 116 (1959) 1563. 140

[86] M. Wielunski, M. Mayer, R. Behrisch, J. Roth, and B.M.U. Scherzer. Nucl. Instr. Meth. B 122 (1997) 113. 142

[87] J.E.E. Baglin, A.J. Kellog, M.A. Crockett, and A.H. Shih. Nucl. Instr. Meth. B 64 (1992) 469. 142

[88] F. Besenbacher, I. Stensgaard, and P. Vase. Nucl. Instr. Meth. B 15 (1986) 459. 142

Index

A

ADC offset 18
Administrator privileges ..... *see* Installation, privileges
Adobe
  Acrobat 3, 57
  Acrobat Reader 3, 57
Andersen .. *see* Screening, *see* Stopping power
Appearance 56
Appearance:progress window 56
Appearance:toolbar 56
Atomic data 73

B

Biersack ..... *see* Stopping power
Bohr ..... *see* Straggling
Bozoian formula 80
Bragg's rule ..... *see* Stopping power

C

Calculate menu 48–52
  Calculate Spectrum 48
  Calculate Spectrum Fast 48
  Cross Section 48
  Density 48
  Exit Angle Beta 48
  Fit Spectrum 48, 49
  Kinematics 48
  Particles*sr 48
  Stopping 48
  Subtract Pile-up 48, 51
CAM file 8, 18, 20
Canberra 8, 18, 20
Chi2 evaluation 50
Chu ..... *see* Straggling
Command line parameters 70
Conventions 2
Cornell geometry ..... *see* Geometry
Cross section
  calculation 48
Cross-section data 78–80
  adding new data 62
  integrated 77
  Mott scattering 80
  non-Rutherford cross-section 80
  R33 file format 34, 62, 204
  RTR file format 34
  Rutherford cross-section 78–79
    high energy deviation 80
    recoil cross-section 79
    scattering cross-section 78
    screening 23, 78

D

Data exchange 58
  Excel 58
  Origin 58
  RUMP 58
  WiNDF 60
Dead layer ..... *see* Detector
Dead time 126
Density conversion 48
Depth profile 30
Detector
  dead layer 69
  electrostatic detector 15, 92
    Delta-E/E 15
    energy resolution 92
  energy calibration 12, 69
    detector nonlinearity 12, 69
    different ion species 12, 69
    non-linear 12, 69

quadratic 12, 69
energy resolution 13, 92
different ion species 13
free flight path 15, 92
plasma effect 69
pulse height defect 69
resolution *see* Detector, energy resolution, *see* Detector, time resolution
semiconductor detector 69
solid angle 13
solid state detector 13, 15, 69
material 15
thickness 15
time resolution 15, 92
time-of-flight detector 13, 15, 92
energy resolution 92
free flight path 15, 92
time resolution 15, 92
top electrode 69
transmission detector 15
type 15
Detector geometry 16
Doolittle ..... *see* Energy loss evaluation
Dual scattering 21

E

Edit menu 11
Copy Data 11
Copy Page 11
Energy
of incident beam 12
Energy calibration ..... *see* Detector
Energy loss
in layer 48
Energy loss evaluation 82–83
Doolittle 82
Runge-Kutta 82
Energy spread of incident beam . *see* Incident beam
Exit angle 12, 14, 48
Experimental data ..... *see* Spectrum data

F

File format
idf 7
nra 7
xnra 7
File menu 7–10
Exit 10
New 7
Open 7
IDF 7
nra 7
xnra 7
Print 9
Read Spectrum Data 8
ASCII 8
Canberra 8
IPP 8
ISI 8
MCERD 8
User 8
RUMP
Read RBS File 9
Read Sample Description File 9
Write Sample Description File 9
Save 7
IDF 7
nra 7
xnra 7
Save as 7
Write Spectrum Data 8
Fit error 50, 51
Fit spectrum 48, 49
accuracy 50
calculate fit error 50
fit error 50, 51
max iterations 50

G

Gamma distribution 112
γ-ray spectrum 52
Genie-2000 ..... 3, 8
Geometrical straggling 16, 103
Geometry
Cornell 12, 48, 49, 104
General 104
IBM 12, 48, 49, 104, 118

H

Help menu 57

About 57
Home Page 57
IBANDL Cross-Sections 57
Register 57
User's Guide 57

I

IBA data furnace 60
IBANDL 62
IBM geometry ..... *see* Geometry
Incident angle 12, 14
Incident beam 13
charge state 13
energy 12
energy spread 13
incident ion species 12
number of particles 13
Installation 3
privileges 3
registration 3
system requirements 3

K

Kinematics 74–76
calculation 48
elastic scattering 74
backscattering 74
recoils 74
nuclear reactions 74

L

L'Ecuyer ..... *see* Screening
Layer
manipulation 29
Layer roughness ..... *see* Surface roughness
License agreement ix
Live time 18, 52, 126
Live time correction 18, 126

M

Max iterations 50
Multiple scattering 21, 107–108

N

NDF 60
Nuclear energy loss straggling . *see* Straggling
Nuclear stopping 86–89
krypton-carbon potential 86
universal potential 87
ZBL potential 88

O

OLE automation 70, 145–203
data types 151
methods 145
objects 145
Options menu 56
Create Reaction List 56
Preferences 56

P

Parameters .... *see* Command line parameters
Particles*sr 13
calculation 48
Payment vii
Payne 94
Pile-up 18, 26, 127–134
accurate model 26, 127–132
calculation from experimental data 48, 51
fast model 26, 127, 132–134
pile-up rejector 20, 52, 132
pair resolution time 20, 52, 132
subtraction 48, 51
Pile-up rejector ..... *see* Pile-up
PIXE 52
Plasma effect ..... *see* Detector
Plot
pan 55
zoom in 55
zoom out 55
Plot menu 55
Autoscaling 55
Delete Experimental Data 55
Delete Simulated Data 55
Legend 55
Rescale x-Axis 55
Rescale y-Axis 55
Unzoom 55
x-Axis 55
y-Axis 55
Plural scattering 21, 107–110

Privileges ..... *see* Installation
Progress window 56
Publications ..... *see* SIMNRA
Pulse height defect ..... *see* Detector
Pulse rise time ..... *see* Rise time

R

R33 file format ..... *see* Cross-section data
Reactions menu 34
Real time 18, 52, 126
Registration ..... vii, 3, 57
Rise time 18, 52
Roughness ..... *see* Surface roughness
RTR file format ..... *see* Cross-section data
RUMP 58, 71, 82
  RBS file 9, 58
  sample description file 9, 58
Runge-Kutta 82
Rutherford cross-section *see* Cross-section data

S

Scattering angle 12, 14
Scattering kinematics ..... *see* Kinematics
Screening
  Andersen 23, 78
  L'Ecuyer 23, 78
Semiconductor detector
  seeDetector 215
Setup menu 12–20
  Calculation 21
  Experiment 12
  Experiment: More Options
    Detector Geometry 16
    Detector Type 15
    Live Time and Pile-up 18
SIMNRA
  publications ii
  reference ii
  version history x
Solid state detector ..... *see* Detector
Spectrum data 8
  ASCII 8
  CAM file 8
  Canberra 8
  IPP 8
  ISI 8
  MCERD 8
  reading 8
  RUMP 9
  user defined 8, 61
  writing 8
SRIM ..... *see* Stopping power
Stopping power 22, 85–91
  Andersen-Ziegler 22, 85
    heavy ions 87
    helium 86
    hydrogen 85
    nuclear stopping 85–87
  Bragg's rule 29, 90
  calculation 48
  cores and bonds model 90
  correction factor 29
  in compounds 90
  KKK stopping 22, 90
  SRIM 3, 22, 56, 66, 90
    download 66
    installation 66
    program directory 56, 66
    trouble shooting 66
  SRIM 97 ..... 22, 89
  User defined 22, 68
  Ziegler-Biersack 22, 87
    heavy ions 89
    helium 88
    hydrogen 87
    nuclear stopping 88, 89
Straggling 93–105
  Bohr theory 23, 94, 95
  charge state fluctuations 96–97
  Chu theory 23, 95
  electronic energy loss 93–100
    accuracy of 100
    step width control 100
  geometrical 16
  geometrical straggling 103
  in compounds 103
  multiple scattering 21, 107–108
  non-statistical broadening 94
  nuclear energy loss straggling 103
    Bohr theory 103

Payne 94
plural scattering 21, 107–110
Symon 94
Tschalär 94
Vavilov theory 94
Yang theory 23, 96–97
Substrate roughness ... *see* Surface roughness
Surface roughness 111–124
layer roughness 29, 30, 111–116
number of steps 26
parameter for calculation 26
rough film ..... *see* layer roughness
rough substrate . *see* substrate roughness
substrate roughness 29, 30, 116–124
Symon ..... *see* Straggling

T

Target menu 28–32
Foil 32
Target 28
Time-of-flight detector ..... *see* Detector
Toolbar 5, 56
Tools menu 53
data reader 53
integrate spectrum 53
nearest elements 53
Top electrode ..... *see* Detector
Tschalär ..... *see* Straggling

U

Uninstallation 3
Universal potential 87
User.dll 61

V

Vavilov ..... *see* Straggling
Version ii
Version history ..... *see* SIMNRA

W

WiNDF 60

X

X-ray spectrum 52

Y

Yang ..... *see* Straggling

Z

ZBL potential 88
Ziegler ..... *see* Stopping power